Founded 1925

Incorporated
by Royal Charter 1961

"To promote the advancement of radio, electronics and kindred subjects by the exchange of information in these branches of engineering.

VOLUME 42 No. 7 JULY 1972

THE RADIO AND ELECTRONIC ENGINEER

The Journal of the Institution of Electronic and Radio Engineers

The Engineer's Employment Prospects

DESPITE the evidence in the 'Situations Vacant' advertisements of a general shortage of labour, and especially of professional men, the British Press has in the past year taken a most pessimistic view of the employment situation. Discouraging to the young and most depressing to the older man, are headlines such as: 'Industrial jobs are finishing at a net rate of 6000 a week as inflation forces companies to make economies.'

Admittedly such sweeping statements may apply to outmoded industries but to advertise a considerable shortage on one hand and yet to comment so unfavourably about the future on the other is, to say the least, confusing. Historians may well question our present-day inability to realize fully the potential of 20th-century technology—surely revealed in the 'situations vacant' columns. Whilst competition for jobs is rampant in small areas it is almost non-existent in those fields, including perhaps radio and electronics, which afford the greatest scope for worldwide improvement in man's living standards.

In every country the main economic problem is that of first ensuring maximum opportunity for gainful employment—gainful in terms of individual satisfaction, *as well as* contributing to the national wealth. Reconciliation of these interests with national solvency is, in countries like Great Britain, decided by a freely elected Government. In turn, such a Government can only determine economic policy according to the best information at its disposal. In an imperfect world, the 'best' information available to Government may, in fact, be determined by those sectional interests most able to *afford* 'persuasion'.

Distinguishing 'self-interest' from national need requires a Government capable of assessing the value of new technologies—those that give opportunity to improve individual standards of living as well as those which profit the economy of the country as a whole.

In turn this requires a Government— and its administrators—to secure public and private investment in technology. For only by technology can living standards be improved—the avowed policy of every freely elected Government—but it is doubtful, whether enough has been done to ensure full employment of technological resources. As far back as 1963 an 'Economic Committee' recommended that an interdepartmental enquiry, under the leadership of the Minister for Science, should 'consider what the Government might do to create a climate of opinion more favourable to engineering and technology generally, and so to improve the quality of people coming forward for technological training and to make better use of technologists'.

At that time the IERE and other Institutions had worked together for over a year as 'The Engineering Institutions Joint Council' in seeking general agreement on the introduction of a common qualification of reasonably high standard, and a common title, such as 'Chartered Engineer', as being most beneficial for the status of the engineering profession as a whole. This combined effort by the professional bodies was greatly encouraged by the then Minister for Science and was ultimately recognized by the granting of a Royal Charter to 'The Council of Engineering Institutions'.

Among the original purposes of CEI was to mount a strong and continuing public relations drive so as to create a climate of opinion more favourable to technology, and a higher public regard for the professional engineer. It is still essential that all Institutions should demonstrate that the various branches of engineering require professional engineers of ability and integrity, whose work is vitally important to the economic future of the country.

This is the background against which the Council of the Institution believes that it would have been wrong to have supported such resolutions as were proposed at the recent Special General Meeting, which is reported elsewhere in this *Journal*.

G. D. C.

Contributors to this issue

Dr. C. W. Sherring studied at Exeter University, where he obtained a B.Sc. degree in physics in 1967 and a Ph.D. degree in infra-red spectroscopy in 1970. Since that time he has been engaged in developing photoconductive photo-voltaic and pyroelectric detectors at the Plessey Company's Allen Clark Research Centre.

Mr. R. S. Simkins joined the Plessey Company at Towcester in 1955 developing protective coatings for electronic components. He transferred to the Allen Clark Research Centre in 1962 and worked on photolithography with thin film circuits and chromium on glass masks for microcircuitry, and more recently on infra-red devices and arrays.

Mr. C. J. Rogers graduated from Lanchester Polytechnic with a combined honours degree in physics and chemistry in 1969, and gained an M.Sc. in solid state physics from Bath University in 1970. Since then he has been working on the growth and diffusion of lead-tin telluride at the Allen Clark Research Centre.

Mr. T. J. Waterfield studied for a B.Sc. honours degree in applied physics at the City University, London. After graduating in 1972, he spent a year working on a new integrated circuit process, and in the following year gained an M.Sc. in optoelectronics from the University of Essex. His present work at the Allen Clark Research Centre is concerned with the device physics of lead-tin telluride photodiodes and with the design of suitable amplifiers for use with these detectors.

Mr. W. H. Rolls obtained his B.Sc. degree in physics at Reading University in 1964. Since then he has worked at the Allen Clark Research Centre of the Plessey Company on the development of infra-red detectors based on the II–VI and IV–VI alloy systems.

Mr. Sumadi Sosroprawiro received his M.Sc. degree in radio engineering from the Kiev Polytechnical Institute, U.S.S.R., in 1965. From 1966 to 1968 as the Head of Laboratory of the National Electrotechnical Institute of the Indonesian Institute of Sciences he was concerned with semiconductor devices. In 1968 he moved to the National Institute for Instrumentation as the head of the Electronic Department concerned with the servicing, maintenance and design of electronic instruments. In August 1970 Mr. Sumadi received a fellowship for training in medical electronics in the University of Nijmegen, where the work described in his paper was done.

Mr. A. F. Tyler served an apprenticeship at the College of Electronics, Royal Radar Establishment, Malvern, between 1958 and 1964, during which time he obtained his Higher National Diploma, the College of Electronics Diploma, and Graduate Membership of the I.E.E. He then worked for four years in the Instrumentation Section of Imperial Metal Industries Ltd., Summerfield Research Station, Kidderminster, before taking up his present appointment as a Technical Officer in the Department of Space Research at Birmingham University in 1968. Whilst at the University, he has worked mainly on circuit development for rocket-borne experiments, and the U.K. IV satellite. He has attended research vehicle launches from Woomera, South Australia, and the Western Range, California.

Professor D. P. Howson (Fellow 1969, Member 1961) is currently Dean of the Board of Studies in Engineering at the University of Bradford. A fuller biography was published in the January 1972 *Journal*.

Mr. R. W. J. Barker and **Mr. B. L. Hart** (Member 1961, Graduate 1955) are Senior lecturers at Portsmouth Polytechnic and North East London Polytechnic respectively. Notes on their careers were published in the March 1972 issue of the *Journal*.

D.C. 537.312.62: 621.372/5: 029.65/6

Applications of the Josephson Effects in the Millimetre and Submillimetre Wavelength Regions

T. G. BLANEY, B.Sc., Ph.D.*

Based on a paper presented at the Conference on Infra-red Techniques, held in Reading from 21st to 23rd September 1971

SUMMARY

The Josephson effects, which arise at a suitable junction between two pieces of superconducting material, have several applications at millimetre and submillimetre wavelengths. Devices based on the effects can be used as video detectors, harmonic mixers and frequency analysers, often with unique properties. These and other possible applications are described, and the current experimental situation using the 'point contact' type of junction is outlined.

* *Division of Electrical Science, National Physical Laboratory, Teddington, Middlesex.*

1. Introduction

In 1962, Josephson made several predictions regarding the tunnelling of superconducting electrons through a thin insulating barrier separating two pieces of superconductor.[1, 2] Since their experimental realization, these effects have given rise to a whole new family of measuring devices.[3] Their application in the microwave region has been clear from the start, but in the last few years there has been interest in operation to much higher frequencies. At the present time, the ultimate high-frequency 'cut-off' of the effects is a matter of contention, but it is certain that they will retain their usefulness well into the far infra-red.

In this paper the applications of the Josephson effects to radiation detection, mixing and frequency measurement at millimetre and shorter wavelengths are discussed.

2. Theory

The Josephson effects arise when two pieces of superconducting material are separated by some sort of barrier which hinders the passage of superconducting electrons from one side to the other except under certain conditions. The types of barrier which have been shown to work in practice include the thin insulating film (e.g. an oxide layer 10^{-9} m thick), a normal (i.e. non-superconducting) metal film (about 10^{-6} m thick), or even a superconductor of lower critical current than the superconductor on each side (e.g. a superconducting constriction 10^{-6} m long with a 10^{-6} m $\times$ 10^{-7} m cross-section).

Josephson's original treatment was for insulating barriers and we shall assume that it can also be applied to other systems. In such a structure (called a Josephson junction or JJ), superconducting electrons are able to tunnel quantum mechanically through the barrier and thus the junction can carry a supercurrent, I_s. On the basis of the microscopic theory of superconductivity Josephson predicted that

$$I_s = I_0 \sin \phi \qquad \text{.....(1)}$$

where I_0 depends on junction structure, material and temperature, ϕ is the phase difference between the wave-like functions (analogous to the wave functions of elementary quantum mechanics) which describe the superconducting state on each side of the junction. In a d.c. experiment, the junction exhibits zero resistance until the current I_0 is exceeded: for $I_s < I_0$, ϕ adjusts itself to satisfy equation (1). Once I_0 is exceeded, there is a transition to the normal resistance (approximately ohmic) of the junction (Fig. 1).

However, even when a voltage V exists across the junction, some superconducting properties remain. In addition to the normal current which then flows, there is also a supercurrent which is, in general, a function of time. This arises because the phase difference ϕ becomes time dependent such that

$$\frac{\partial \phi}{\partial t} = \frac{2e}{\hbar} V \qquad \text{.....(2)}$$

where e is the charge of an electron, and $\hbar$ is Planck's constant divided by 2π.

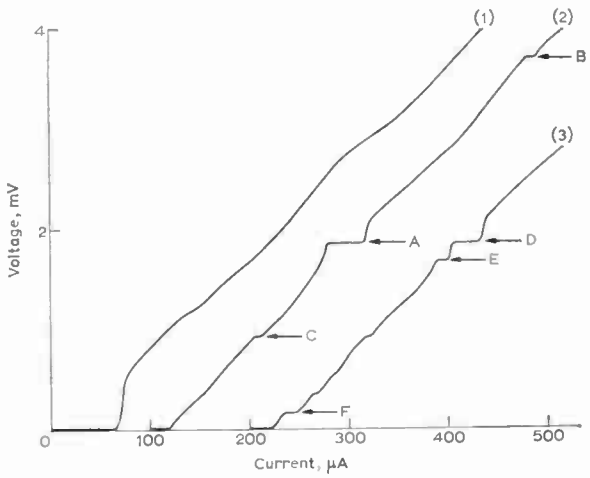

Curve (1): no monochromatic radiation incident on junction.

Curve (2): with radiation from an HCN laser operating at 891 GHz (337 μm). Current zero for this curve at 100 μA on scale.

A—fundamental laser frequency step, $2eV_0 = \hbar\omega$.

B—harmonic step, $2eV_0 = 2\hbar\omega$.

C—subharmonic step, $2 \times 2eV_0 = \hbar\omega$

Curve (3): with radiation from an HCN laser operating at two frequencies 891 and 805 GHz. Current zero at 200 μA on scale.

D—fundamental laser frequency step for 891 GHz, $2eV_0 = \hbar\omega_1$.

E—fundamental laser frequency step for 805 GHz, $2eV_0 = \hbar\omega_2$.

F—step corresponding to mixture of 891 and 805 GHz lines, $2eV_0 = \hbar(\omega_1 - \omega_2)$.

Fig. 1. Voltage-current characteristics for a niobium–niobium point contact Josephson junction at 4·2 K.

Josephson also made predictions regarding the junction's response to magnetic fields, but these will not concern us here.

We now consider the consequences of subjecting the junction to a voltage $V = V_0 + V_1 \cos \omega_1 t + V_2 \cos \omega_2 t$ where V_0 is a steady d.c. voltage and V_1 and V_2 are the amplitudes of voltages produced across the junction by incident radiation composed of two circular frequencies ω_1 and ω_2. We have neglected any possible phase difference between the radiation signals, but this is not important to the present argument. By integrating equation (2) and substituting into equation (1), an expression for I_s is obtained. Using mathematical identities, the expression for I_s becomes

$$I_s = I_0 \sum_{k=-\infty}^{\infty} \sum_{l=-\infty}^{\infty} \left[(-1)^{k+l} J_k \left(\frac{2eV_1}{\hbar\omega_1} \right) J_l \left(\frac{2eV_2}{\hbar\omega_2} \right) \cdot \sin \left(\frac{2eV_0 t}{\hbar} + \phi_0 - k\omega_1 t - l\omega_2 t \right) \right] \quad \ldots(3)$$

where J_k and J_l are Bessel functions of the first kind of integer order k and l, and ϕ_0 is a constant of integration.

It can be seen that, under these conditions, oscillating supercurrents can exist in the junction, not only at the fundamental frequencies ω_1 and ω_2 but also at a frequency $\omega_0 = 2eV_0/\hbar$ determined solely by the d.c. voltage V_0, and at frequencies determined by mixtures of ω_0, $k\omega_1$ and $l\omega_2$ (where k and l are integers). When $\omega_0 = k\omega_1 + l\omega_2$ there is a non-oscillating (i.e. d.c.) supercurrent term in equation (3). Thus over a certain range of d.c. current (corresponding to $-\pi/2 \leqslant \phi_0 \leqslant \pi/2$) there is no change in d.c. voltage: this shows itself as a constant-voltage 'step' on the voltage-current characteristic of the device (Fig. 1). The appearance of such steps indicates the presence of oscillating supercurrents in the junction, and the voltages at which steps occur enable one to calculate the frequencies present. The simple relationship linking step voltage and frequency ($2eV = \hbar\omega$) is exact to within the bounds of current absolute experimental accuracy (about 2 parts in 10^6) and is certainly reproducible to about 1 part in 10^7. The relationship may be used to maintain the standard of potential difference in terms of frequency.[4]

In the limit of $V_0 = 0$, $V_2 = 0$, $k = 0$ we find that

$$I_s = I_0 \left[J_0 \left(\frac{2eV_1}{\hbar\omega_1} \right) \sin \phi_0 \right]$$

This shows that for small radiation signals ($2eV_1 < \hbar\omega_1$), the measured d.c. supercurrent at zero voltage is reduced by incident radiation, which, to generalize, may be broad-band rather than monochromatic. Thus by monitoring the change, ΔI, in the maximum zero voltage supercurrent, broadband radiation may be detected. For very small signals

$$\Delta I \propto \frac{V_1^2}{\omega_1^2} \quad \ldots(4)$$

and thus this is a square-law detector.

The discussion above assumed that the junction was being fed from a voltage source (i.e. very low impedance). In practice, for the types of junctions which will interest us here, operation from a current source (i.e. of high impedance) is much more realistic, but does considerably complicate the mathematics. However, it is possible to show that with a current source the results are generally the same, with the occurrence of steps at the appropriate voltages, mixing, harmonic generation and, under suitable conditions, square-law detection.

As regards the frequency range of operation of the Josephson effects, there is no fundamental limit at low frequencies. Prima facie, at the high frequency end, one might expect the effects to disappear when the quantum energy of the incident photons becomes greater than the superconducting energy gap (the energy required to excite electrons from the superconducting state to the normal resistive state). However, the detailed theory indicates that the effects persist beyond the gap energy and fall off rather slowly at higher frequencies (see, for example, Ref. 5). Experimentally, Josephson phenomena have been observed at frequencies corresponding to over ten times the energy gap.[6] The highest energy gap materials presently known have gaps in the region of 5 meV (equivalent to radiation wavelength of about 0·25 mm). The experimental work described in this paper was mainly carried out on junctions of niobium, which has an energy gap of about 3 meV.

Of course, the Josephson effects only occur at temperatures below the superconducting transition temperature of the materials used, and this usually means operation in liquid helium.

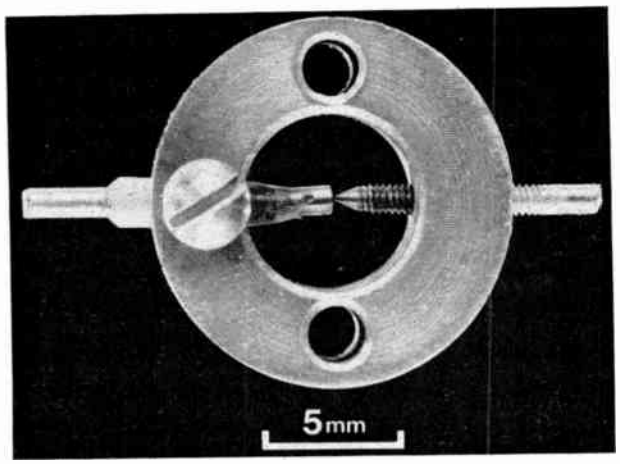

Fig. 2. A simple type of point contact junction used at N.P.L. as a mixer. The junction is formed at the contact between the tip of a pointed 14 B.A. niobium screw and a flat-ended piece of niobium wire. The junction is held together with a ring of niobium and the flat side of the contact is insulated from this ring by a sleeve of epoxy resin.

3. Experimental Types of Junctions

Many types of JJ have been made (see, for example, Ref. 3). For use at high frequencies, the first criterion which determines usefulness is that of impedance and the ease with which radiation power can be matched into the device. For work at millimetre and submillimetre wavelengths, where single-mode waveguide, over-moded waveguide and optical-type techniques are used, a device of comparatively high impedance is usually necessary. For this reason, the 'point contact' device is currently the best in this region.

A point contact consists of a sharply-pointed superconducting wire in contact with the flat surface of a second piece of superconductor. Depending on the thickness of the surface oxide layers on the material and the mechanical pressure exerted on the contact, the link between the two sides could be by tunnelling through the oxide or by way of very narrow constrictions of metal through the punctured oxide skin. The advantages of this type of junction are its low capacitance (possibly less than 1 pF), and relatively high resistance (up to several hundred ohms), and the possibility of adjustment while in operation. Its great disadvantage is its mechanical fragility and sensitivity to vibration. Although fairly stable point contact JJs can be made,[7-9] a device which combined similar impedance properties with long-term stability and complete reliability through many thermal cycles would be a great step forward. Given further work, 'weak-link' devices made from either an evaporated metal film[10] or a single crystal layer-structure superconductor[11] could do this.

Figure 2 shows a very simple type of point contact JJ used at the N.P.L. for harmonic mixing in the terahertz region.[9] The device is initially adjusted at room temperature, operates in a liquid helium storage vessel and, with suitable precautions, can be very stable if kept at liquid helium tdmperatures.

3.1. *Low-level Video Detection of Broadband Sources*

A brief review of the experimental status of point-contact JJs as broadband detectors is presented. The experimental results are not, as yet, fully understood.

The frequency response in the broadband detection regime is being measured at N.P.L. by the technique of Fourier transform spectroscopy using a lamellar grating interferometer with a mercury arc lamp source. Typically, the contact is mounted in liquid helium with its axis normal to the axis of a light pipe (over-moded waveguide) which brings the chopped radiation (originating in the interferometer) to the junction from the top of the cryostat. In the simplest experiments, the junction is biased at a constant current set just greater than I_0). Changes in the observed maximum supercurrent, ΔI, produced (at the chopping frequency) by the incident radiation can then be observed in terms of a voltage. The signal is transformer-coupled to an amplifier and then passed through a phase-sensitive detection system.

A typical result is shown in Fig. 3(a). This shows the

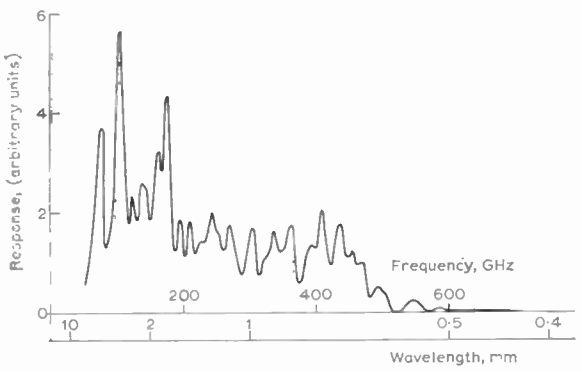

Fig. 3(a). Variation with frequency of the response (in arbitrary linear units) of a niobium–niobium point contact to radiation from a mercury discharge lamp as measured by a lamellar grating interferometer. Nominal resolving power, 7·5 GHz. Junction temperature 4·2 K. Constant current bias giving a nominal d.c. voltage of 50 μV (Josephson frequency 24 GHz). Maximum signal evel in experiment about 5 μV. Post-detection time-constant, 1 s.

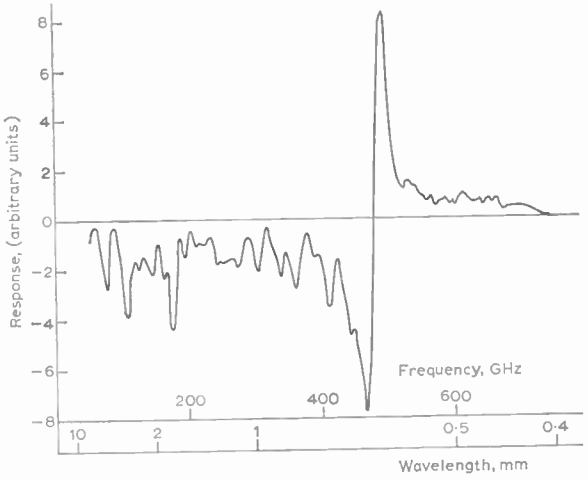

Fig. 3(b). As Fig. 3(a), but with the junction biased at a nominal d.c. voltage of 1·00 mV (Josephson frequency, 484 GHz). Maximum signal level in experiment about 250 nV, but signal/noise not appreciably worse than in the case of Fig. 3(a). Unit of response on vertical scale about twenty times smaller than in Fig. 3(a).

response (in arbitrary units) of the whole system (source, interferometer and detector): it is not an absolute response curve. As a rough first approximation, one might assume that the source energy increases as the square of the frequency in this region and that the interferometer has a flat response. Thus, if equation (4) was obeyed, the result in Fig. 3(a) would be approximately a flat line. The actual results, with the highly structured response curves are due to many factors, although at present even a qualitative analysis of such results is seldom possible. The curves in Fig. 3 should not be taken as representing all Nb–Nb junctions at 4·2 K.

Factors determining response can be grouped under two main headings. Firstly, the resonances of the cavity containing the junction are certainly important, and probably give rise to much of the structure in the curves. Secondly, there are the properties of the junction itself. If the voltage-current characteristic of the junction is changed by adjustment, there are, in general, extensive changes in the response curve. The general fall-off of the response as the frequency increases probably arises, at least in part, from the decreasing impedance presented to the radiation by the junction capacitance.

Recently, it has been found that the JJ will also operate as a square-law detector when biased at currents much greater than I_0. Under these conditions the d.c. voltage, V_0, across the junction can become large enough that the Josephson frequency ν_0 ($= \omega_0/2\pi = 2eV_0/h$ or 484 MHz/μV) falls within the frequency range of the detected radiation. Theory shows[12] that the video signal disappears at ν_0, but there are large resonant peaks of opposite sign on either side of ν_0. This behaviour is observed in practice. Figure 3(b) shows the response of the same junction used in Fig. 3(a), but now operated with a finite voltage across it. This is thus a detector the peak response of which can be continuously frequency tuned by simply varying the voltage across it.[13]

Another mode of operation involves placing the junction in a resonant cavity.[14] This, used with a broadband source, shows a very narrow band-width response when the voltage is adjusted so that ν_0 is equal to a cavity resonance frequency. The narrowing of the response is claimed to be due to feedback of the Josephson oscillation to the junction by the cavity producing an effective Q-factor much greater than the cavity Q. Once again, this is a square-law detector at low radiation levels.

Some JJ detector properties are shown in Table 1. In the author's experience, the best response is in the wavelength region down to about 0·6 mm but other workers[15] have observed appreciable response to about 0·3 mm. Theoretical estimates of noise equivalent power (taking into account only the fundamental limits of noise produced by the junction itself) indicate figures around 10^{-15} W Hz$^{-\frac{1}{2}}$ at 3 mm wavelength. In practice, the problems of efficiently coupling energy into the junction, interference from sources other than that under study (the system being sensitive down to zero frequency) and possible very fine instabilities in the point contacts themselves have not allowed this figure to be achieved yet. The speed of response of point contacts is not definitely known. It seems likely that the limit will be set by the electrical characteristics of the device rather than any fundamental limit in the time-constant of the Josephson phenomena.

Table 1. Some video detection properties of point contact Josephson detectors

Property	Performance	Reference
Operating temperature	below ~ 10 K	
Frequency range	up to ~ 1 THz (0·3 mm)	15
Radiation power level†	$\lesssim 10^{-8}$ W (at $\lambda = 3$ mm)	
Responsivity	up to 10^{5} V W^{-1} (at $\lambda = 3$ mm)	
Noise equivalent power (best achieved)	5×10^{-15} W Hz$^{-\frac{1}{2}}$ (at $\lambda = 3$ mm)	12
	10^{-14} W Hz$^{-\frac{1}{2}}$ (at $\lambda = 2$ mm)	14
Response time	$\lesssim 10^{-8}$ s (direct measurement)	15
	$\lesssim 10^{-10}$ s (inferred from mixing experiment)	17

† This is an estimate of the power level below which, with the present systems used by the author, the response can be expected to be square-law.

The high sensitivity (possibly an order of magnitude better than any other detector at these wavelengths) of these detectors gives them potential for spectroscopic purposes (e.g. in astronomy) in a spectral region where broadband sources are extremely weak. The tunability could also be useful, although the highly structured frequency response curves in the present systems are a drawback. The further advantage of very high speed (probably more than two orders of magnitude faster than other sensitive detectors in this region) could make them suitable for the study of transient phenomena (e.g. pulsed plasmas).

3.2. *Frequency Analysis and Mixing*

As remarked earlier, the JJ exhibits constant-voltage steps on its V–I characteristic when subjected to radiation from monochromatic sources. Measurements of step voltage can be directly related to source frequency and thus the JJ can be used as a frequency analyser.[6, 16] An example of this using a hydrogen cyanide gas laser is given in Fig. 4. This laser will operate strongly at three frequencies, and the JJ provides a continuous monitor of the frequencies emitted as the laser cavity is adjusted. For the strongest emission line (891 GHz, 337 μm), steps corresponding to junction-generated harmonics are readily observed up to four times the fundamental frequency. Steps corresponding to subharmonics of the fundamental frequency are also often seen (as in Fig. 4), although to do this, it is not necessary that the junction should actually generate subharmonics of the incident frequency, and in fact probably does not do so to any great extent.[16]

Steps have also been observed using the deuterium cyanide laser (operating at 1540 and 1578 GHz)[16] and the water vapour laser (operating at 2430 GHz and 3822 GHz).[17, 18] To observe steps with these laser sources at least a few milliwatts of radiation power is normally required.

With lower frequency sources, harmonic generation is much more striking in that many steps are observed. For example, with a 70 GHz klystron, step structure has been seen to over 100 harmonics or about 8 THz in frequency.[6]

The properties of JJs give rise to steps at voltages corresponding to the frequencies of mixtures of external sources as well as their harmonics (Figs. 1 and 4). In practice, it is also possible to detect voltages across the junction at the harmonic and mixed frequencies of external sources without these frequencies being mixed with internal Josephson frequency. (This would not be expected from the simplified theoretical treatment given earlier.) Thus the device can be operated in much the same way as a conventional harmonic mixer, but the unprecedented harmonic generating capability opens up new possibilities.

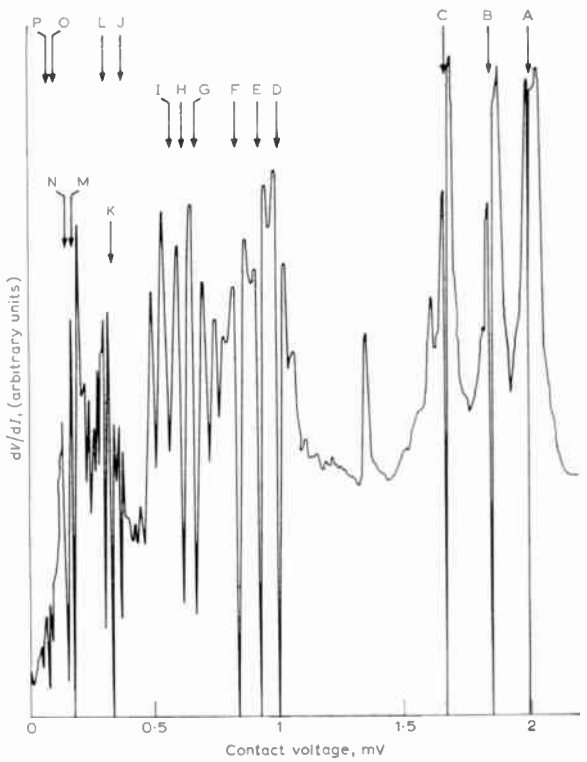

Fig. 4. Differential resistance, dV/dI, versus voltage for a niobium–niobium point-contact junction subjected to radiation of three frequencies (964, 891 and 805 GHz) from an HCN laser. Steps on the V–I characteristic appear as downward-going spikes on the plot above. The features on the curve correspond (through the Josephson relation $2eV = \hbar\omega$) to the following frequencies (in GHz) A 964; B 891; C 805; D ½ × 964; E ½ × 891; F ½ × 805; G ⅓ × 964; H ⅓ × 891; I ⅓ × 805; J 2 × (891 − 805); K (964 − 805); L 2 × (964 − 891); M (891 − 805); N (964 − 891); O ½ × (891 − 805); P ½ × (964 − 891).

Conventional non-linear resistive mixers used in this region (e.g. metal-semiconductor and metal–oxide–metal diodes) seldom generate more than about 10 or 20 harmonics which can be used for mixing purposes,[19] and then only with rather large input radiation powers. With the JJ, hundreds, or possibly thousands of usable harmonics are generated. The amplitude of junction-generated harmonics does fall off with increasing harmonic number, n (possibly with approximately the Bessel function dependence of equation (3)), but not nearly so quickly as with the non-linear resistive mixers where a $1/n^2$ dependence is the best which can be expected.[20] The highest order harmonic mixing so far reported is that of the 401st harmonic of a 9·5 GHz klystron with the 3822 GHz emission from a water vapour laser.[17] This used an adjustable point-contact JJ and a travelling-wave maser to amplify an i.f. of 9 GHz. This and three other Josephson mixing experiments are outlined in Table 2. The last two results quoted in this table were achieved by using a device of the type shown in Fig. 2, and the i.f. signal was used to phase-lock the klystron to the laser.[22] The mixer was found to be considerably more stable than other mixers used at around 1000 GHz.

Table 2. Some Josephson mixing experiments

Frequencies† mixed (GHz)	I.F. (MHz)	Type of junction	Reference
3822 − 401 × 9·5 (H_2O laser) (klystron)	9000	Nb–Nb adjustable point contact at 2 K	17
891 − 100 × 8·9 (HCN laser) (klystron)	60	ditto	21
964 − 27 × 35·7 (HCN laser) (klystron)	60	Nb–Nb preset point contact at 4·2 K	22
891 − 49 × 18·2 (HCN laser) (klystron)	60	ditto	25

† Frequency figures only approximate.

One application of these remarkable properties is the direct accurate measurement of the frequencies of far infra-red lasers in terms of the standard frequency, the caesium clock at about 9 GHz.

Secondly, a JJ could be used as the mixing element in a heterodyne receiver for use in the submillimetre region. For example, a reliable (and relatively inexpensive) microwave source at, say, about 10 GHz with only a few per cent frequency tuning could provide, via harmonic generation in a JJ, a local oscillator with continuous frequency tuning at submillimetre wavelengths. One interesting application of such a receiver might be in submillimetre radio astronomy, particularly in the field of interstellar molecular spectroscopy.

It remains to say that the use of Josephson mixers is at an early stage and no formal measurements of conversion loss, noise figure, etc., have yet been reported. Being a cryogenic device, one would expect the noise performance to be good.

4. Other Possibilities

In principle, the Josephson frequency oscillations of a junction could be used as a tunable source of radiation or as a local oscillator in a heterodyne receiver.

As a heterodyne detector, the major difficulty would be the lack of stability of the frequency of the local oscillator. The natural linewidth of the Josephson

oscillation (arising from modulation of the bias voltage by noise originating in the junction itself) could amount to tens or hundreds of megahertz. This could be improved by coupling the junction to a highly resonant cavity, but this would make tuning much more difficult.

The natural linewidth problem still exists if a junction is used as a radiation source. Also, the emitted radiation is weak: for a point contact 10^{-10} or 10^{-9} W (at about 5 mm wavelength) is about the best which can be expected. An array of junctions might provide a useful power level[23] but the technological difficulty of constructing such a device for use at millimetre and shorter wavelengths is formidable.

Although not fully proven in practice, it has been calculated[24] that if a JJ is mounted (in a special geometry) in a cavity or resonator it should be possible to detect the magnetic field of the electromagnetic radiation in the cavity. It has been estimated that individual millimetre-wave photons could be detected in this way, much as a photomultiplier operates in the optical region.

5. Conclusions

Josephson junctions have unique properties with several applications in the detection, mixing and frequency measurement of radiation at millimetre and submillimetre wavelengths. The development of Josephson techniques for these purposes is still at an early experimental stage and requires much work before the ultimate performance is achieved. The upper frequency limit of operation is not yet known, but seems unlikely to be much greater than 10 THz. The junctions call for the use of temperatures in the liquid helium range, but this should be less of a problem as such cryogenic facilities become more common, even on a large commercial scale. In any case, optimum thermal noise performance will only be achieved in electronic devices cooled to low temperatures.

The point contact junction has an acceptable performance for use in the laboratory, but devices with much better characteristics, especially as regards long-term stability, are needed. With further development, some of the already existing types of junction may well meet this requirement.

6. References

1. Josephson, B. D., 'Possible new effects in superconducting tunnelling', *Phys. Letters* (*Netherlands*), **1**, pp. 251–3, 1st July 1962.
2. Josephson, B. D., 'Supercurrents through barriers', *Advances in Phys.*, **14**, pp. 419–51, October 1965.
3. Clarke, John, 'Electronics with superconducting junctions', *Phys. Today*, **24**, pp. 30–7, August 1971.
4. Finnegan, T. F., Denenstein, A. and Langenberg, D. N., 'A.C.-Josephson effect determination of e/h: a standard of electrochemical potential based on macroscopic quantum phase coherence in superconductors', *Phys. Rev. B.*, 4, pp. 1487–522, 1st September 1971.
5. Werthamer, N. R., 'Non-linear self-coupling of Josephson radiation in superconducting tunnel junctions', *Phys. Rev.*, **147**, pp. 255–63, 8th July 1966.
6. McDonald, D. G., Kose, V. E., Evenson, K. M., Wells, J. S. and Cupp, J. D., 'Harmonic generation and submillimeter wave mixing with the Josephson effect', *Appl. Phys. Lett.*, **15**, pp. 121–2, 15th August 1969.
7. Zimmerman, J. E., Thiene, Paul and Harding, J. T., 'Design and operation of stable r.f.-biased superconducting point-contact quantum devices, and a note on the properties of perfectly clean metal contacts', *J. Appl. Phys.*, **41**, pp. 1572–80, 15th March 1970.
8. Buhrman, R. A., Strait, S. F. and Webb, W. W., 'Stable superconducting point-contact weak links', *J. Appl. Phys.*, **42**, pp. 4527–8, October 1971.
9. Blaney, T. G., 'A simple point-contact Josephson junction for use in the millimetre and submillimetre wavelength regions', *J. Phys. E.*, **4**, pp. 945–8, December 1971.
10. Gregers-Hansen, P. E. and Levinsen, M. T., 'Normal-state resistance as the determining parameter in the behaviour of Dayem bridges with sinusoidal current-phase relations', *Phys. Rev. Lett.*, **27**, pp. 847–9, 27th September 1971.
11. Consadori, F., Fife, A. A., Frindt, R. F. and Gygax, S., 'Construction and properties of weak-link detectors using superconducting layer structures', *Appl. Phys. Lett.*, **18**, pp. 233–5, 15th March 1971.
12. Kanter, H. and Vernon, F. L., Jr., 'Response of superconducting point contacts to high frequency radiation', *Phys. Lett. A* (*Netherlands*), **35**, pp. 349–50, 28th June 1971.
13. Blaney, T. G., 'Effect of bias voltage on the frequency response of point contact Josephson radiation detectors', *Phys. Lett. A* (*Netherlands*), **37**, pp. 19–20, 25th October 1971.
14. Richards, P. L. and Sterling, S. A., 'Regenerative Josephson effect detector for far infrared radiation', *Appl. Phys. Lett.*, **14**, pp. 394–6, 15th June 1969.
15. Grimes, C. C., Richards, P. L. and Shapiro, S., 'Josephson effect far infrared detector', *J. Appl. Phys.*, **39**, pp. 3905–12, July 1968.
16. Blaney, T. G. and Bradley, C. C., 'The Josephson junction as a frequency analyser and mixer of submillimetre radiation sources', *J. Phys. D.*, **5**, pp. 180–4, January 1972.
17. McDonald, D. G., Risley, A. S., Cupp, J. D., Evenson, K. M. and Ashley, J. R., 'Four hundredth order harmonic mixing of microwave and infrared laser radiation using a Josephson junction and a maser', To be published.
18. McDonald, D. G., Evenson, K. M., Wells, J. S, and Cupp, J. D., 'High-frequency limit of the Josephson effect', *J. Appl. Phys.*, **42**, pp. 179–81, January 1971.
19. Baker, J. G., 'Harmonic generators and semiconductor detectors', Chap. 5 of 'Spectroscopic Techniques for Far Infrared, Submillimetre and Millimetre Waves', ed. Martin, D. H. (North-Holland Publishing Co., Amsterdam, 1967).
20. Page, C. H., 'Harmonic generation with ideal rectifiers', *Proc. I.R.E.*, **46**, pp. 1738–40, October 1958.
21. McDonald, D. G., Risley, A. S., Cupp, J. D. and Evenson, K. M., 'Harmonic mixing of microwave and far-infrared laser radiation using a Josephson junction', *Appl. Phys. Lett.*, **18**, pp. 162–4, 15th February 1971.
22. Blaney, T. G., Bradley, C. C., Edwards, G. J. and Knight, D. J. E., 'Phase locking klystrons to far infrared lasers via harmonic mixing in silicon, metal–oxide–metal and Josephson point contacts', *Phys. Lett. A* (*Netherlands*), **36**, pp. 285–6, 13th September 1971.
23. Clark, T. D., 'Generation and detection experiments using point contact junction arrays', *Physica* (*Netherlands*), **55**, pp. 432–8, 1971. (Proceedings of the International Conference on the Science of Superconductivity, Stanford, U.S.A., 26th–29th August 1969.)
24. Chiao, R. Y., 'Response of superconducting weak links to photons', *Phys. Lett. A* (*Netherlands*), **33**, pp. 177–8, 19th October 1970.
25. Blaney, T. G., Knight, D. J. E. and Bradley, C. C. To be published.

Manuscript first received by the Institution on 13th May 1971 and in final form on 14th April 1972. (Paper No. 1456/CC134.)

U.D.C. 557.510.6:621.317.335.3

Design Considerations in the Measurement of Electron Temperature in the Ionosphere

A. F. TYLER*

SUMMARY

Measurements of electron temperature in the ionosphere using rocket and satellite-borne probes have been made for some years by the Department of Electron Physics and Space Research of Birmingham University, using the experimental technique described.
The apparatus, in its latest form, has been developed to provide a more compact and reliable system by exploiting the advantages of linear integrated circuits over the discrete component circuitry used previously. In considering the performance of the experiment, particular attention has been paid to the stability problems associated with the closed-loop system employed.

* *Department of Space Research, University of Birmingham, Birmingham B15 2TT.*

1. Introduction

The technique used in the University of Birmingham electron temperature experiment is an extension of Langmuir probe principles, whereby the exponential current-voltage characteristic of the plasma is investigated by the comparison of differential currents to two identical probes. The technique was first described by Wilson and Garside in 1968.[1] (A complementary technique, using an r.f. probe to measure electron densities, has also been developed in the Department.[2])

The present electronic system, in comparison with earlier experiments, offers higher sensitivity, enabling temperature measurements to be made with greater accuracy, and in conditions of lower electron density. In addition, by periodic transposition of probe connexions, inequalities in contact potential caused by work function differences of probe surfaces may be taken into account.

This experiment has been successfully flown on *Petrel* and *Skylark* rockets, and was flown, in a modified form, on the *Ariel IV* satellite launched in late 1971.

2. Theory

The electron current to a probe immersed in a plasma and maintained at plasma potential is given by

$$I_0 = \tfrac{1}{4} A n e \bar{v}$$

where A is the area of the probe, n is the electron density, $\bar{v}$ is the electron mean velocity, and e is the electron charge.

If the probe potential is made slightly negative with respect to the plasma potential, only electrons with sufficient energy to overcome the retarding potential can reach the electrode. The current is then given by

$$I = I_0 \exp\left(\frac{eV}{kT}\right) \qquad \ldots . (1)$$

where V is the probe potential with respect to plasma potential, k is Boltzmann's constant, and T is the electron temperature. At potentials more positive than plasma potential the current-voltage characteristic is no longer exponential, but is determined by the geometry of the probe. At potentials below plasma potential, all electrons are retarded. Thus, if a ramp voltage is applied to the probe, such that its potential is swept from a few volts below to a few volts above plasma potential, it will exhibit, in the retarding region just negative of plasma potential, an exponential current-voltage characteristic whose form gives a measure of electron temperature.

If two identical probes are now considered at different potentials V_1 and V_2 in the retarding region, it follows from equation (1) that

$$\left(\frac{dI_1}{dI_2}\right)_{dV} = \exp\left[\frac{e(V_1 - V_2)}{kT}\right]$$

Thus the ratio of differential currents to the probes is dependent on electron temperature and the voltage between the probes. If this ratio can be maintained constant, say equal to 2, then the electron temperature

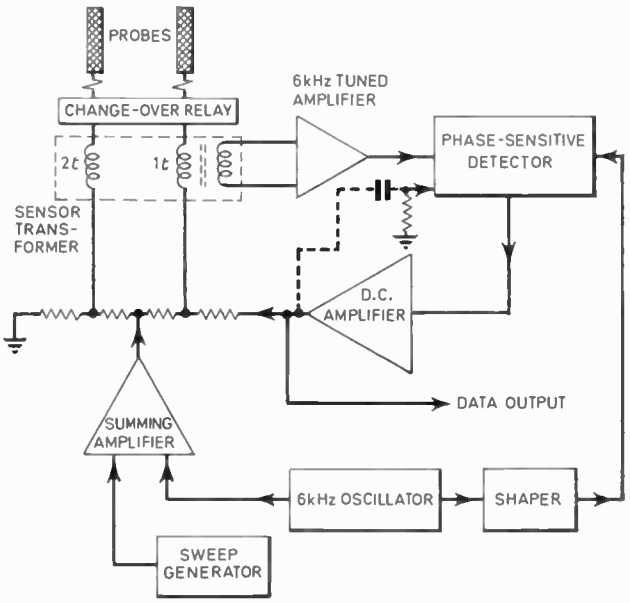

Fig. 1. System block diagram.

may be determined if the voltage difference, $(V_1 - V_2)$, is known,

$$\text{i.e. } \ln\left(\frac{dI_1}{dI_2}\right)_{dV} = \frac{e(V_1 - V_2)}{kT} = \ln 2$$

$$T = \frac{e(V_1 - V_2)}{k \ln 2}$$

$$= 1{\cdot}67 \times 10^4 \, \Delta V \text{ kelvins}$$

where $V_1 - V_2 = \Delta V$ in volts.

3. Experimental Technique

The requirement is for a system in which the ratio of the differential currents to the probes is monitored, and the voltage, ΔV, between the probes adjusted until the desired ratio of two is achieved; then from the measurement of ΔV the electron temperature can be determined. This requirement can be fulfilled by a servo system which controls the voltage between the probes by reference to the ratio of the differential currents. The block diagram of the system is shown in Fig. 1.

Both probe voltages are swept through the electron retarding region by the output from a sawtooth sweep generator. To this sweep is added a 6 kHz dV signal and the differential currents so produced are monitored by a transformer having windings in the probe leads with turns ratio 2 : 1. These transformer windings are arranged such that their fluxes are in opposition, so that when the ratio of the differential currents is 2 : 1 there is no signal induced in the third (sensing) winding which feeds a 6 kHz tuned amplifier. However, if the ratio of the differential currents is not 2 : 1, the resultant signal is amplified and phase-sensed. The output from the phase-sensitive detector (p.s.d.), after amplification, controls the voltage ΔV between the probes, such that the differential currents are changed until the desired ratio of 2 : 1 is achieved. The 6 kHz tuned amplifier also incorporates automatic gain control, since high gain is necessary in the interests of system accuracy, and yet it must be able to cope with the large unbalance signals which are present during the accelerating region of the sweep.

The highest electron temperature likely to be measured is about 3500 K, corresponding to a value for the voltage ΔV of 200 mV, and this is an unsuitable level for most telemetry systems. This voltage is therefore produced at higher level by the potentiometer chain driven by the d.c. amplifier, whose output is telemetered. Thus the maximum temperature anticipated can be made to correspond to a data output of several volts, which may be telemetered with sufficient accuracy.

If the d.c. amplifier output (and hence ΔV) is arranged to be a maximum for no signal input to the 6 kHz amplifier temperature data can easily be recognized as a minimum in the output voltage as the probes are swept through the retarding region. During the accelerating region of the sweep, the current to the probes being more nearly equal, the data output is driven up into saturation in attempting to maintain the desired current ratio.

The technique can be tested in a laboratory simulation of the plasma or, more simply, by connecting semiconductor diodes between the probes and ground, thus using their exponential current-voltage characteristic at the turn-on point to represent the plasma characteristic.

4. Circuit Details

Undoubtedly the sensor transformer is the most critical single component in the successful operation of the system. The turns ratio of the probe windings must be exactly 2 : 1 and this ratio is cross-checked by measurement of winding inductances. This measurement gives ratios of 4 : 1 typically within 0·25%. It is also desirable that leakage inductances should be kept as low as possible, therefore inductance measurements are made on each probe winding with the other short-circuited. Inductances typically less than 1/1000 of those measured on open circuit are obtained. In order to reduce capacitive coupling between the probe windings and the sensing

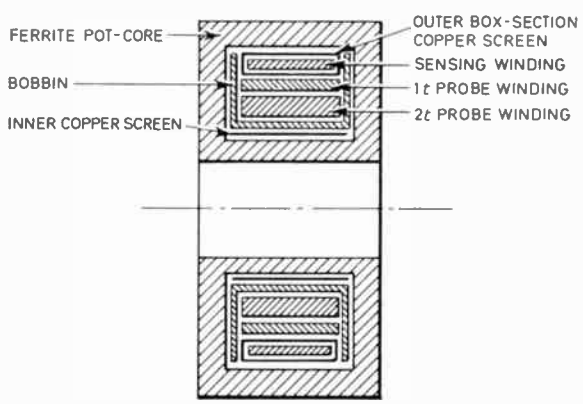

Fig. 2. Section through sensor transformer.

winding an efficient screening system is essential. It is imperative that such coupling be reduced virtually to zero, since the probe windings carry the 6 kHz dV signal. The construction of the transformer is illustrated in Fig. 2.

In earlier experiments, the transformer was mounted in close proximity to the probe. However, since it was found desirable in the interests of accuracy periodically to transpose the sensor connexions, the transformer, together with the relay which performs the switching, has been relocated within the electronics module. Thus the coaxial cables connecting the transformer windings to the probe, which is necessarily deployed at relatively large distance from the vehicle during flight, present considerable capacitance, resulting in 6 kHz current flow. It is necessary to maintain a null in such capacitive currents to avoid saturation of the 6 kHz amplifier, and for this purpose two trimmers are provided in order that a null may be achieved in both relay states. Any residual capacitive currents may be distinguished from electron current by their phase relationship to the phase sensitive detector reference input, and will therefore be rejected. The transformer, relay and probe arrangement is shown in Fig. 3.

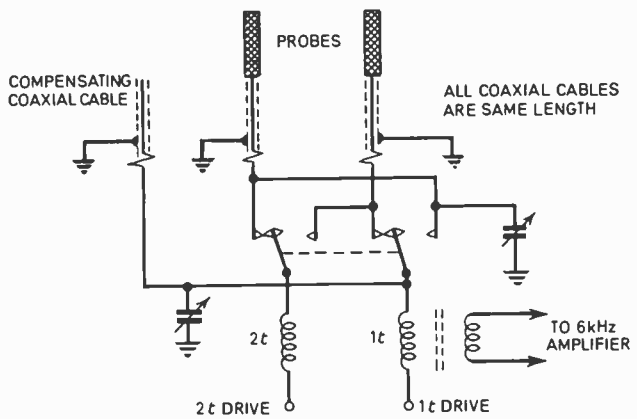

Fig. 3. Transformer, relay and probe arrangement.

The sensing winding of the transformer feeds the 6 kHz tuned amplifier, which has a first stage using discrete components. The noise figure obtained could not be matched by integrated circuits available at the time when the system was developed. The second stage uses an operational amplifier, and is tuned by means of a twin-T network providing frequency-dependent negative feedback. The last stage also utilizes an operational amplifier, and incorporates automatic gain control in the form of transistors which provide increased negative feedback once a pre-set output amplitude is exceeded. The complete amplifier has a centre-frequency gain of 95 dB, and 3 dB bandwidth of 1 kHz. The tuning was intentionally kept flat, so that phase change was not too rapid around the centre frequency, thus allowing for a small amount of drift in amplifier tuning and/or oscillator frequency. The twin-T type of tuning was employed to eliminate inductors and, by the use of metal oxide resistors and silver mica capacitors for the network, good stability has been achieved, phase-shift remaining typically within 10° of its value at ambient temperature over the range −20 to +70°C.

The p.s.d. uses a junction field effect transistor as a shunt chopper, its gate being driven by the reference signal from the 6 kHz oscillator. The f.e.t. was chosen since it gave better isolation between reference and signal inputs than a bipolar transistor and a junction device offered lower 'on' resistance than m.o.s. types. The chopper is followed by an operational amplifier having some a.c. feedback, thus providing a degree of smoothing. The reference input used is a narrow (20 μs) gating pulse rather than a symmetrical square-wave. This was found to result in better rejection of quadrature signals appearing at the p.s.d. input.

An operational amplifier is used for the d.c. amplifier, which provides further smoothing by means of additional a.c. feedback. This stage also incorporates a complementary emitter follower within the feedback loop in order to provide very low output impedance. This is necessary since the potentiometer chain providing the voltage ΔV is required to supply probe current while maintaining a substantially constant voltage ratio.

The 6 kHz oscillator providing the dV signal uses an operational amplifier in a Wien bridge configuration, with variable feedback controlled by an f.e.t. to give amplitude stability. As with the tuned amplifier, the desire to eliminate inductors led to the selection of this type of circuit. Oscillator frequency remains typically within 20 Hz of 6 kHz over the temperature range −20 to +70°C without any special precautions being taken. The oscillator output is attenuated, since the dV signal applied to the probes is required to be 30 mV peak-to-peak and a simple discrete component phase-shifter is used in order that the correct phase-relationship between signal and reference inputs to the p.s.d. may be established. The reference signal is provided by an operational amplifier in open-loop, driven by the 6 kHz oscillator, and with an offset voltage applied to one input to enable the output mark/space ratio to be adjusted for the desired 20 μs gating pulse width. Stability of reference pulse width is desirable if the system sensitivity is to remain constant, and this is ensured by the use of f.e.t.-controlled feedback, giving oscillator amplitude stability.

The saw-tooth sweep waveform, normally of 250 ms period, is produced by a constant-current source charging a capacitor. An operational amplifier in a bootstrap configuration is used to provide the charging current. A second operational amplifier, in open-loop, operates as a comparator and discharges the capacitor when the sweep voltage reaches the desired maximum level. The output of the second operational amplifier provides a pulse suitable for the synchronization of other experiments, and, after frequency division, for operation of the probe switching relay typically every twenty sweeps. The sweep output is connected to that part of the sensor assembly supporting the probes, thus providing a guard-ring system between the probes and the parts of the sensor assembly at earth potential.

The saw-tooth sweep waveform, with superimposed 6 kHz dV signal, which is applied to the probes is provided by a summing amplifier, incorporating a complementary emitter follower within the feedback loop.

Stabilized power supplies are provided by integrated circuit voltage regulators. Two systems are used, one to provide power for the 6 kHz amplifier, the other powering the remainder of the circuitry. The total current consumption of the system is approximately 25 mA per (10 volt) line.

5. Constructional Details

Printed-circuit board construction is used, the boards being housed in a package measuring about 10 cm × 7 cm × 6 cm and weighing approximately 350 g. All connexions between the package and the launch vehicle are filtered to avoid telemetry interference. A small amount of silicone rubber conformal potting is used around the transformer connexions and vibration trials and flight have proved that no further encapsulation is necessary.

6. System Performance

As is necessary in any closed-loop system, the gain was made as high as possible, consistent with noise and drift considerations so that accuracy should be high. Inevitably, this resulted initially in an unstable closed-loop system. An open-loop Nyquist plot verified the instability, the transient response test being carried out as follows:

The loop was broken at the point where the d.c. amplifier drives the potential divider providing the voltage ΔV between the probes. A d.c. voltage was then applied to the divider and adjusted for a suitable value of ΔV. The sweep generator output was disconnected from the summing amplifier input and replaced by a d.c. voltage adjusted so that the diodes simulating the plasma during the test were biased to the exponential part of their characteristic. A third input was then applied to the summing amplifier in the form of a sinusoidal test signal, the amplitude and phase of the modulation appearing at the d.c. amplifier output being compared with this test signal to provide the information for the Nyquist plot. A suitable stabilizing network indicated by the modification of the Nyquist plot was found to be a simple CR-network connected between the d.c. amplifier output and the input to the operational amplifier associated with the p.s.d., as indicated in Fig. 1. The resistor in the network is in fact provided by the input bias resistor for the operational amplifier. The value of capacitor chosen was a compromise between adequate stability margin and transient response. The stability predicted by the Nyquist plot was then verified by closed-loop operation of the system. The optimum value of the compensating capacitor arrived at for the prototype system has been found to be applicable to all subsequent systems.

It must be remembered that the test described above assumes the diode characteristic to be a reasonable approximation to that of the plasma. This has been shown to be the case by tests in a laboratory simulation of the plasma, and by results obtained during flight.

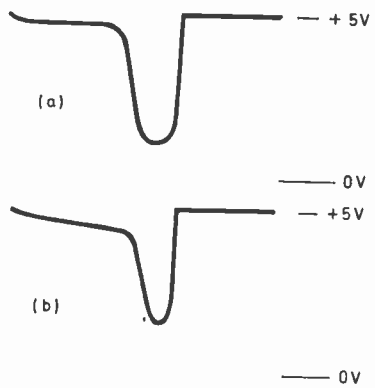

Fig. 4. Typical data outputs.

(a) Using diodes; (b) From flight measurements.

Typical data outputs, obtained using diodes and from flight measurements, are shown in Fig. 4.

The electron temperature range of the system is normally 0–3500 K, but this is easily changed by selecting a different ratio for the potential divider providing the voltage ΔV, no other modifications being necessary.

The overall accuracy of the system is not easily determined, the sensitivity being dependent upon such factors as electron temperature and density, and probe configuration. At high electron densities ($> 10^3$ cm^{-3}) a reasonable estimate of accuracy would be within 5% over the full temperature range. It is in conditions of low electron density and low electron temperature that system accuracy suffers, due to the finite error signal necessary to maintain the loop closed. A very approximate estimate of the limiting conditions may be obtained by feeding the probe windings from an external oscillator arranged to provide known differential current. The external oscillator beats with the 6 kHz dV oscillator to produce modulation of the data output at the beat frequency. The amplitude of modulation on the data output then gives the maximum possible data change corresponding to the particular electron density represented by the differential current provided. By this means it is found that with a minimum electron temperature, say 200 K, the accuracy of the system is maintained within 10% down to an electron density of about 10^2 cm^{-3}. However, this technique gives the maximum sensitivity, since the oscillator frequency is adjusted for the lowest beat frequency possible (< 1 Hz).

In practice the transient response of the system imposes a limitation such that the 5% accuracy is no longer maintained in densities of less than 10^3 cm^{-3}. Although by no means ideal, this accuracy is sufficient for many applications.

7. Conclusions

The system described provides an accurate and reliable method for determining electron temperatures from a single measurement, accepting the limitations already mentioned. Hence future development will be towards greater accuracy at low electron densities and tempera-

tures. In its present form, however, the system fully justifies the use of linear integrated circuits in terms of reliability, small size and simplicity of assembly and setting-up.

8. Acknowledgments

The author wishes to thank Professor J. Sayers and Mr. J. H. Wager for the interest taken in the development of the system. He is especially grateful for the helpful advice given throughout by Dr. J. W. G. Wilson. The research here described forms part of the space research programme supported by the Science Research Council.

9. References

1. Wilson, J. W. G. and Garside, G., 'A new technique for measuring electron temperatures in the ionosphere', *Planetary and Space Science*, **16**, pp. 257–72, 1968.
2. Bryan, H. W., Wall, J. and Wager, J. H., 'An improved radio-frequency probe for the measurement of electron densities in the ionosphere', *The Radio and Electronic Engineer*, **42**, pp. 217–24, May 1972.
3. 'The Application of Linear Microcircuits', Vol. 1, SGS (U.K.) Ltd., 1969.

Manuscript first received by the Institution on 3rd March 1972 and in final form on 10th May 1972. (Paper No. 1457/IC 65.)

Displays and Instrumentation for Short-field Aircraft*

Flight-deck displays and instrumentation for future civil short-field aircraft were discussed at a joint meeting of the Institution's Aerospace, Maritime and Military Systems Group and the Royal Institute of Navigation held in London on 5th April last.

L. W. Dowdall and M. Fay (Hawker Siddeley Aviation, Hatfield) summarized the market pressures that point towards the early adoption of civil QStol transports. Mr. Dowdall reviewed the growth in airfield congestion, runway length and community noise exposure. Runways, he noted, had increased from 1500 ft in the 1920s to 12 000 ft by the early 1960s. Coupled with this massive appetite for real estate, present aircraft operations expose more and more of the public to noise, with the area of the 90PNdB footprint soaring from about 1 square mile to something over 35 square miles in the same 40-year period. By way of balance, the projected new generation of airliners promises a reduction in both field length and noise, down to and beyond the 1920s values.

Mr Fay continued by outlining some of the airframe, engine and flight-control solutions envisaged, ranging from the minimum-technology-risk Rtol (reduced take-off and landing) aircraft to full V/Stol, capable of vertical or near-vertical ascent and descent.

Mr Fay then spoke about some of the problems associated with the guidance and control of Civil Stol transports. Clearly, first- and possibly second-generation Stol aircraft are going to be operated from the more developed airfields, and will probably have to rely on present-day approach aids. But, despite the airline pilots' reluctance, Mr Fay saw the acceptance of the two-segment approach, with its 6° outer and 3° final glide slopes, as being inevitable. Looking further ahead, the adoption of steeper approach and climb-out gradients would require the use of vectored thrust or lift fans, direct-lift control, or any combination of these. More on-board electronics would be necessary to control these devices, and the speaker not only envisaged the pilot staying firmly within the control loop of the aircraft, but further foresaw responsibility being restored to the cockpit and away from ground control, through the introduction of electronic cockpit displays. Mr Fay referred to a set of alternative studies for short take-off and landing aircraft designs with significantly lighter wing loadings than those at present employed. As a result of the inherently greater gust response, however, extensive on-board electronics would still be needed.

The next speaker, Group Captain H. A. Merriman (Officer Commanding RAF Wittering), discussed flight-instrument requirements for semi-jetborne flight.

In this mode of flight, the normal relationships between aircraft weight, indicated airspeed and angle of incidence no longer hold true, and the flight path can no longer be controlled by varying engine thrust alone. Many variables, such as indicated air-speed, percentage total thrust employed and vectored-thrust nozzle angle, can all be correlated to show the great range of equilibrium conditions possible. The semi-jetborne pilot's task is further complicated by the tendency of the aircraft to lose stability, in both static and dynamic senses and around all axes, as air-speed decreases.

Climb-out from a short ground roll and accelerating transition to wing-borne flight is comparatively easy.

*Reprinted, by permission of the Editor, from *Flight International* 11th May 1972.

Instrument approaches, obviously necessary in year-round schedule civil services, present a greater problem.

Several approach procedure options exist and these were listed as follows:

(a) Deceleration to landing conditions in level flight, before reaching the glidepath. In this case, the transition is easy to achieve, but time spent on the glideslope with high power settings and low stability is lengthy. Such a procedure is clearly unattractive to commercial operators.

(b) Deceleration to landing conditions steadily throughout the glidepath phase. This is more economic in terms of time and fuel expended, but it exposes the pilot to a continuously changing set of variables, making accurate glidepath holding difficult.

(c) Flying down the glidepath virtually fully wing-borne and making the transition either when in visual contact with the ground or at some late, predetermined point on the glidepath. The former is easy to fly with Harrier-type aircraft that have high negative specific excess power characteristics, with transitions being made from quite low altitudes and within very short distances. The full instrument transition of the latter method, however, is probably the most difficult case for the pilot to fly, stemming from the high rate of change in the variables involved. On the other hand, this is the case that comes closest to Cat 3 conditions and could be developed from the fully automatic landing systems already in use.

Gp. Capt. Merriman then turned to the question of pilot information, emphasizing the differences between conventional and semi-jetborne requirements. While indicated airspeed becomes virtually meaningless, angle-of-attack data assume prime importance. An accurate indication of ground speed may well be essential, particularly if such information is also shown in a time-to-go form. Crosswinds assume far greater importance during transition, and some indication of the velocity vectors in both pitching and directional planes would be very valuable.

How is this information to be displayed? Clearly, head-up displays are useful in conditions of fleeting visual contact with the ground, though many pilots are critical of a number of aspects of this type of presentation. Despite collimation of the display (the symbols are, effectively, an infinite distance away), some pilots insist that a change of eye focus is still necessary between symbology and the real-world background, and more are unhappy with the mix of raw digital data and the more readily assimilated analogue presentation.

Analogue information, for example velocity vectors, must also be presented in such a form as to prevent the display disappearing off the edge of the reflector glass, or being seen to wander erratically in turbulence. A presentation of the desired glideslope and runway centreline, overlapped with velocity vectors, would probably be the easiest to follow.

The speaker felt that artificial stability on all axes will be shown to be essential, and that control of aircraft incidence could well prove the most important single aspect of such an automatic flight-control system.

Mr D. C. Price (Elliott Flight Automation) took trends in avionics, as applied to civil V/Stol aircraft, as his topic. Mr Price foresaw, within the period leading up to the introduction of civil Stol service, the widespread displacement of conventional aircraft instruments by integrated electronic navigation flight-control and display systems. This, in turn, should enable the equipment manufacturers to offer improvements in performance and costs.

Stol aircraft will pose stringent problems in guidance accuracy and crew work-load, and close attention will have to be given to the man-machine relationship. Mr Price favoured head-down multi-mode displays, feeding the crew with data so edited as to contain only information relevant to a given situation. He described a hypothetical flight-deck panel with six head-down displays and some eight standby instruments. The pilot and co-pilot could each view two of the displays (one acting simply as back-up), while the two centrally mounted displays could be used for monitoring engine and other essential services. The primary crew displays would be used in the electronic attitude-director or horizontal-situation aspects, depending on flight mode. The speaker demonstrated the way in which mode selection could be varied to correspond with changing flight conditions, ranging from a Mona-style navigational display to a zero-visibility roll-out using electronically sensed runway and taxiway markers.

Mr Price felt that such systems for Stol aircraft must be designed for compatibility with busy, well instrumented airports and more remote, less lavishly equipped airfields. A close watch will have to be kept on any change in air traffic control strategy, and there is a real need for continuing discussion between all interested parties.

The final paper was by Dr. G. H. Hunt and Mr. J. N. Barrett (Ministry of Defence) and discussed MoD assessment of an instrument flight display for V/Stol transports. While these trials had been confined to a ground simulator, the Royal Aircraft Establishment team had broken new ground in the type of display employed. The RAE equipment gives a permanent horizontal-situation-type presentation, with altitude, vertical speed command, slideslip and range-to-go data all presented on the periphery of the portrait-format 5 in × 4 in head-down cathode-ray tube.

Much use is made of cleverly devised and readily assimilated cues, such as a scaled aiming mark termination to the main vector, providing a warning of a potential under- or overshoot situation.

Dr. Hunt outlined the work on symbology and illustrated some of the modifications which have been found necessary. He said that this type of display had not only proved practicable but had also produced the course of simulation exercises carried out by 27 pilots.

Other points of interest contained in Dr. Hunt's remarks included the assumption that the parent aircraft would employ full four-axis autostabilization.

HUGH COWIN

U.D.C. 621.373.54

A New Monostable Circuit with Zero Stand-by Power

R. W. J. BARKER, M.Sc., C.Eng., M.I.E.E.*
and
B. L. HART, B.Sc., C.Eng., M.I.E.R.E.†

SUMMARY

The novel interconnexion of a bridge timing circuit, a switched comparator, and a complementary transistor latching scheme, permits the design of a monostable circuit which consumes 'zero' standby power and has a pulse width $T = CR \pm 3\%$ (C and R being externally connected timing components) for a rail voltage in the range 3V to 30V.

*Department of Electrical and Electronic Engineering, Portsmouth Polytechnic, Anglesea Road, Portsmouth PO1 3DJ.

†Department of Electrical Engineering, North East London Polytechnic, Dagenham, Essex RM8 2AS.

1. Introduction

Zero standby power is an obvious advantage for a monostable circuit, especially when it may be triggered at long and infrequent intervals. One of the problems in the design of such circuits, namely the accurate definition of pulse duration when saturated transistor switches are used, has recently been discussed[1] and it was shown that a modified complementary circuit could give a time duration accurate to within $\pm 12\%$. However, one of the shortcomings of the circuit described was the need for inordinately large timing capacitors for delays in the millisecond, second and minute ranges. This paper considers a circuit which gives a pulse width predictable in duration to $\pm 3\%$, even for long delays, for a decade change in power supply voltage, when an input trigger pulse is applied or a push-button operated.

2. Circuit Description

One practical realization of the circuit technique‡ is shown in Fig. 1. R, C, R1, R2 constitute the bridge circuit; a high gain d.c. coupled differential amplifier, A, is the comparator; TR1 and TR2 are arranged to function as a complementary latch. TR3 with its associated components illustrates one of several possible pulse triggering schemes; the push-button, PBS, shown dotted, is a manual triggering facility. TR4, which is an optional feature, conducts only at the termination of the delay period, speeding up the discharge of timing capacitor, C. An output pulse can be taken from a number of points in the circuit, e.g. the collector of TR1 or TR2. In the stable state, the biasing arrangements ensure that all transistors are 'off' and thus A has no power supply from which to draw current; hence the standby power dissipation is zero. A trigger pulse causes TR1 to switch on and saturate. This establishes a supply rail ($\sim E$) for A. Since the p.d. across C cannot change instantaneously, the output of A goes positive, TR2 is switched into saturation and keeps TR1 saturated when the trigger is removed. The quasi-stable regime is thus initiated and the circuit remains in this state until the charging of C through R causes the potential of the inverting terminal of A to just exceed that of the non-inverting terminal. When this occurs, the output of A drops in potential and TR2 turns off, causing the circuit to revert to the stable state. As the collector of TR1 falls in potential, TR4 is driven into conduction causing C to discharge. The current pulse at the collector of TR4 can be conducted to earth, as shown, or applied to the base of a transistor which fulfills the function of TR3 in another, similar, circuit. Assuming an infinite gain for A, the pulse width (or time delay), t_d, produced by the circuit is given by,

$$t_d = CR \log_e \left[\frac{R_1+R_2}{R_1}\right]. \qquad \text{.....(1)}$$

t_d is therefore sensibly independent of E (and temperature, T); this is a direct result of the bridge scheme.

The choice,

$$\left[\frac{R_1+R_2}{R_1}\right] = \mathrm{e} = 2{\cdot}718, \qquad \text{.....(2)}$$

‡ Patent applied for.

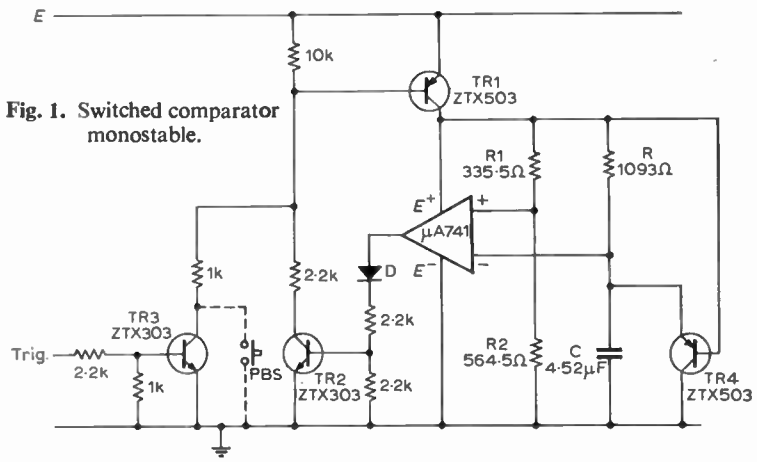

Fig. 1. Switched comparator monostable.

give the equipment designer a simple relationship for t_d, i.e.

$$t_d = CR. \qquad \text{.....(3)}$$

3. Results

Figure 1 indicates the nominal values of the passive components used; except for R_1 R_2, R, C, which were measured. R_1 and R_2 were, in fact, selected to satisfy (3) as closely as possible with the components available.

t_d was measured at the lower and upper supply rail limits for satisfactory operation of the circuit with the particular sample of μA741 used. Table 1 summarizes the results.

Table 1

E	t_d (measured)	t_d (calculated using eqn (1)
3V	4·95 ms	4·87 ms
30V	4·99 ms	4·87 ms

For these tests, TR4 was removed as reverse breakdown in its emitter-base junction occurs when $E > 5$V—this can be circumvented by putting a diode in the emitter lead of TR4.

Figure 2 shows the superimposed traces of the waveforms at the input terminals of A, and illustrates the exponential charging of C, followed by the termination of the quasi-stable state when both input terminals are at approximately the same potential. In this case, $E = 5$V and TR4 was in circuit.

4. Discussion and Conclusions

The discrepancy between predicted and measured values of t_d is due largely to the approximations inherent in (1) and the time delay that occurred in A as a result of switch-off transients. Let us consider each briefly.

The end of the quasi-stable regime commences when the potential between the terminals of A is ε, where ε is given by,

$$\varepsilon = v_{os} + \left(\frac{E}{A_d}\right) \qquad \text{.....(4)}$$

where v_{os} is the input offset voltage of A and A_d is the differential voltage gain of A.

There is therefore a time error Δt_d where,

$$\frac{\Delta t_d}{t_d} = \frac{\varepsilon}{0{\cdot}37E}. \qquad \text{.....(5)}$$

Substitution of typical data gives an error of approximately 0·3% due to these factors. An offset nulling facility would reduce this error by a large proportion.

The switch-off delay in the particular sample of μA741 used was 30 μs. For other units tested, the delay was as low as 18 μs. Clearly, the longer t_d, the smaller the error due to this factor. The situation can be improved by an alternative choice of device type for A, but it is probable that a greatly reduced supply voltage range will be inevitable with some of the purpose-built comparator types.

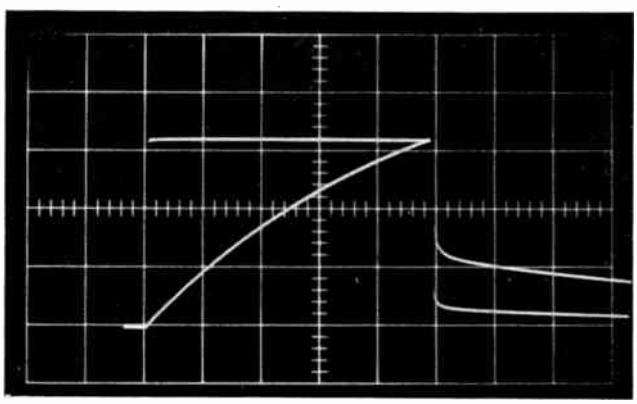

Fig. 2. Superimposed waveforms of the input terminals of A in Fig. 1 during the quasi-stable state.

$E = 5$V, vertical sensitivity 1V/div—both channels, horizontal timebase speed 1 ms/div.

A time delay of seconds or minutes without an inordinately large value of C (with its associated leakage) is possible by increasing R to lie in the megohm range and using an alternative amplifier type for A, e.g. μA740, which has an f.e.t. input stage. For very long delays the accuracy is largely determined by the quality of the capacitor as well as the tolerance of the timing components.

A simple circuit variation, which works satisfactorily, results from interchanging C and R in the bridge network and at the same time interchanging the connexions to the inputs of A—this gives the 'differentiation' timing method as opposed to the 'integration' mode discussed above.

5. Reference

7. Hart, B. L. and Baker, R. W. J., 'A pulse-duration-stabilised complementary monostable', *Int. J. Electronics*, to be published.

Manuscript received by the Institution on 2nd June 1972. (Short Contribution No. 156/CC135.

U.D.C. 621.383.41:535.61-1

Lead–Tin Telluride Photodiode Arrays for Detection in the 8–14 μm Band

W. H. ROLLS, B.Sc.,*
T. J. WATERFIELD, M.Sc.,*
R. S. SIMKINS,*
C. W. SHERRING, Ph.D.*
and
C. J. ROGERS, M.Sc.*

Based on a paper presented at the Conference on Infra-red Techniques held in Reading from 21st to 23rd September 1971.

SUMMARY

This paper describes the lead–tin telluride system and its application to the fabrication of fast sensitive infra-red detectors both as single elements and arrays. The electrical and optical properties are discussed with emphasis on the sensitivity of the single elements, and the uniformity in both spectral response and sensitivity for the arrays. $D^*_{\lambda p}$ (12·1 μm, 800, 1) values up to $2{\cdot}9 \times 10^{10}$ cm Hz$^{\frac{1}{2}}$ watt^{-1} have been achieved for unbiased single detectors and 14×1 element arrays have been measured with a spread in D^*_λ values as good as 2·2 : 1.

* *Allen Clark Research Centre, The Plessey Company Limited, Caswell, Towcester, Northants.*

1. Introduction

Two systems of ternary alloys have been used to exploit the 8–14 μm band. These are $Cd_yHg_{1-y}Te$ and $Pb_xSn_{1-x}Te$. Both systems yield ingots with variable composition if grown from the melt, but the $Pb_xSn_{1-x}Te$ alloys can be readily transported in a vapour phase epitaxy system with little or no change in composition. This method is used to produce single crystal layers of the alloy, for $0{\cdot}75 < x < 0{\cdot}88$, using lead telluride as the substrate.[1] Hydrogen is used as the carrier gas and layers between 100–200 μm thick are grown at a rate of 2–3 μm per hour. The composition of the slice is extremely uniform (better than 0·2%) as shown by x-ray diffraction and electron beam microprobe analysis and spectral response measurements. This alloy system exhibits non-stoichiometry of the crystal lattice, a metal excess being n-type and a tellurium excess p-type. By annealing the crystal slice at a selected temperature with a metal rich alloy powder of the same lead/tin ratio, the as-grown p-type slice is converted at the surface to n-type. This conversion has been demonstrated for compositions having values of $0{\cdot}73 < x < 1{\cdot}0$.[2] Typical values of junction depth are between 1 and 5 μm, depending on composition, and are obtained by annealing at 450°C for about 3 days.

The band gap variation with composition shown in Fig. 1 is approximately 0·005 eV/%. This compares favourably with $Cd_yHg_{1-y}Te$ alloys which have a variation of about 0·01 eV/%. At 77 K the band gap is zero for a value of $x = 0{\cdot}60$ and this zero value is temperature dependent.

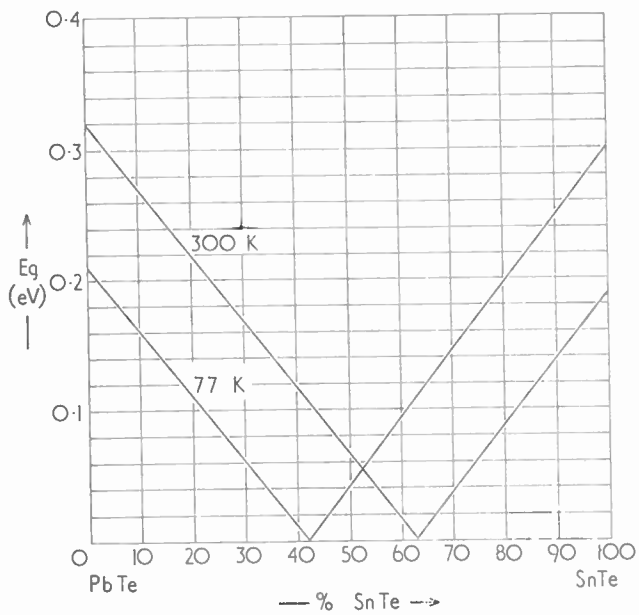

Fig. 1. Band-gap variation with composition for lead–tin telluride alloys. (After Butler *et al.*[3])

2. Single Devices

Since both surfaces of the diffused slice are n-type, one side is etched to expose the p-type material. Tin contacts are evaporated onto both the n- and p-type surfaces. Mesa diodes of 0·6–0·8 mm diameter are etched concentric with the n-type contact which is 0·2 mm

diameter. Lead–tin telluride is easily damaged either mechanically or by thermal shock. To avoid mechanical damage in the device the chip size is made larger, e.g. 1·5 mm^2, than the active mesa area. The device is mounted onto a gold-plated ceramic package and a 0·0254 mm (0·001 in) gold wire soldered to the contact. Thermal compression or ultrasonic bonding cannot be used because of induced damage.

Lead–tin telluride alloys have a high value of refractive index of about 6·0. This results in a radiation reflective loss of about 50% for one surface. A quarter-wave thickness of zinc selenide is evaporated onto the diode surface to form an anti-reflexion coating which reduces the loss to 10–20%. The responsivity of the diodes and the quantum efficiency is determined by the slope resistance, R_0, at the operating bias. Values of R_0 range from 20–300 Ω with responsivities up to 500 V W^{-1}. The quantum efficiency is defined as the ratio of the carriers collected to incident photons and values as high as 0·9 have been obtained. Under reverse bias conditions, the slope resistance is much higher than at zero bias and slope resistances up to 2·5 kΩ have been observed with reverse bias currents less than 1 mA, with corresponding responsivities up to $1{\cdot}2\times10^4$ V W^{-1} (Fig. 2).

For most applications it is more useful to use a figure of merit which contains a signal/noise ratio, in this case D^*_λ:

$$D^*_\lambda = \frac{S}{N}\frac{(B)^{\frac{1}{2}}}{W_{\text{r.m.s.}}A^{\frac{1}{2}}} = \frac{R}{N}(BA)^{\frac{1}{2}} = \frac{A^{\frac{1}{2}}}{P_n} \text{ cm Hz}^{\frac{1}{2}}\text{ W}^{-1}$$

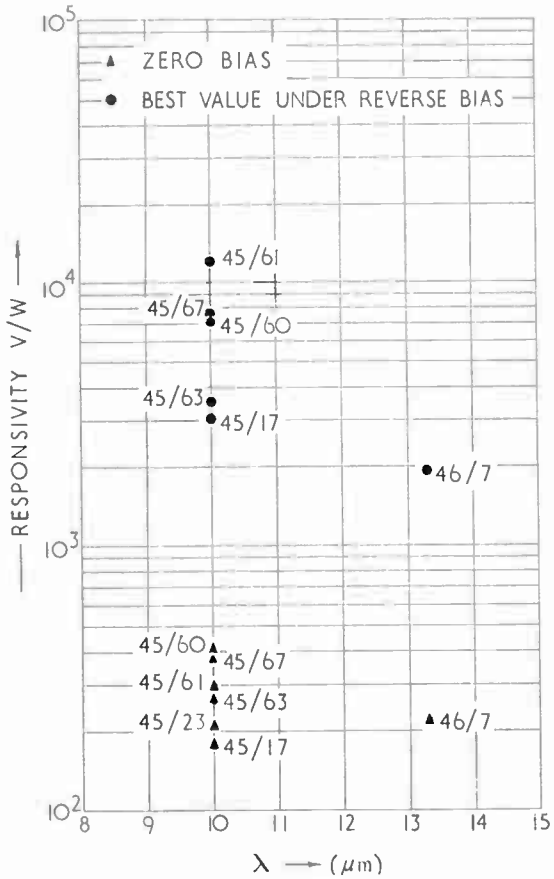

Fig. 2. Variation of responsivity with λp for lead–tin telluride detectors.

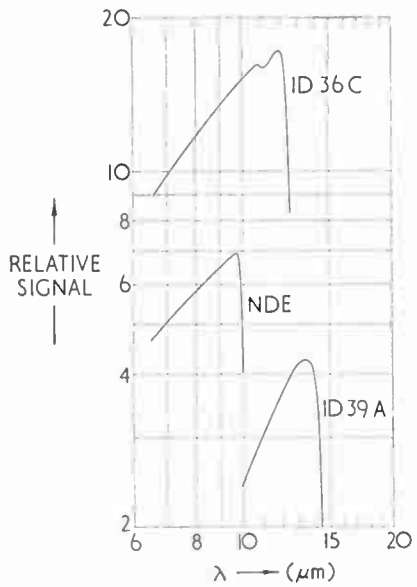

Fig. 3. Spectral response of three detectors.

where S is root mean square of the signal voltage
N is root mean square of the noise voltage
B is the electrical bandwidth
$W_{\text{r.m.s.}}$ is the radiant flux (W cm^{-2})
A is the area of the detector (cm^2)
R is the responsivity (V W^{-1})
P_n is the noise equivalent power (W Hz$^{-\frac{1}{2}}$).

For an ideal diode the only noise is the shot noise of the device. However, there is a contribution from current noise due to surface and contact effects. This occurs when the diode is operated at any point other than zero volts bias. The effect of background radiation is to forward-bias the detector and current noise is evident at frequencies above 1 kHz when a voltage (zero current bias) amplifier is used. When the device is operated close to zero volts bias by the use of a transformer coupling, current amplifier or voltage amplifier with reverse bias, current noise is eliminated at frequencies above 100 Hz. Typical shortcircuit currents vary between 50–200 μA for 2π field of view. The quantum efficiency of the device can be obtained from the short-circuit current and the background temperature. Values of $D^*_{\lambda p}(\lambda_p, 800, 1)$ up to $2{\cdot}9\times10^{10}$ cm Hz$^{\frac{1}{2}}$ W^{-1} at 12·1 μm and $2{\cdot}8\times10^{10}$ cm Hz$^{\frac{1}{2}}$ W^{-1} at 13·3 μm have been measured. Spectral response curves are shown in Fig. 3.

The response speed of the detectors has been measured at 3·0 μm using an InAs laser† and at 10·6 μm by heterodyning the outputs from two CO_2 lasers.‡ Rise-times between 20 ns and 100 ns have been observed. The detectors are RC-limited in their response due to the

†Wilson, J., Royal Radar Establishment (Private communication).
‡Woods, P., National Physical Laboratory (Private communication).

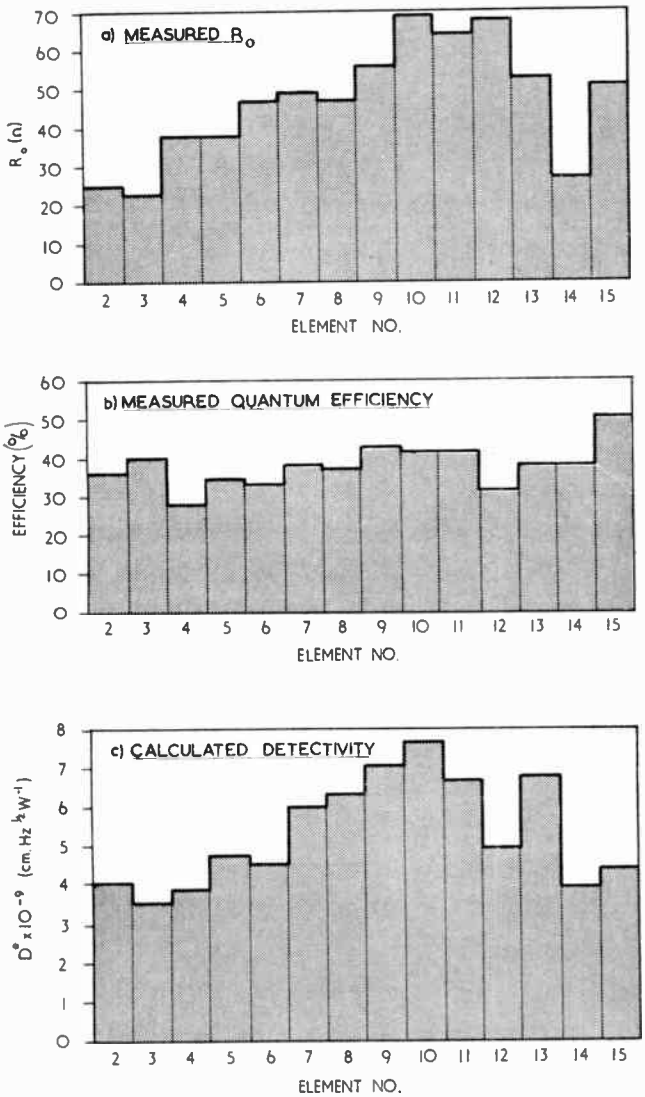

Fig. 4. Results for a 14 × 1 array with an element size of 4×10^{-4} cm².

high value of dielectric constant of about 560 which gives junction capacitance of approximately 1 μF cm^{-2}. For a typical device area of $2{\cdot}5 \times 10^{-3}$ cm² and an effective load resistance of 25 Ω from a 50 Ω device in parallel with a 50 Ω input c.r.o., the *RC* time-constant is 62·5 ns. Close correlation between the rise-times measured at 3·0 μm and 10·6 μm using the same detector also indicates a time-constant limitation, otherwise the different absorption processes at the two wavelengths would give different rise-time values.

3. Arrays

The epitaxial growth of lead–tin telluride produces material which is extremely uniform in composition and quantum efficiency. The x-ray and electron beam microprobe analysis show that the composition is uniform within ±0·5%. A comparison of the spectral responses of detectors fabricated from a single slice shows a uniformity in peak wavelength better than ±0·1 μm. However, it is the slope resistance at zero bias or under reverse bias which determines the detectivity of the device. Figure 4 shows the results from a 14 × 1 array with an element size of 4×10^{-4} cm² and a pitch of 250 μm. The D^*_λ results are calculated from the slope resistances at zero current bias and the corresponding quantum efficiencies assuming Johnson noise. This assumption has been shown to be valid for many devices at frequencies greater than 5 kHz. Early diodes were operated at zero current bias. More recent results, as indicated in Section 2, have shown that the devices are Johnson-noise-limited down to 100 Hz when operated at zero volts bias. (This array was not bloomed with zinc selenide.) More recent arrays with 20 elements, 250 μm square and a 1 : 1 mark/space ratio have shown good uniformity in quantum efficiency and spectral response. This is over a 1 cm length of material. A spread in current responsivity of less than 1·4 : 1 has been obtained with arrays 0·5 cm long, and zero bias resistance values have been frequently greater than 100 Ω.

As the element size decreases so the problem of contact resistance becomes more severe. This increases faster than the decrease in contact area would suggest. Improved contacts can be achieved by heating the device to partly alloy the contact to the top surface. Lower resistance contacts are formed when the bonding to the gold wire takes place away from the active area of the device. Figure 5 shows a layout for a 15 × 1 array. The bonding pads are much larger than the contact area and are removed from it using an underlying insulator to prevent shorting down the side of the mesa. At this time the insulator is KPL photoresist. Tests showed that a 1·5 μm thick layer could stand 200 V on an area of 5×10^{-4} cm² without breakdown. Reproducible contact resistances of about 3 Ω can be achieved by this method and temperature cycling of a lead–tin telluride slice with a photoresist layer on it showed that the insulator is stable under operating conditions. No cracking or lifting of the resist was evident after many cooling cycles.

The calculated values of R_0 for different compositions are higher than those obtained in practice. This is due mainly to surface effects. Surface states form an inversion layer on the n-type surface giving rise to surface channels. This is particularly the case for high tin content alloys where the n-type carrier concentration may be as low as 5×10^{15} cm^{-3}. The zinc selenide coating used to reduce reflexion losses also acts as a passivation layer on the device. Some variation of the characteristics occurs for the coated devices which are exposed to the atmosphere. Encapsulation of the device in an evacuated Dewar prevents this variation. In practice the saturation

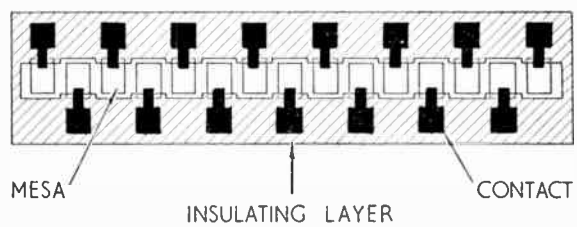

Fig. 5. Diagram showing construction of a 15-element lead–tin telluride detection array.

current shows a perimeter rather than an area dependence, hence the smaller elements have lower values of R_0 than expected on the basis of bulk conduction.

The noise of single detectors is conveniently measured using transformer coupling to the amplifier. An alternative is to use a pre-amplifier with many transistors in parallel to give a low noise equivalent resistance (n.e.r.). For a multi-element array it is impracticable to use either of these methods. Each element requires a separate output amplifier before signal processing can be carried out. Most of the single detectors have low values of n.e.r. between 10–100 Ω. It is also desirable to utilize the fast rise-time of these devices without degrading the D_λ value. The high capacitance values require the use of a low input impedance amplifier where the input resistance should be 1–2 Ω. Suitable choice of input bipolar transistor or f.e.t. combined with a feedback resistance can yield a low-noise amplifier with R_{in} about 1 Ω. The detector will now operate close to the optimum bias point of zero volts and fast response may also be achieved. Recent arrays have shown resistance values up to 300 Ω which is approaching the noise equivalent resistance of some available transistors, and soon it should be possible to build amplifiers which no longer limit the performance of the device. Ideally the amplifiers would be sited close to the array itself and operate at 77 K. This will increase the cooling requirements further and may be impractical for large arrays.

4. Conclusions

Photovoltaic detectors for use in the 8–14 μm band have been fabricated to give fast response and high sensitivity. Arrays of these devices show considerable promise for thermal imaging applications, due to their uniformity of response and the absence of $1/f$ noise down to low frequencies.

5. Acknowledgments

The authors wish to thank Mr. D. V. Eddolls for helpful discussions. This work was carried out in part under a C.V.D. contract and is published by permission of the U.K. Ministry of Defence (Navy Department) and the directors of the Plessey Company.

6. References

1. Rolls, W., Lee, R. and Eddington, R. J., 'Preparation and properties of lead–tin telluride photodiodes', *Solid State Electronics*, **13**, p. 75, 1970.
2. Butler, J. F. and Harman, T. C., 'Long-wavelength infra-red $Pb_{1-x}Sn_xTe$ diode lasers', *Appl. Phys. Letters*, **12**, p. 347, 15th May 1968.
3. Butler, J. F., Calawa, A. R. and Harman, T. C., 'Diode lasers of $Pb_{1-y}Sn_ySe$ and $Pb_{1-x}Sn_xTe$', *Appl. Phys. Letters*, **9**, p. 427, 15th December 1966.

Manuscript first received by the Institution on 10th June 1971 and in final form on 3rd May 1972. (Paper No. 1458/CC136.)

British and American Guides to SI Units

The publication which should now be in use throughout the country by scientists, technologists of every discipline, teachers and many others as a practical guide to the use of the International System of Units (SI),* has been revised by the British Standards Institution in order to bring it into line with the latest international agreements. The Publication is PD 5686: 1972 'The use of SI units'.†

The SI has been developed to a point far beyond that achieved by any alternative or previous system of units and finalized, insofar as that is possible, but a few detailed developments which have taken place in the system are reflected in the latest edition of PD 5686.

The mole (symbol mol), the unit for 'amount of substance', has been confirmed as the seventh base unit of SI. Its use will normally be confined to technical and scientific applications. The special names and symbols of the pascal (Pa) for newton per square metre and siemens (S) for reciprocal ohm (conductance) have been given full recognition within the system and it is expected that use of these names and symbols will gradually become widespread. The centimetre, not included in the earlier editions, is now listed as an acceptable sub-multiple of the metre in recognition of its widespread use.

Information is given on a Directive of the EEC issued at the end of 1971, which requires that members should change their legislation within five years so as to make the major SI units obligatory and delete reference to certain other non-SI units.

The BSI publication has its counterpart (also just into a second edition) issued by the U.S. National Bureau of Standards.‡ The contents of this are naturally similar to PD 5686 and thus include the official definitions and symbols of the SI base units: for length (metre), mass (kilogram), time (second), electrical current (ampere), thermodynamic temperature (kelvin), luminous intensity (candela), and amount of substance (mole). There are also tables of various groups of non-SI units, some (e.g., hour, litre) considered permanent auxiliaries to the SI units, others (e.g., nautical mile, bar) to be retained for a 'limited time', and still others (e.g., micron, kilogram-force) whose use is 'generally deprecated'.

Evidence of international agreement on symbols and units between the Western and Eastern Hemispheres is to be welcomed—it has not always been a strong point in the past. The two publications reveal what a cynic might regard as a much needed piece of 'horse-trading' on two comparatively small, but important, spelling differences: The U.S. 'gram' has been adopted for the SI in the place of 'gramme', and the Americans have now conformed in spelling 'metre' instead of 'meter'.

*'The use of SI units: the metric system and the Institution's Journal' *The Radio and Electronic Engineer*, **32**, pp. 61–4, July 1966.

†Obtainable from BSI Sales Branch, 101 Pentonville Road, London, N1 9ND. Price including postage 85p (plus 20p for orders under £2).

‡'The International System of Units (SI)' edited by Chester H. Page and Paul Vigoureux, National Bureau of Standards Special Publication 330, 1972 edition. Price 30 cents. U.S. Government Printing Office, Washington, D.C. 20402).

U.D.C. 621.317.361.029.66/7: 621.273.826

Absolute Measurement of Submillimetre and Far Infra-red Laser Frequencies

C. C. BRADLEY, B.Sc., Ph.D.,*

G. EDWARDS, B.A., D.Phil.†

and

D. J. E. KNIGHT, M.A., D.Phil.†

Based on a paper presented at the I.E.R.E. Conference on Infra-red Techniques held in Reading from 21st to 23rd September 1971.

SUMMARY

The frequencies of the hydrogen cyanide and water vapour laser emissions have been measured directly against a fundamental frequency standard by harmonic generation and mixing and beat frequency detection in point contact diodes. The value obtained for the HCN laser (337 μm) is 890 760·2 $\pm$ 0·2 MHz and for the H_2O laser (118 μm) 2 527 952·5 $\pm$ 1·5 MHz. In addition some preliminary measurements have been made on the 10·7 THz H_2O laser line.

* *Division of Electrical Science, National Physical Laboratory, Teddington, Middlesex.*

† *Division of Quantum Metrology, National Physical Laboratory, Teddington, Middlesex.*

1. Introduction

The direct measurement of laser frequencies as opposed to using wavelength measurements and the speed of light is an important new step in applications to very high resolution spectroscopy and the development of time and frequency standards. Hitherto only in the microwave region and below has it been possible for an oscillator frequency to be compared directly with the caesium standard at 9 GHz or with secondary standards such as quartz crystal oscillators, since these standards are themselves in this region. The advent of submillimetre and infra-red lasers has enabled measurements to be made up to 88 THz (3·39 μm) by using harmonic mixing techniques to bridge the difference between microwave and infra-red frequencies.[1] In theory it is possible to obtain accuracies of the order of one in 10^{11} whereas the indirect wavelength determinations are usually limited by the accuracy of the present value of the speed of light which is about 3 in 10^7 (Ref. 2).

The first direct determination of a laser frequency was made by Hocker *et al.*[3] in 1967 in which the output of an HCN laser oscillating at several frequencies in the 800–1000 GHz region was mixed with a high harmonic of a millimetre wave klystron in a point-contact tungsten-silicon diode. The frequencies were determined by tuning the klystron to give suitable beat frequencies which could be amplified and measured on a spectrum analyser. The klystron frequency was measured by down conversion against a quartz crystal oscillator using standard techniques. The recent extensive development of submillimetre and infra-red gas lasers[4, 5] has produced nearly 100 continuous wave laser lines with wavelengths longer than 20 μm and some 200 lines in the region around 10 μm.

Frequency measurements by direct mixing with klystron harmonics using the Hocker *et al.* techniques become very difficult beyond 3 THz (100 μm) and the extension to the 88 THz region is achieved by harmonic mixing experiments with several lasers suitably chosen to produce beat frequencies in the 1–200 GHz region.[6] For example, the 32 THz (9 μm) CO_2 laser frequency is measured by successive mixing of the 12th harmonic of the HCN 891 GHz (337 μm) laser line with the 10·7 THz (28 μm) H_2O laser line and then the 3rd harmonic of the latter with the CO_2 frequency.[7–9]

Using these techniques direct frequency measurements in DCN, H_2O, D_2O, CO_2, CO and He Ne lasers have been made during the last four years.[1, 10–13] The highest frequency measured (to approximately one in 10^6) is the 88 THz (3·39 μm) He–Ne laser emission.[1]

One of the most important aspects of this work was the development of suitable mixers having response times appropriate to near infra-red frequencies. A very considerable advance was the replacement of the microwave silicon–tungsten point-contact mixer by a metal–oxide–metal type for frequencies beyond 3 THz.[12] The cut-off frequency for this diode is in excess of 88 THz as illustrated by the measurement of the 3·39 μm He–Ne laser line. A parallel development has been the use of superconducting point contact devices based on the

Josephson effects.[14] In particular it has been shown that it is possible to mix up to the 400th harmonic of an X-band klystron with the 78 μm (3·8 THz) water vapour laser line in a niobium–niobium point contact and to obtain a beat frequency which can be amplified and measured.[14] This ability to obtain extremely high harmonic mixing is probably superior to that for the metal–oxide–metal or metal semiconductor point contacts but at the present time the upper frequency limit is set empirically at the 3·8 THz region which is some 20 times lower than for the latter.[15]

The work described in the present paper forms part of a programme to determine the speed of light to one part in 10^8 by the direct measurement of wavelength and frequency of the 9 μm CO_2 laser emission using successive stages of harmonic mixing and beat frequency detection with a millimetre wave klystron, an HCN laser and an H_2O laser as transfer oscillators.[16] This paper is concerned with measurements of frequency and frequency locking of the HCN laser at 891 GHz and the frequency measurement of the 2·5 THz (118 μm) and 10·7 THz (28 μm) H_2O laser lines.

2. Submillimetre Lasers

2.1. *The Hydrogen Cyanide Laser*

This laser is the most powerful continuous wave source presently known in the 1–10 THz region. There are several fairly strong lines which are generated under d.c. discharge excitation conditions, namely, at 890, 805 and 964 GHz. These occur due to suitable population inversions in the rotation levels in the 11′0 and 040 vibration states of the HCN molecule.[17]

The dimensions and operating conditions for a hollow cathode discharge in a 50/50 mixture of CH_4 and N_2 which forms HCN molecules are given in Table 1. The laser is not cooled because it is found that the output is optimum for a wall temperature of about 100 °C. In order to obtain as narrow a frequency output as possible it is extremely important to have very stable striations in the discharge positive column.[18] Typically the output at 891 GHz is a few kilohertz wide under these conditions. (A non-striated discharge increased the emission width by about one order of magnitude.) The invar stabilized cavity is near confocal with 10 m radius mirrors separated by 8 m and the energy is coupled out using a 45° 0·05 mm thick polythene intracavity beam divider. The double mirror arrangement at one end means that the output coupling is varied from 0 to $4r^2$ by tuning the mirror at right angles to the main cavity, where r is amplitude reflectance of the beam divider. The main cavity is tuned to give single mode output since at this frequency the laser Doppler gain profile is much less than the cavity mode spacing $c/2L$, where L is the cavity length and c is the velocity of light. The output is 50–75 mW at 891 GHz and some two or three times down on this at 964 and 805 GHz, as measured by a Golay cell using the manufacturer's calibration.†

2.2. *The Water-vapour Laser*

The H_2O molecule gives many emission lines in the submillimetre and far infra-red regions arising from perturbations of rotational levels in the 100, 020 and 001 vibrational states.[19] The main interest is in the 118 μm (2·5 THz) and 28 μm (10·7 THz) lines. The construction of the laser is basically similar to that of the HCN laser and the appropriate dimensions and operating conditions are given in Table 1. The discharge is water cooled. For strong emission at 2.5 THz (118 μm) the cavity is near confocal with 8 m radius mirrors separated by 6 m. The output coupling is a 45° 0·01 mm thick polypropylene film with a two-mirror system similar to that for the HCN laser. Although reasonable power at 10·7 THz (28 μm) can be obtained using this cavity a considerable improvement in terms of mode purity and output power results from extending the length to 8 m and using a folded confocal arrangement, that is one plane and one 15 m radius mirror. About 100 mW at 10·7 THz, and 10 mW at 2·5 THz are typical.

Table 1. Operating conditions for HCN and H_2O lasers

	Frequency	Length (m)	Diameter (mm)	Cavity	Current (A)	Voltage (kV)	Pressure (torr)	Output Power (mW)
HCN laser	891 GHz	8·5	100	confocal	0·7	4·5	0·13	75
	805 GHz	8·5	100	confocal	0·7	4·5	0·13	25
	964 GHz	8·5	100	confocal	0·7	4·5	0·13	30
H_2O laser	2·5 THz	6·0	50	confocal	1·0	2·8	0·3	20
	3·8 THz	8·0	50	folded confocal	1·0	3·3	0·4	10
	10·7 THz	8·0	50	folded confocal	0·5	4·8	0·4	100

2.3. *Metal-Oxide–Metal Diodes*

If R, r_s and C are the barrier resistance, spreading resistance and junction capacitance of a point contact rectifier (Fig. 1), the barrier voltage produced by a signal of frequency ω is proportional to $(1+\omega^2 r_s^2 C^2)^{-\frac{1}{2}}$ in the approximation $r_s \ll R$. For a metal-semiconductor point-contact diode such as tungsten–silicon the roll-off

† Pye-Unicam Golay cell.

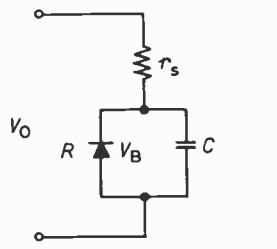

$$\frac{V_B^2}{V_0^2} = \frac{1}{(1+r_s/R)^2 + (\omega C r_s)^2}$$

Fig. 1. Equivalent circuit of diode.

frequency is about 3 THz[20] and they are little used above this frequency. To extend the usefulness of point-contact diodes up to infra-red frequencies it is at least necessary to reduce r_s and/or C. In metal-oxide–metal (m.o.m.) devices this is achieved by having a metal in place of a semiconductor (reducing r_s) and by using very fine whiskers, which may decrease C. Rectification is then achieved by electron tunnelling through a thin oxide film between the two metals.

The diodes used in the present experiments consisted of a fine tungsten whisker (electrolytically etched to the required dimensions in potassium hydroxide solution) which was brought into light contact with a metal post by means of a differential screw (Fig. 2). Typically the whisker had a length of 1 to 2 mm, a diameter between 2 and 8 μm and a tip radius of 50 nm. The post material used was either nickel or 'pencil lead' (graphite) as these appeared experimentally to give the best results. (Approximately 20 metals and alloys have been tested as posts at Q-band frequencies; all give rise to rectification.)

The action of m.o.m. diodes may be considered as a two-stage process: (a) the whisker acts as a travelling-wave antenna in the radiation field; (b) currents pass from the antenna to the junction where rectification occurs. The validity of (a) has been demonstrated experimentally,[21] the detected signal showing the usual dependence for an antenna[22] on the angle between the radiation Poynting vector and the whisker. In particular, there is an angle for which optimum coupling occurs, and the dimensions in Fig. 2 were designed so that this was the case for the 891 GHz and 2·5 THz radiations. The diode construction was kept as open as possible so that the radiation from laser and microwave sources could be focused on to the diode over a wide angular range (Fig. 2).

The rectification stage has been considered by Green *et al.*[23] who showed that a theoretical model based on the tunnelling of electrons through a metal–insulator–metal junction can qualitatively explain some of the experimental data.

The adjustment of the diode for optimum beat signals depends critically on the mechanical adjustment and the radiation power levels. It can be important at the highest frequencies to form the junction in the presence of the radiation. Good contacts only last a matter of a day or so at the present time although improved fabrication techniques may eventually eliminate this problem.

2.4. *Laser Beam Focusing*

The outputs of the two lasers were focused onto the point-contact diode as shown in Fig. 3. A TPX (poly 4 methyl pentene-1) lens of 90 mm focal length was used for the HCN emission.[24] Assuming an 8 m confocal cavity and about 1 m distance between the laser output window and the lens a focused spot diameter of about $2 \times \lambda_{0\cdot89\ \mathrm{THz}}$ was obtained. In the case of the 2·5 (and 10·7) THz H_2O lines an off-axis paraboloid was used for focusing to reduce absorption losses. Spot diameters of about $5 \times \lambda_{10\cdot7\ \mathrm{THz}}$ and $3 \times \lambda_{2\cdot5\mathrm{THz}}$ were calculated from the known beam parameters in the laser cavities.[25]

3. Frequency Measurements

The basic requirement of the point-contact diode in these measurements is not only to respond to the very high frequencies but also to generate high order harmonics in order to do the mixing experiments listed in Table 2. It is found that this depends quite heavily on fairly arbitrary factors such as pressure and area of the contact. The only operating criterion is to obtain a particular beat frequency by a trial and error process and to optimize by making adjustments to the contact and the relative powers of the radiations falling on it. The direct current–direct voltage characteristics of the diodes are usually non-linear but it is not easy to draw conclusions from these about their high frequency harmonic generation properties.

The HCN laser frequency was measured in a similar way to the original method of Hocker *et al.*[3] The output of a 74 GHz klystron was detected by a commercial run-in silicon–tungsten point-contact diode. The laser radiation was focused by a polythene or TPX lens onto the contact through a cone-shaped aperture in the diode mount. The tunsten whiskers were typically 25 μm diameter and pointed to a few hundred nanometres

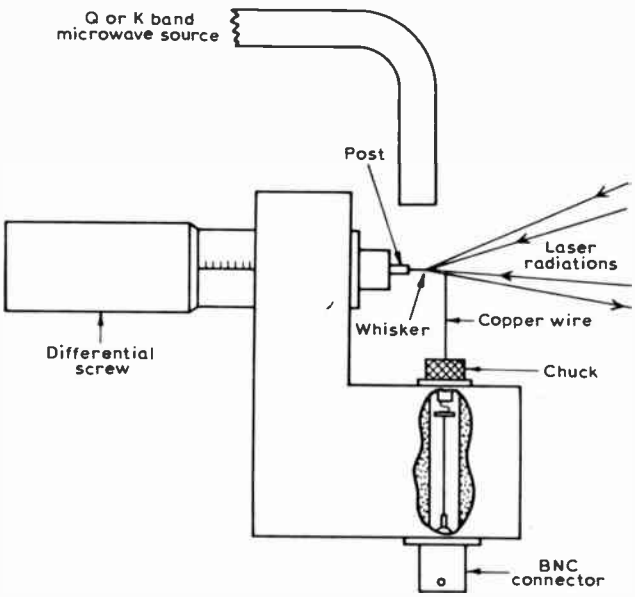

Fig. 2. Free space diode mount.

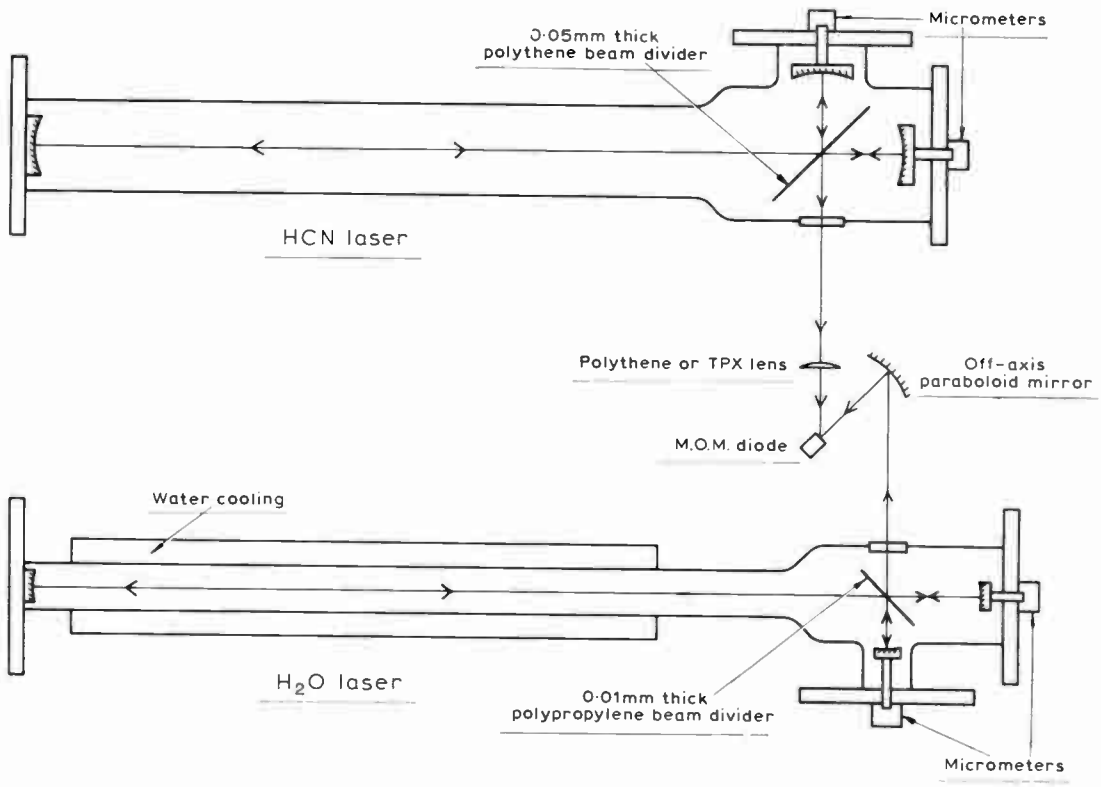

Fig. 3. HCN and H_2O laser outputs focused onto point-contact diode.

Table 2. Harmonic mixing

Laser 1	Laser 2	Microwaves	Mixing
HCN 891 GHz	—	74 GHz	$891 - 12 \times (\sim 74) \simeq 30$ MHz
HCN 891 GHz and 805 GHz	—	29 GHZ	$891 - 805 + 3 \times (\sim 29) \simeq 30$ MHz
HCN 891 GHz and 964 GHz	—	36 GHz	$964 - 891 + 2 \times (\sim 36) \simeq 30$ MHz
HCN 891 GHz	H_2O 2528 GHz	36 GHz	$3 \times 890 - 2528 + 4(\sim 36) \simeq 30$ MHz
HCN 891 GHz	H_2O 10718 GHz	29 GHz	$12 \times 891 - 10718 + (\sim 29) \simeq 30$ MHz

diameter. Rectified d.c. signals of the order of 10 mV were obtained for a few milliwatts of input power at 891 GHz. The 74 GHz klystron was tuned to produce a beat frequency between its 12th harmonic and 891 GHz in the 30 MHz region and was amplified and displayed on a spectrum analyser. The klystron was phase locked to a reference signal multiplier from a quartz crystal oscillator. A special harmonic mixing technique was used in the last stage to get beyond the 30 GHz limit of the silicon-varactor comb generators (Fig. 4) which avoided the complications of using the conventional double phase-locked system in which the 74 GHz klystron is locked to a harmonic of a lower frequency phase-locked klystron. Phase noise from the 15 MHz reference quartz crystal broadened the beat frequency to about 20 kHz at half height (Fig. 5). A value for the laser centre frequency at 891 GHz is given in Table 3.

In addition to these measurements experiments were carried out using the free-space-mounted metal–oxide–metal point-contact diode to observe mixing between the 891, 805 and 964 GHz lines from the HCN laser. By suitably tuning the laser these three lines can be made to oscillate simultaneously and hence it is only necessary to focus the output from this laser onto the point contact with a polythene or TPX lens. The difference frequencies,

Table 3. Laser frequencies

Laser	Frequency (MHz)	R.M.S. error (MHz)
HCN	890 760·2	± 0·2
H_2O	2 527 952·5†	± 1·5

† With laser set to the Lamb dip.

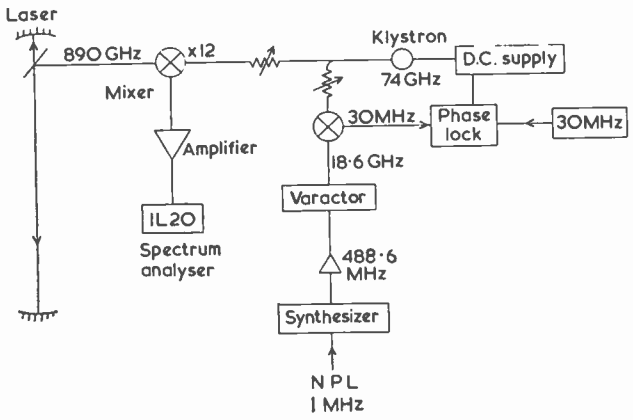

Fig. 4. Microwave system for the measurement of the HCN laser frequency at 891 GHz.

which are listed in Table 2 were provided by harmonics of 29 and 36 GHz klystrons. The microwave radiation was directed on to the diode by an open-ended waveguide situated vertically above it (Fig. 2). Figure 6 shows the fundamental and second harmonic of the beat frequency between the 891 and 964 GHz lines. The beat signal was observed using a low-noise 0–1000 MHz amplifier and a 1–110 MHz spectrum analyser. A typical signal was 40 dB above the noise. The width of the beat notes was less than 20 kHz since any broadening due to laser cavity instabilities cancels to first order. Similar results were obtained for the beat frequency between the 891 and 805 GHz lines.

Since the HCN laser is an important transfer standard from frequency measurements in the infra-red region a technique has been developed to frequency-lock the output at 891 GHz to an absorption reference. This has been achieved in a relatively simple manner by locking to a near-coincident absorption line in difluoroethylene ($CH_2{=}CF_2$) at 890 759·60 ± 0·08 MHz with a stability of about two parts in 10^8 r.m.s. over several minutes. More extensive details are given by Bradley *et al.*[26] Theory and experiment have shown[27] that this absorption line is not affected by stray electric or magnetic fields by greater than a few parts in 10^{10}. The method consists of frequency modulating the laser by applying a 400 Hz signal to a piezo-electric crystal holding one of the cavity mirrors. The modulated output passes through a cell containing the gas and is received by a phase-sensitive detector. A d.c. correction signal is then fed back to the laser using a motor-driven potentiometer and amplifier.

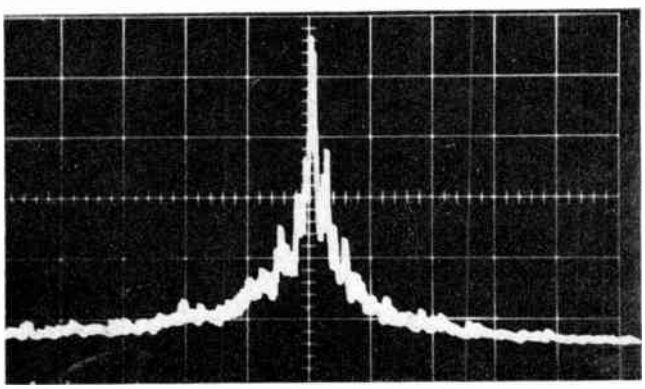

Fig. 5. Beat frequency signal between 891 GHz and 12th harmonic of 74 GHz.

3.1. *The* 2·5 THz H_2O *Laser Line*

The frequency of the 2·5 THz H_2O laser line was measured by mixing with the 3rd harmonic of the 891 GHz HCN laser line together with the 4th harmonic of a 36 GHz phase locked klystron in the metal–oxide–metal diode (Table 2). Rectified signals of about 10 mV for 10 mW of 2·5 THz power were obtained. Careful adjustments were made to the diode contact and the relative powers of the three radiations in order to observe the beat frequency which was detected using a low noise preamplifier and a 1–110 MHz spectrum analyser. The average signal was approximately 20 dB above the noise level with a 10 kHz bandwidth in the spectrum analyser (Fig. 7). The full width of the signal was about 75–100 kHz at half height of which approximately 20 kHz was contributed by the microwaves. The beat frequency signal was only occasionally steady to better than ±1 or 2 dB and more frequently showed fluctuations of ±5 dB with a period of a few seconds. These fluctuations could not be correlated proportionally with any amplitude changes in the laser output levels since these were much more steady. Thermal drift of the beat frequency amounted to ~60 kHz/minute. The H_2O laser operated in single mode and it was possible to set to the Lamb dip. The frequency was measured as the mean of six readings and is shown in Table 3. The value agrees well with that obtained by Frenkel *et al.*[11] using direct mixing with a klystron harmonic in a silicon point-contact diode (2 527 952·8 ± 0·1 MHz r.m.s.). The main source of innacuracy in the figure given in Table 3 is from the setting of the HCN laser on line centre at 891 GHz since this frequency was not monitored directly at the time of the 2·5 THz measurements.

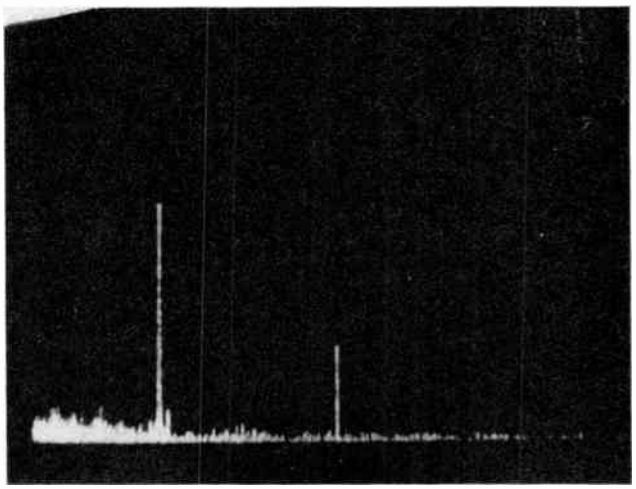

Fig. 6. Beat frequency signals between 891 and 964 GHz radiation.

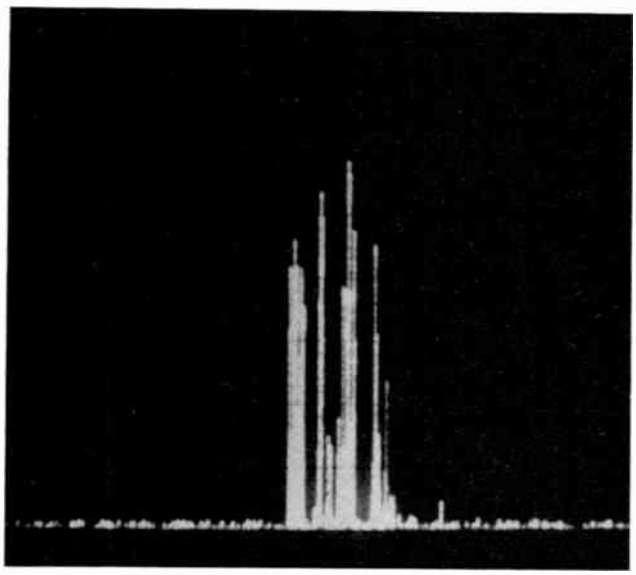

(a) Unlocked 36 GHz klystron (0·1 MHz/div).

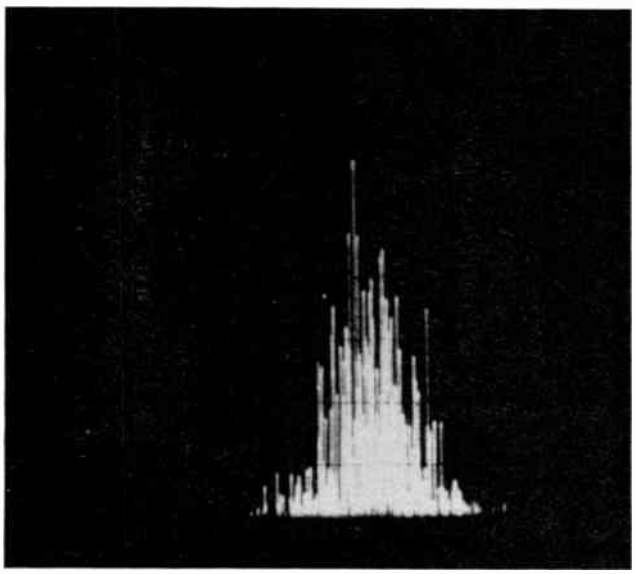

(b) Phase-locked 36 GHz klystron (0·05 MHz/div).

Fig. 7. Beat frequency signal between 3 × 891 GHz and 2·53 THz radiations.

3.2. *The* 10·7 THz H_2O *Laser Line*

This frequency was measured by mixing with the 12th harmonic of the 891 GHz HCN laser line and 29 GHz radiation from a klystron. The latter is tuned to produce a beat frequency in the 50 MHz region. The signal was considerably more difficult to obtain than that for the 2·5 THz line and was typically 10–15 dB above noise using similar amplification and detection to the above. The experimental arrangement was similar to that shown in Fig. 3. Further details are to be found in Reference 28.

4. Conclusion

The frequencies of the 891 GHz HCN laser line and the 2·5 and 10·7 THz H_2O laser lines have been measured. The metal–oxide–metal contact diode has been demonstrated as a wideband mixer in a free space configuration. Some practical problems are being investigated with a view to extending reliable operation towards the 88 THz region.

5. Acknowledgments

The authors wish to thank Dr. K. D. Froome, Dr. A. Horsfield and Dr. N. W. B. Stone for advice and encouragement and Mr. J. Dromey for technical assistance.

6. References

1. Evenson, K. M., Day, G. W., Wells, J. S. and Mullen, L. O., 'Extension of absolute frequency measurements to the c.w. He–Ne laser at 88 THz', *Appl. Phys. Letts.*, **20**, pp. 133–5 1st February 1972.
2. Froome, K. D., 'A new determination of the free-space velocity of electromagnetic waves', *Proc. Royal Soc. A*, **247**, pp. 109–22, 9th September 1958.
3. Hocker, L. O., Javan, A., Ramachandra Rao, D., Frenkel, L. and Sullivan, T., 'Absolute frequency measurement and spectroscopy of gas laser transitions in the far infrared', *Appl. Phys. Letts*, **10**, pp. 147–9, 1st March 1967.
4. Gebbie, H. A., Stone, N. W. B. and Findlay, F. D., 'A stimulated emission source at 0·34 mm wavelength', *Nature*, **202**, p. 685, 16th May 1964.
5. Gebbie, H. A., Stone, N. W. B., Findlay, F. D. and Robb, J. A., 'Interferometric observations on far infrared stimulated emission sources', *Nature*, **202**, pp. 169–170, 11th April 1964.
6. Knight, D. J. E., 'Harmonic Frequency Coincidences between Gas Laser Transitions in the Far Infra-red', (Report No. QU8, National Physical Laboratory, Teddington, Middlesex, England.)
7. Evenson, K. M., Wells, J. S., Matarrese, L. M. and Elwell, L. B., 'Absolute frequency measurements of the 28 and 78 μm c.w. water vapour laser lines', *Appl. Phys. Letts.*, **16**, pp. 159–61, 15th February 1970.
8. Daneu, V., Sokoloff, Sanchez, A. and Javan, A., 'Extension of laser harmonic-frequency mixing techniques into the 9 μm region with an infrared metal–metal point contact diode', *Appl. Phys. Letts.*, **15**, pp. 398–400, 15th December 1969.
9. Evenson, K. M., Wells, J. S. and Matarrese, L. M., 'Absolute frequency measurements of the CO_2 c.w. laser at 28 THz (10·6 μm)', *Appl. Phys. Letts.*, **16**, pp. 251–3, 15th March 1970.
10. Hocker, L. O. and Javan, A., 'Absolute frequency measurements on new c.w. HCN submillimetre laser lines', *Physics Letters*, (*Netherlands*) **25A**, pp. 489–90, 9th October 1967.
11. Frenkel, L., Sullivan, T., Pollack, M. A. and Bridges, T. J., 'Absolute frequency measurements of the 118·6 μm water-vapour laser transition', *Appl. Phys. Letts*, **11**, pp. 344–5, 1st December 1967.
12. Hocker, L. O., Small, J. G. and Javan, A., 'Extension of absolute frequency measurements to the 84 μm range', *Phys. Letters* (*Netherlands*), **29A**, pp. 321–2, 2nd June 1969.
13. Sokoloff, D. R., Sanchez, A., Osgood, R. M. and Javan, A., 'Extension of laser harmonic-frequency mixing into the 5 μ regions', *Appl. Phys. Letts.*, **17**, pp. 257–9, 15th September 1970.
14. McDonald, D. G., Risley, A. S., Cupp, J. D. and Evenson, K.M., 'Harmonic mixing of microwave and far infra-red laser radiation using a Josephson junction,' *Appl. Phys. Letts.*, **18**, pp. 162–4, 15th February 1971.
15. Blaney, T. G., 'Applications of the Josephson effects in the millimetre and submillimetre wavelength regions', *The Radio and Electronic Engineer*, **42**, pp. 303–8, July 1972.
16. Bradley, C. C., Edwards, G., Knight, D. J. E. and Woods, P., 'Towards a new determination of the speed of light', *Physics Bulletin*, **23**, pp. 15–8, January 1972.

17. Lide, D. R. and Maki, A. G., 'On the explanation of the so-called CN laser', *Appl. Phys. Letts.*, **11**, pp. 62–4, 15th July 1967.

18. Fuller, D. W. E., Hines, J. and Compton, B., 'Short-term frequency stability of the HCN maser', *Electronics Letters*, **5**, p. 448, 18th September 1969.

19. Benedict, W. S., Pollack, M. A. and Tomlinson III, W. J., 'The water vapour laser', *I.E.E.E. J. Quantum Electronics*, **QE-5**, pp. 108–24, February 1969.

20. Becklake, E. J. S., Cram, L. A. and Prewer, B. E., 'Spectral response of a point-contact diode in the submillimetre range', *Electronics Letters*, **4**, pp. 601–2, 27th December 1968.

21. Matarrese, L. M. and Evenson, K. M., 'Improved coupling to infrared whisker diodes by the use of antenna theory', *Appl. Phys. Letts.*, **17**, pp. 8–10, 1st July 1970.

22. Jasik, H. (editor), 'Antenna Engineering Handbook' (McGraw-Hill, New York, 1961).

23. Green, S. I., Coleman, P. D. and Baird, J. R., 'The MOM electric tunnelling detector', Symposium on Submillimetre Waves, Polytechnic Institute of Brooklyn, 1970. To be published.

24. Chantry, G. W., Evans, Hellen M., Fleming, J. W. and Gebbie, H. A., 'TPX, a new material for optical components in the far infrared spectral region', *Infrared Physics*, **9**, pp. 31–3, January 1969.

25. Kogelnik, H. and Li, T., 'Laser beams and resonators', *Proc. I.E.E.E.*, **54**, pp. 1312–27, October 1966.

26. Bradley, C. C., Knight, D. J. E. and McGee, C. R., 'Frequency-locking an HCN laser to a molecular absorption line'. *Electronics Letters*, 7, pp. 381–2, 1st July 1971.

27. Duxbury, G., Jones, R. G., Burroughs, W. J., Bradley, C. C. and Stone, N. W. B., 'Molecular absorption in near coincidence with the HCN 337 μm emission', Symposium on Submillimetre Waves, Polytechnic Institute of Brooklyn, 1970. To be published.

28. Bradley, C. C. and Edwards, G., To be published.

Manuscript first received by the Institution on 6th May 1971 and in final form on 14th April 1972. (Paper No. 1459/IC 66.)

The Authors

Dr. C. C. Bradley gained a B.Sc. degree in physics at the University of Birmingham in 1958 and went on to work for a Ph.D. of the University of Cambridge in the Royal Society Mond Laboratory, his thesis being on electron transport in liquid metals. He joined the National Physical Laboratory in 1961, working on high pressure properties of metals and semiconductors until 1965 and subsequently on submillimetre wave lasers. Dr. Bradley then spent two years in the U.S.A., first as Visiting Scientist at the Francis Bitter National Magnet Laboratory, MIT, Cambridge, Massachusetts, carrying out research on cyclotron resonance in semiconductors, and then as a member of the staff of the National Bureau of Standards, Boulder, Colorado, where he worked on the direct measurement of the frequency of submillimetre wave lasers. He returned to his present position in the Division of Electrical Science at the National Physical Laboratory in 1969, to continue development of high power, high stability submillimetre wave lasers and their application to frequency measurements and resonance studies.

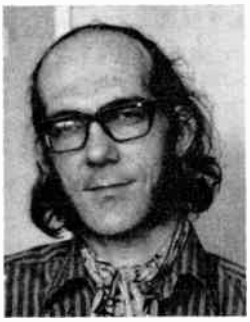

Dr. G. J. Edwards received his B.A. degree in physics in 1964 at Jesus College, University of Cambridge, and in 1968 was granted the D.Phil. degree of the University of Sussex for a thesis on Fermi surfaces of metals. He went as a post-doctoral fellow to Michigan State University for four years to do research on low temperature solid-state physics. Dr. Edwards took up his present post in the Quantum Metrology Division of the National Physical Laboratory in 1970, where he has been working on a new determination of the speed of light.

Dr. D. J. E. Knight obtained his B.A. degree in physics at Exeter College, University of Oxford, in 1961, and in 1965 received the D.Phil. for a thesis on millimetre wave harmonics generation. For the next two years he was a staff member of the Research Laboratories of RCA Victor Ltd., Montreal, where he did research on the interaction of earth satellites with ionospheric plasmas. Dr. Knight joined the Quantum Metrology Division of the National Physical Laboratory in 1966 to work on the extension of frequency measurements to the submillimetre wave region.

U.D.C. 621.375.7

Maximum Power Transfer in Parametric Circuits

Professor D. P. HOWSON,
D.Sc., C.Eng., F.I.E.E., F.I.E.R.E.*

SUMMARY

This paper establishes the conditions under which maximum power transfer in a parametric circuit with port immittances having positive real parts will be achieved with conjugate matching at input and output, and links these results with earlier work which showed, for modulator and mixer circuits, when source and load resistance might also be equal.

* *University of Bradford, Postgraduate School of Electrical and Electronic Engineering, Bradford 7.*

1. Introduction

For a two-port consisting of linear, constant-coefficient elements it is well known[1] that maximum power transfer from input to output is achieved if the source impedance is conjugately matched to the input impedance, and the load impedance to the output impedance—see Fig. 1. In this paper the possibility of achieving maximum power transfer with conjugate matching at input and output will be studied for the case of a two-port consisting of at least one linear, periodically-varying element together with linear, constant-coefficient elements.

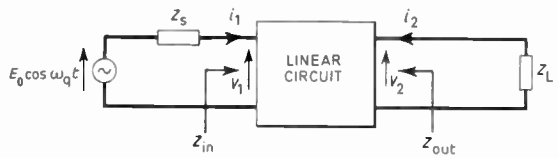

Fig. 1. Linear two-port network.

The necessary condition for a non-linear element to appear time-varying is that the non-linearity is wholly controlled by a current or voltage—variously designated the pump, local oscillator or carrier source—independent of the input signal. This usually means that the controlling source provides a voltage across the non-linear element much larger than the corresponding input voltage component—recent work on modulators has suggested a ratio of at least three to one[2] and a common guideline is ten to one. Such a circuit is a satisfactory representation of a range of circuits, such as the series, shunt and ring modulators, the parametric amplifier, and various types of upconverter and downconverter[3, 4] for the purpose of examining their fundamental properties. The characteristic property of such a circuit is that, although the output may be a linear function of the input, it is usually at a different frequency, and furthermore currents and voltages at a range of frequencies—the modulation frequencies—will appear at different parts of the circuit. This paper examines under what conditions maximum power transfer will be achieved with conjugate matching at input and output in a circuit of this type with a restriction that the input and output immittances have positive real parts.

2. Maximum Power Transfer with Conjugate Matching

Calculations on circuits with periodically-varying parameters are greatly facilitated if it can be assumed that any tuned circuits present are 'ideal', in the sense that they present either a zero or an infinite impedance to all but a few modulation frequencies, and at these frequencies the impedance has a finite real part. Because the modulation frequencies may be quite widely spaced this approximation is often realistic and leads to results surprisingly close to the measured results. It will therefore be assumed in all subsequent work in this paper.

Circuit models based on this assumption will include in many cases current at only the signal frequency passing through the source impedance, or voltage at only the signal frequency occurring across it. For such circuits, examining *only* the input mesh of the linear network of Fig. 1, it will not be possible to determine whether or not

the network contains a periodically-varying component. The multi-frequency nature of the circuit, assuming it to contain a periodically-varying element, will not be detectable from a measurement of the currents through or voltages across Z_s, and the input impedance of the network at signal frequency will not be a function of Z_s since the circuit is linear. Therefore the maximum power transfer theorem will apply to this circuit just as to a conventional linear circuit—as can be seen from the usual form of the proof.[5]

The input power to the circuit is, from Fig. 1,

$$P_{in} = i_1^2 R_{in} = \frac{E_o^2 R_{in}}{(R_s+R_{in})^2+(X_s+X_{in})^2} \quad \text{.....(1)}$$

Taking R_{in} as a constant for the moment, differentiate to find the optimum value of X_{in}:

$$\frac{dP_{in}}{dX_{in}} = \frac{-2E_o^2 R_{in}(X_s+X_{in})}{(R_s+R_{in})^2+(X_s+X_{in})^2}$$

and is zero when

$$X_{in} = -X_s \quad \text{.....(2)}$$

Substituting this value into (1) gives

$$P_{in} = \frac{E_o^2 R_{in}}{(R_s+R_{in})^2} \quad \text{.....(3)}$$

and differentiation with respect to R_{in} shows that the maximum value requires

$$R_s = R_{in} \quad \text{.....(4)}$$

as long as R_s and R_{in} are always positive, as has been assumed throughout this calculation. Therefore

$$Z_{in} = Z_s^* \quad \text{.....(5)}$$

for maximum power transfer from source to network, and it can be similarly shown that

$$Z_{out} = Z_L^* \quad \text{.....(6)}$$

for maximum power transfer from network to load, if current at the output frequency *only* passes through the load, or voltage at the output frequency *only* occurs across it. Because the circuit is assumed linear, maximum power transfer from input to output will follow if the power transfers into and out of the network are maximized.

Because of the assumptions about the nature of the source and load impedances, the restriction that current at a single frequency passes through source and/or load is equivalent to stating that power at a single frequency is dissipated in the source and/or load terminations. The conclusions reached in this section may therefore be stated:

Conclusion A: Maximum power transfer from input to output is obtained in a linear two-port, some of the components of which are periodically-varying, if the circuit is conjugately matched at source and/or load, and *when power is only dissipated at one frequency in the respective source and/or load resistances.* The conventional parametric upconverter is a well-known case in point.

The implication of the result is that all diode mixer and modulator circuits that have 0dB minimum loss for ideal (passive) diodes[6] will be conjugately matched at input and output, since none of these circuits can dissipate power at unwanted modulation frequencies in the terminations. The matching condition for these circuits will hold for minimum loss whether the diodes are ideal or not.

3. Maximum Power Transfer in Other Circuits

The theorem that is given above is of little value if it is found that maximum power transfer is achieved with conjugate matching at the ports in many other types of parametric circuit. It is unfortunately not possible to prove the negative of the above theorem, and certainly a few groups of circuits exist that do not satisfy the criterion, but for which conjugate matching is necessary for maximum power transfer. These will be discussed a little later. *Generally, however, it is true that if power is dissipated at more than one frequency in a termination, maximum power transfer is achieved with some form of matching at that port other than conjugate matching.*

The reason for this is that, in the majority of such cases, the impedance looking into the port depends upon the termination at the port.[7, 9] The assumption of the independence of Z_s and Z_{in} made in order to differentiate (1) is therefore no longer valid and therefore (5) and (6) will not follow.

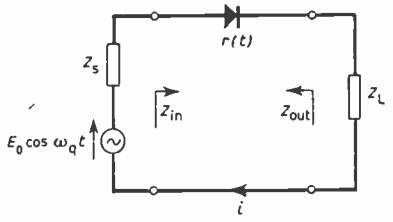

Fig. 2. Equivalent circuit of modulator.

This result can be seen more clearly from the constant-coefficient multiple-loop equivalent circuit that can be drawn for the modulator[7] of Fig. 2—see Fig. 3. The diagram also shows that a similar result will follow—in general, and with Z_L replacing Z_s—for the output impedance, which may be determined by removing the signal generator from the input loop and replacing it by a generator at the output frequency in the output loop.

It is possible to take the mismatching argument further in particular cases. Figure 3 refers to the series modulator, and the following can be proved for this circuit:

If, in a series mixer or modulator, unwanted dissipation occurs in the source resistance at output frequency, then for minimum loss the input resistance will be *greater* than the source resistance. Also, if unwanted dissipation at the signal frequency occurs in the load resistance, the optimum output resistance will be *greater* than the load resistance.

These results follow because under either of these circumstances, the relevant port impedance is a compromise between two conditions. For minimum loss,

conjugate matching is the natural condition. On the other hand, considering the first result, it can be seen from Fig. 3 that unwanted dissipation at the output frequency is represented in the equivalent circuit by an added parasitic source resistance in series with the load resistance and therefore for minimum unwanted dissipation the source resistance should be as small as possible. These two conflicting requirements lead to the stated result, the actual value of source resistance in a particular case being a compromise between them. The second result can be argued similarly. By duality the same results hold for port and terminating *conductances* in the shunt modulator.

For other modulators with equivalent circuit of series or shunt form, such as the ring and star modulators, similar results follow.

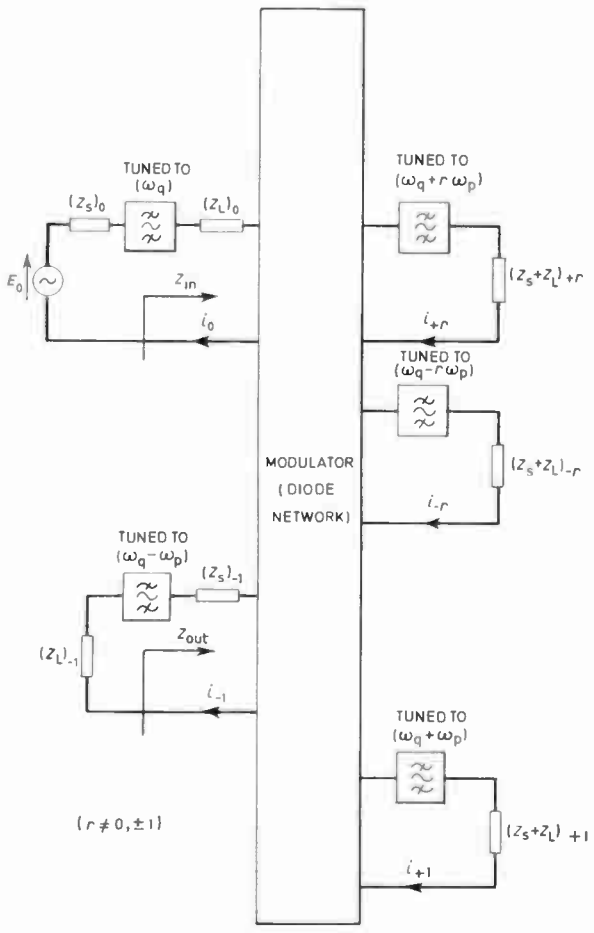

Fig. 3. Multiple-loop equivalent circuit for modulator.

Returning to a consideration of conditions for a conjugate match at one or both ports to coincide with minimum loss, an examination of the effect of unwanted dissipation at frequencies other than the signal and output frequencies will now be made. Remembering that the matching with which this paper is concerned occurs at a single frequency only, in either input or output loop in Fig. 3, it can be seen that unwanted dissipation at a port will not affect the matching for minimum loss unless the impedance in which the unwanted dissipation occurs is a function of that particular terminating impedance.

Therefore,

Conclusion B: Maximum power transfer from input to output is achieved with conjugate matching at input and/or output, if the source and/or load impedances can be adjusted at the matching frequency without affecting impedance values at the other modulation frequencies.

This could happen if the terminating impedance was a high Q tuned circuit at the matching frequency, together with other components.

Furthermore, if unwanted loss occurs in the source termination of a parametric circuit at frequencies other than those of the signal or output, then the source termination can be replaced, for any particular set of circuit component values, by two elements, one tuned to the signal frequency and lossless elsewhere, and a second with appropriate loss at the other modulation frequencies. If, additionally, the circuit happened to have maximum power transfer for $Z_s = Z_L$, the second component could be considered to depend upon Z_L (rather than its actual dependence on Z_s) without alteration of any values. For those circuits in which the periodically-varying element is resistive and an even function of time, $Z_s = Z_L$ for maximum power transfer implies a symmetrical pattern[8] of terminating impedances at other modulation frequencies. This in turn implies that the modified circuit, Z_L replacing Z_s in the second component of the source impedance, has also maximum power transfer for $Z_s = Z_L$. Therefore, because the source impedance has now only dissipation at signal frequency, it will be conjugately matched at the input. Therefore the original circuit will also. Similar considerations apply for the load termination. These may be summarized by:

Conclusion C: If, in a circuit containing periodically-varying resistance which is an even function of time, unwanted loss occurs in the terminations solely at frequencies other than those of the signal or output, conjugate matching will occur at input and output for maximum power transfer as long as this implies equal source and load impedances.

An example will be found in Table 1.

The matching of other modulation frequencies present in the currents or voltages at the input or output of the two-port is rather different from that obtaining for the input and output frequency. Because dissipation at other frequencies gives no useful return, matching is unlikely to occur, other than in all-resistive circuits. Indeed, it is more normal, in tuned structures, to go to some trouble to ensure that such frequencies are presented with either an open or a short circuit.

4. Results for Series and Ring Modulators†

Table 1 shows calculations of input and output impedance for several different types of series and ring modulator circuit, assuming the circuit diodes behave

† Results for the shunt modulator, or for some forms of star modulator, may be inferred from these by duality.

Table 1. Series and ring modulators

		Source impedance	Load impedance	Source resistance for minimum loss	Input impedance for minimum loss	Load resistance for minimum loss	Output impedance for minimum loss
Series modulator circuit no.	1	R_s	R_L	500 Ω	1500 Ω	500 Ω	1500 Ω
	2	R_s	R_L at $(\omega_p-\omega_q)$; 0 elsewhere	576 Ω	820 Ω	1152 Ω	1152 Ω (a)
	3	R_s at ω_q; 0 elsewhere	R_L at $(\omega_p-\omega_q)$; 0 elsewhere	26 Ω	26 Ω (a)	26 Ω	26 Ω (a)
	4	R_s at ω_q; 0 elsewhere	R_L	1152 Ω	1152 Ω (a)	576 Ω	820 Ω
	5	R at ω_q; 0 elsewhere	0 at ω_q; R elsewhere	1000 Ω	1000 Ω (a)	1000 Ω	1000 Ω (c)
Ring modulator circuit no.	1	R_s	R_L	1000 Ω	1000 Ω (a)	1000 Ω	1000 Ω (c)
	2	R_s at ω_q; 0 elsewhere	R_L at $(\omega_p-\omega_q)$; 0 elsewhere	26 Ω	26 Ω (a)	26 Ω	26 Ω (a)
	3	R_s at ω_q; 0 elsewhere	R_L at $(\omega_p-\omega_q)$; ∞ elsewhere	1570 Ω	1570 Ω (a)	638 Ω	638 Ω (a)

Note: Square-wave switching, 1:1 mark space. (a) = Conclusion A; (c) = Conclusion C.

as time-varying resistances. Formulae used are largely based on Tucker's earlier work on input impedance,[9] and have been extended to output impedance, and to show the matching at input and output for minimum loss, the numerical calculations being based upon the assumption that the diodes switch from an incremental forward resistance to 10 Ω to an incremental reverse resistance of 100 kΩ under the influence of the local oscillator voltage. It will be seen that in all the cases corresponding to the rules deduced in the previous section the circuits are matched at the appropriate ports, but that for other conditions the mismatch may need to be very considerable, up to three to one in the resistively-terminated series modulator. This would have repercussions on system design using this circuit.

The 'narrow-band' and 'broad-band' microwave mixer circuits can also be considered. In these circuits the image frequency $(2\omega_p-\omega_q)$, is very close to the signal frequency, ω_q, because in turn the local oscillator, ω_p, and signal frequencies, ω_q, are very close together. In the 'narrow-band' mixers high Q tuned circuits are used to distinguish the image and signal frequencies, so that unnecessary dissipation at the image frequency may be avoided, the circuits having then a minimum loss of 0dB with ideal diodes. It follows in consequence of the previous discussion that all such 'narrow-band' mixers must be conjugately matched at input and output for minimum loss. In the 'broad-band' mixers, however, the tuned circuits are lower Q and cannot distinguish the image from the signal frequency. Dissipation at the former frequency then occurs in the input circuit, and the minimum loss is 3dB with ideal diodes. The optimum source and load resistances are not equal. From the discussions of this paper it follows that, although such circuits may be conjugately matched at the output port, there must be a mismatch at the input port for minimum loss. This is well known for certain forms of the circuit,[10] but is clearly a general property of all forms of 'broad-band' mixer with the exception of circuits such as the constant-resistance ring modulator under conditions when image-frequency currents or voltages cannot be supported—see Table 1.

It has been shown elsewhere[11] that the minimum loss condition is a good approximation to the minimum system noise condition for present-day mixers and i.f. amplifiers.

A previous work[8] quoted earlier also offers insight into the problem of modulator and mixer circuit terminations, predicting whether input and output terminations will be equal from a knowledge of the form of frequency selectivity at each port. The basis for these conclusions follows from an examination of the symmetry of the circuit matrix, and is valid despite an erroneous statement in the paper concerning conjugate match for minimum loss, which the present paper corrects.

5. Conclusions

It has been shown possible to predict conditions for which two-ports including one or more elements with periodically-varying parameters will achieve maximum power transfer from source to load when conjugately matched at each port, in those cases where the port impedances or admittances have a positive real part. This has been illustrated with reference to series and ring diode modulators, and it has been further pointed out that earlier work which assessed whether source and load

resistances were equal under these conditions could usefully be used in conjunction with the new results.

6. References

1. Spence, R., 'Linear Active Networks' (Wiley, New York, 1970).
2. Gardiner, J. G. and Yousif, A. M., 'Multi-frequency analysis of switching diode modulators', *The Radio and Electronic Engineer*, **41**, p. 17, January 1971.
3. Tucker, D. G., 'Circuits with Periodically-varying Parameters' (Macdonald, London, 1964).
4. Howson, D. P. and Smith, R. B., 'Parametric Amplifiers' (McGraw-Hill, New York, 1970).
5. van Valkenburg, M. E., 'Network Analysis' (Prentice Hall, Englewood Cliffs, N. J., 1964).
6. Page, C. H., 'Frequency conversion with positive non-linear resistors', *J. Nat. Bur. Stand.*, **56**, p. 179, 1956.
7. Duinker, S., 'General properties of frequency-converting networks', *Philips Res. Repts*, **13**, pp. 37–78 and 101–148, 1968.
8. Howson, D. P., 'Terminating impedances in diode modulators', *The Radio and Electronic Engineer*, **38**, p. 147, September 1969.
9. Tucker, D. G., 'The input impedance of rectifier modulators', *Proc. Instn Elect. Engrs*, **107B**, p. 273, 1960.
10. Strum, P. D., 'Some aspects of mixer crystal performance', *Proc. Inst. Radio Engrs*, **41**, p. 875, 1953.
11. Vugrinic, J., 'Input impedance considerations for a diode mixer . . .', Summer School on Circuit Theory, Prague, 1968.

Manuscript first received by the Institution on 20th December 1971 and in final form on 10th March 1972. (Paper No. 1460/CC137.)

STANDARD FREQUENCY TRANSMISSIONS—June 1972

(Communication from the National Physical Laboratory)

June 1972	Deviation from nominal frequency in parts in 10^{10} (24-hour mean centred on 0300 UT)			Relative phase readings in microseconds N.P.L.—Station (Readings at 1500 UT)		June 1972	Deviation from nominal frequency in parts in 10^{10} (24-hour mean centred on 0300 UT)			Relative phase readings in microseconds N.P.L.—Station (Readings at 1500 UT)	
	GBR 16 kHz	MSF 60 kHz	Droitwich 200 kHz	GBR 16 kHz	†MSF 60 kHz		GBR 16 kHz	MSF 60 kHz	Droitwich 200 kHz	GBR 16 kHz	†MSF 60 kHz
1	—	—	0	—	—	17	—	0	+0·1	—	642·0
2	—	—	0	—	—	18	—	+0·1	0	—	641·3
3	—	+0·1	0	—	645·9	19	—	0	+0·1	—	640·6
4	—	+0·1	0	—	645·0	20	—	0	0	—	640·3
5	—	+0·1	0	—	643·9	21	—	+0·1	0	—	638·0
6	—	+0·1	0	—	643·0	22	—	0	0	—	637·4
7	—	+0·1	0	—	642·1	23	—	0	0	—	637·5
8	—	0	0	—	644·0	24	—	0	0	—	637·2
9	—	+0·1	0	—	643·5	25	—	0	+0·1	—	637·2
10	—	0	0	—	643·7	26	—	0	+0·1	—	637·2
11	—	0	0	—	645·7	27	—	0	+0·1	—	638·3
12	—	0	0	—	643·5	28	—	−0·1	+0·1	—	637·6
13	—	0	0	—	643·4	29	—	+0·1	+0·1	—	636·4
14	—	0	0	—	643·5	30	—	0	0	—	636·6
15	—	0	+0·1	—	642·5						
16	—	+0·1	+0·1	—	641·9						

All measurements in terms of H.P. Caesium Standard No. 334, which agrees with the N.P.L. Caesium Standard to 1 part in 10^{11}.

† Relative to AT Scale; $(AT_{NPL} - \text{Station}) = +468{\cdot}6$ at 1500 UT 31st December 1968.

The GBR and MSF Transmitters at Rugby are off the air for maintenance until the end of July.

U.D.C. 621.376.23: 621.383.4: 621.391.63

A Photoconductive Detector Suitable for Optical Communications Systems

D. V. EDDOLLS, M.Inst.P.*
H. E. G. LUXTON, B.Sc.*
R. O'ROURKE, B.Sc.*
C. W. SHERRING, Ph.D.*
and
H. C. WRIGHT, B.Sc.*

Based on a paper presented at the I.E.R.E. Conference on Infra-red Techniques held in Reading from 21st to 23rd September 1971.

SUMMARY

This paper describes a photoconductive detector which, through the use of a microwave bias, is capable of demodulating a low-level signal at information bandwidths greater than 1 MHz. The principle of operation is described and the advantages over d.c. biased photoconductors highlighted. The dependence of photocurrent gain on semiconductor properties and limitations on performances are discussed.
A system operating at 1 μm wavelength using a Gunn oscillator and miniaturized microwave components is described. This detector, which uses germanium as the photoconductor, has a noise equivalent power (n.e.p.) of 5×10^{-9} W in a noise bandwidth of 10 MHz and a 10–90% rise-time of 80 ns. The system has also been operated with silicon and indium arsenide. Finally, a comparison is made between microwave biased photoconductive detectors and avalanche photodiodes.

* *Allen Clark Research Centre, The Plessey Company, Limited, Caswell, Towcester, Northants.*

1. Introduction

It has been shown[1] that a photoconductive detector is capable of achieving significant gain at large information bandwidths when it is operated with a high frequency bias supply provided by a microwave field. The practical realization of this technique can be understood by reference to Fig. 1, which shows a photoconductor mounted in the high electric field region of a re-entrant microwave cavity. The change in conductivity of the photoconductor, caused by the absorption of incident light, produces a change in the reflection coefficient of the microwave cavity. This results in a modulation being impressed upon the reflected microwave power, the amplitude fluctuations of which will be a reproduction of the amplitude fluctuations in the incident light beam. This signal is then detected, amplified and displayed.

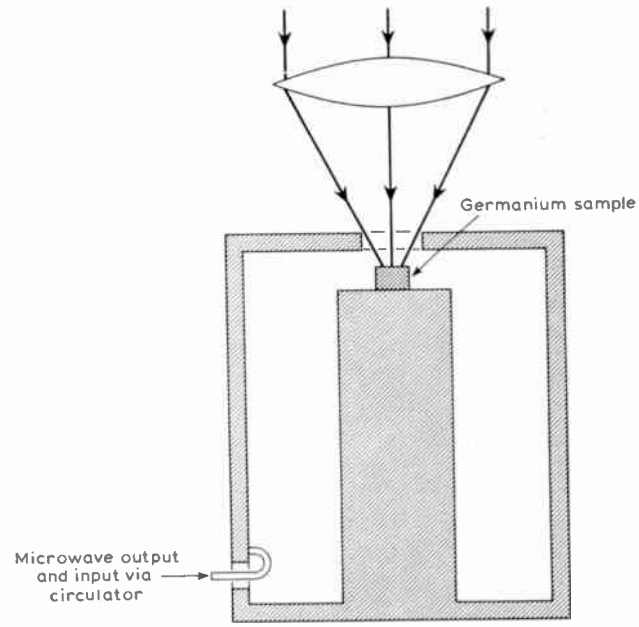

Fig. 1. Schematic diagram of a microwave-biased photoconductor.

2. Comparison with D.C. Biased Photoconductors

In order to appreciate the significance of microwave biasing it is necessary to consider the disadvantages of d.c. biased intrinsic photoconductors. These may be divided into two broad groups. The first group has trapping centres which have a high capture cross-section for minority carriers. The second is comprised of those with no traps. The first group, in which only one type of trap is operative, gives high response but a long time-constant due to the slow discharge of the traps after stimulation ceases. This is shown in Fig. 2(b) where photoconductivity results from the square input pulse of Fig. 2(a). The gain of the second trap-free group is limited by recombination between the excited carrier pairs as they are swept into the contact area by the applied field. This gives the small but fast response shown in Fig. 2(c).

If a trap-free photoconductor is driven by a microwave bias field it is possible to achieve high gain without degradation of response-time as shown in Fig. 2(d). This is possible because if the frequency of the bias field is sufficiently high the motion of the carriers will reverse before they reach the ends of the sample and sweep-out will be drastically reduced. In this way the full generation-recombination lifetime of the photo-pairs can be utilized by applying high fields to the sample.

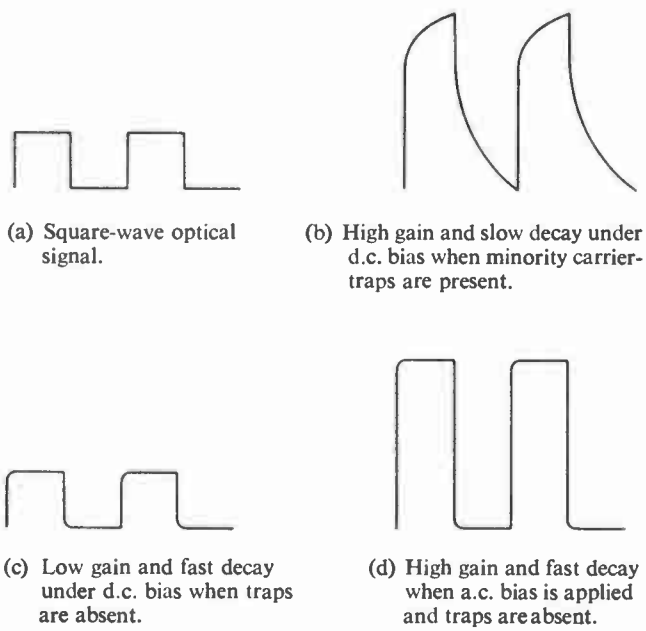

(a) Square-wave optical signal.

(b) High gain and slow decay under d.c. bias when minority carrier-traps are present.

(c) Low gain and fast decay under d.c. bias when traps are absent.

(d) High gain and fast decay when a.c. bias is applied and traps are absent.

Fig. 2. Response of photoconductors.

The high gain available is a result of two effects. The first is a true photocurrent gain in the photoconductor which can be as high as the number of times the photo-carriers traverse the photoconductor before they finally recombine. Further gain is available due to the impedance transformation produced by the microwave circuit from the high resistance of the photoconductor to the low input impedance of the detection system. It is theoretically possible to achieve sufficient gain to overcome the noise of the following amplifier, making low-level detection possible at large information bandwidths.

Summarizing, the following advantages accrue from microwave biasing:

(i) Large gain-bandwidth products are possible with high purity transistor grade materials having a long minority carrier life-time. With d.c. bias the gain-bandwidth is limited by minority carrier sweep out. The use of such high-purity material reduces or eliminates trapping effects which seriously degrade the performance of insulating photoconductors at low light levels.

(ii) Since capacitive coupling to the photoconductor is possible at microwave frequencies, ohmic contacting is no longer necessary. This simplifies fabrication and mounting and eliminates contact noise.

(iii) A theoretical relation limiting the gain-bandwidth product for photoconductors to the reciprocal of the dielectric relaxation time does not apply with blocking contacts, which inject no charge. Thus, very large gain-bandwidth products are possible with high resistivity photoconductors. The use of high-resistivity material results in reduced dissipation and noise.

(iv) The impedance transformation provided by the microwave circuit results in a significant improvement in the performance of extrinsic photoconductors.

3. Available Photocurrent Gain in Microwave-biased Photoconductors

In practice the photocurrent gain is determined through the expression:

$$G = \frac{I_{max}}{\alpha q F} \qquad \text{.....(1)}$$

where I_{max} is the maximum signal current flowing in the amplifier input impedance R, when the cavity is critically coupled. The quantum efficiency of the photoconductor is α, q is the charge on an electron and F is the light flux in photons per second.

The theoretical photocurrent gain, G, attainable with a microwave-biased photoconductor is given in terms of the bias field and the physical properties of the semiconductor by the expression:[2]

$$G = \frac{1}{2\sqrt{2}}\left(\frac{R_s}{R}\right)^{\frac{1}{2}} \cdot \frac{\tau_o(\mu_n+\mu_p)E}{L} \cdot \left[1-\frac{\mu_a E}{\pi f_o L}\right] \qquad \text{.....(2)}$$

where R_s is the photoconductor resistance, τ_o the life-time of the photo-excited pair, L the length of the photoconductor in the direction of the bias field and μ_n, μ_p and μ_a are the electron, hole and ambipolar mobilities respectively. The peak value of the bias field and the frequency are represented by E and f_o, and R is the input impedance of the amplifier.

The right-hand side of eqn. (2) can be divided into three parts. The quotient $(R_s/R)^{\frac{1}{2}}$ is the maximum gain available due to the impedance transformation from the high resistance of the photoconductor to the low input impedance of the broad-band amplifier. The second term represents the true photocurrent gain due to the many transits of the photoexcited carriers in the characteristic lifetime τ_o. Finally, the term in the square bracket accounts for the degradation in gain which results at very high bias fields or low bias frequencies when the motion of the carriers is not reversed before they cross the sample and excessive recombination occurs at the ends. Equation (2) shows that high gain is achieved by using material having a high resistivity, a long life-time and a high mobility. In general a significant improvement in gain will result from operating the photoconductor at a reduced temperature. The maximum transit-time gain available is that obtaining when the carriers are moving with their saturation drift velocities.

A lower limit is set to the bias frequency by the resistivity of the semiconductor. This arises because the free

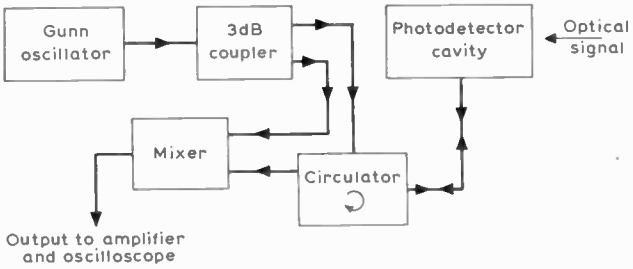

Fig. 3. Schematic diagram of a homodyne detection system.

carrier population tends to redistribute itself so as to oppose an applied field and so screen the interior of the sample. The time constant for this process is τ_d, the dielectric relaxation time. In order that significant screening of the applied field shall not occur the frequency must be greater than the reciprocal of the dielectric relaxation time

$$f_o \geqslant \frac{1}{2\pi\tau_d} = \frac{1}{2\pi\varepsilon_o\varepsilon_r\rho} \qquad \ldots\ldots(3)$$

where ε_o is the permittivity of free space and ε_r the dielectric constant. If the bias frequency is 10 GHz and silicon is used as the photoconductor the minimum resistivity, ρ, to satisfy eqn. (3) is 15 ohm cm. Both silicon and germanium are commercially available with resistivities which are sufficiently high to ensure complete penetration of the electric field. However, it is not generally possible to satisfy this condition with the smaller band-gap materials and the use of indium arsenide, for example, results in a degradation of response.

4. Detection System

The original experimental work on microwave biased photoconductor systems was described by Sommers and Gatchell.[1] Their results demonstrated the high performance available with systems of this type but the use of a klystron as the source of microwave power clearly limited the application of this detector. Work at the Allen Clark Research Centre[3] showed that high performance was still possible if the klystron was replaced by a Gunn oscillator. Subsequently effort has been devoted to developing a system using a Gunn oscillator and miniaturized microwave components.

A block diagram of the Plessey system is shown in Fig. 3. Microwave power from the Gunn oscillator is split by the 3 dB coupler and the output from one port is passed by a circulator to the photodetector cavity. The reflected power having a modulation impressed upon it is returned through the third port of the circulator to the mixer where it is combined with the direct output from the 3 dB coupler. The detected signal is then amplified and displayed. The advantages of this homodyne detection system over a superheterodyne system are that improved stability is achieved by the use of a single Gunn oscillator source and improved noise performance results because the signals that are combined at the mixer are coherent. The microwave system is shown in Fig. 4. All of the components, apart from the microwave cavities, are commercially available. A production system could operate without the circulator and by integrating the Gunn oscillator, 3 dB coupler and mixer in a single assembly a further significant reduction in size would result.

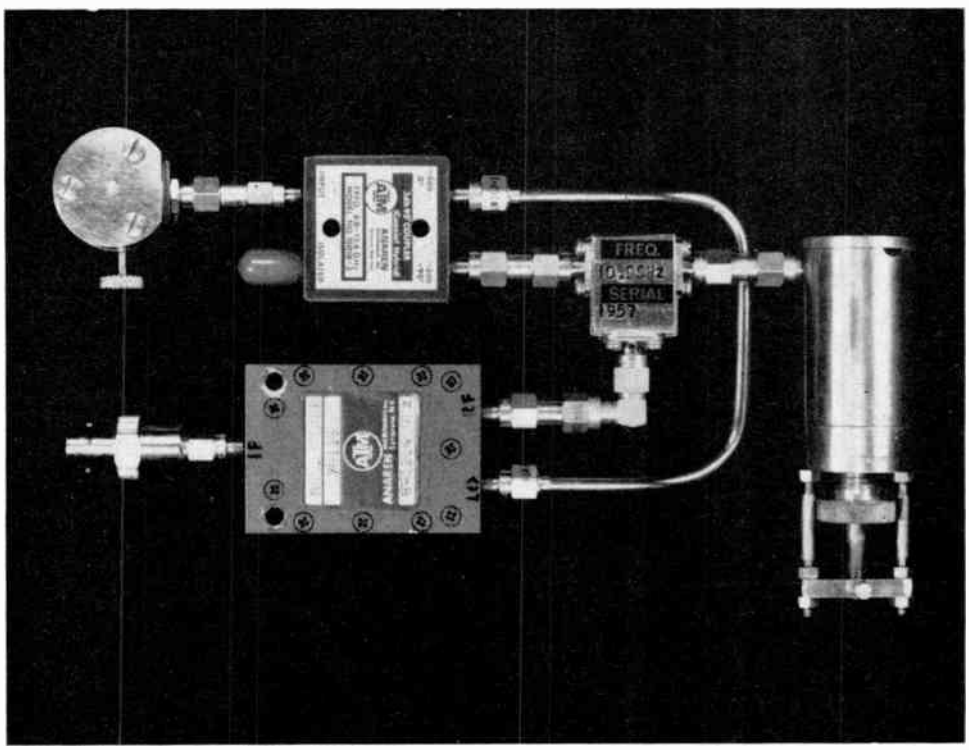

Fig. 4. Microwave-biased 1·06 μm photoconductor system layout.

5. Experimental Results

The system shown in Fig. 4 was developed for operation at wavelengths up to 1·5 μm and therefore uses germanium as the photoconductor. The material is prepared using lapping and etching techniques aimed at producing a high-quality surface having a low recombination velocity. The sensitive surface is provided with an antireflexion coating of zinc selenide of thickness appropriate to the wavelength. Finally, the photoconductor is mounted in the cavity using a proprietary cement to ensure that a blocking contact is made. The optical source was a Plessey GAL3 GaAs lamp and the bandwidth of the amplifier was 10 MHz. The n.e.p. of this system was 5×10^{-9} W and the 10–90% rise-time 80 ns. By using signal processing at the amplifier the rise-time was reduced to 40 ns but with a corresponding increase in n.e.p. to 10^{-8} W. Silicon photoconductors have also been operated in this system and an n.e.p. of 5×10^{-10} W in a 6 MHz bandwidth was measured. However, this material was of poor quality and trapping effects degraded the 10–90% rise-time to 10 μs.

6. Microwave Cavity Design

The microwave bias is applied to the photoconductor by mounting it in the high electric field region of a reentrant TEM mode cavity which is resonant at X-band frequencies. Radiation is incident on the photoconductor through an optical port in the side wall of the cavity. The geometry of the optical port permits the use of $F/4$ optics. Microwave coupling to the cavity is by a loop which is adjustable so that both the impedance and the bandwidth can be optimized. Optimum performance should be obtained when the cavity is critically coupled, that is when the cavity presents a matched load to the 50 ohm line.

Ideally the cavity should be designed so as to concentrate the electrostatic energy in the photoconductor. It has been shown[1] that the photocurrent gain is proportional to the ratio E^2/W where E is the peak electric field and W the energy stored in the cavity. This ratio is a property of the empty cavity and can be determined experimentally by measuring the change in the resonant frequency caused by a perturbation of the field in the gap. The dependence of the factor E^2/W has been investigated both analytically and experimentally. The results confirmed that optimum performance is obtained by using a coaxial line cavity designed to maximize the shunt impedance.

7. Noise

Noise in a microwave-biased photodetection system arises from four sources. These are shot noise associated with the photocurrent and the dark current, noise arising in the Gunn oscillator and Johnson noise in the 50-ohm input impedance of the detection system. Calculations have shown photocurrent shot noise to be negligible and dark current noise to make only a small contribution to the total noise in the system. The noise level in the detector input impedance can be reduced to about 2–3 dB above the thermal limit by a good amplifier design. Photocurrent gains of 100–200 have been measured with the present detector and with the noise contributions listed above this would give rise to a limit of detection of $2\text{–}3\times10^{-9}$ W in a 10 MHz noise bandwidth. In practice noise arising in the Gunn oscillator limits the minimum measurable signal to 5×10^{-9} W. The observed noise is the sum of a number of small contributions including bias circuit oscillations, amplitude modulation on the Gunn oscillator and microphonic noise. Although a homodyne system is used phase shifts arising in the various components and imperfect isolation make it impossible for complete cancellation to occur.

8. Extension to Wavelengths beyond 1·5 μm

A significant feature of the microwave-biased photoconductor is that no specialized materials technology is required, the samples being prepared by conventional lapping and etching techniques. Hence when the microwave-biasing and detection circuitry have been developed the system can be operated at any wavelength provided a suitable semiconductor is available.

An assessment has been made of the feasibility of developing a 10 μm detector using either lead–tin telluride or cadmium–mercury telluride. Both materials have a band-gap appropriate to 10 μm detection and the introduction of traps, which degrade the gain-bandwidth product, is not necessary. All available fast detectors operating beyond 1·5 μm operate at reduced temperatures. Most materials in which traps have been deliberately introduced to give the correct wavelength response, e.g. mercury-doped germanium, have to be cooled to 4·2K and intrinsic detectors operate at 77K. One potential advantage of microwave-biasing is the possibility of using the improved sensitivity offered to allow operation at higher ambient temperatures thus effecting a considerable reduction in system complexity.

Measurements have been made on indium arsenide photoconductors at room temperature to assess degradation effects when narrow gap semiconductors are used.[4] The material used had a resistivity of 0·0085 ohm cm. The best n.e.p.s measured with the sample under d.c. and microwave-bias were $2\cdot8\times10^{-9}$ W Hz$^{-\frac{1}{2}}$ and $1\cdot2\times10^{-10}$ W Hz$^{-\frac{1}{2}}$ respectively. Improvements by a factor of up to 30 were obtained in some instances. The effects of free carrier screening were estimated by comparing the performance of indium arsenide with that of germanium. The resistivity of the latter material was sufficiently high for screening effects to be neglected. The degradation in performance due to imperfection in the microwave system was assessed using germanium. The additional atrophy in the performance of indium arsenide, which is a consequence of free carrier screening, was then found to be a factor of ten. However, since both lead–tin telluride and cadmium–mercury telluride can be obtained with resistivities of 0·01 ohm cm or higher, improved photoconductor performance at 10·6 μm and 77K should be possible with microwave-biasing.

9. Applications

The microwave-biased photoconductor has internal photocurrent gain preceding the principal source of noise. It is therefore suitable as a low-level broadband detector,

the obvious applications being in optical communications systems and laser radar. In a communications system using an optical fibre link the sensitive area of the photoconductor could be significantly reduced below that used in the present system. This would have the double advantage of increasing the theoretically available current gain and reducing the microwave drive power required and possibly the level of oscillator noise. On the other hand laser radar systems require a detector diameter of typically 0·5 mm (0·02 in.) One method of increasing the detector area without degrading the performance of the system would be to admit the radiation through an optical port in the end plate of the cavity. This would necessitate the use of a high conductivity semiconductor window to avoid distortion and consequent reduction of the electric field.

In considering applications of this detector it is necessary to compare it with the avalanche photodiode. Both devices have internal current gain, however the avalanche gain process in the diode is fundamentally noisy due to its statistical nature. At high levels of multiplication the avalanche noise exceeds the Johnson noise in the amplifier input impedance. In general this limits the useful multiplication gain to values less than 100. However, the gain-bandwidth product of the avalanche photodiode generally exceeds 50 GHz. The high sensitivity in the microwave-biased photoconductor arises from transit-time gain in which the only noise contribution is shot noise which is insignificant. Photocurrent gains greater than 1000 have been realized in practice with gain-bandwidth products of 5 GHz.[1] Calculations assuming the limiting noise level to be twice Johnson noise indicate that n.e.p.s below 10^{-8} W in a 100 MHz bandwidth should be available. In practice with a 10 GHz bias frequency the photoconductor cavity will limit the available bandwidth to about 50 MHz. Larger bandwidths will require bias frequencies approaching 20 GHz.

10. Conclusion

In spite of the relatively limited effort so far expended on microwave-biased photoconductive systems they have achieved a level of performance comparable with the avalanche photodiode in the bandwidth range up to 50 MHz. The low voltage supply (8 V for the Gunn oscillator) and simplified semiconductor technology required coupled with the improvement in performance that results as the size of the photoconductor is reduced, makes this detector an obvious choice for an optical fibre communications system. Furthermore the simple fabrication procedure and the range of materials available should make the microwave-biased photoconductor the preferred detector for many broadband applications.

11. Acknowledgment

This work was supported by the former Ministry of Technology and is published by permission of the Directors of The Plessey Company.

12. References

1. Sommers, H. S. and Gatchell, E. K., 'Demodulation of low-level broad-band optical signals with semiconductors', *Proc. Inst. Elect. Electronics Engrs*, **54**, pp. 1553–68, November 1966.
2. Eddolls, D. V. and Wright, H. C., 'Photocurrent gain in a.c. biased photoconductors', *Brit. J. Appl. Phys. (J. Phys. D.)*, Series 2, **1**, pp. 1449–57, November 1968.
3. Bass, J. C., Eddolls, D. V. and Knibb, T. F., 'Microwave-biased photodetector system with an integral Gunn-effect oscillator', *Electronics Letters*, 4, pp. 429–30, October 1968.
4. Sherring, C. W. and Eddolls, D. V., 'Free carrier screening in a microwave biased InAs photoconductor', *Infrared Physics*, **11**, pp. 203–6, December 1971.

Manuscript first received by the Institution on 22nd May 1971, and in final form on 17th April 1972. (Paper No. 1461/CC138.)

Contributors to this issue

Dr. T. G. Blaney graduated in 1963 from King's College in the University of Durham (now the University of Newcastle upon Tyne) with a B.Sc. in Physics. From the next four years he did research in the Cavendish Laboratory, Cambridge, on the electronic properties of metals at low temperatures in the presence of high magnetic fields, (in particular, the magnetoacoustic effect) and in 1967 he was awarded the Ph.D. of the University of Cambridge. Dr. Blaney then went as a Research Associate in the Physics Department and Materials Research Centre of Case Western Reserve University, Cleveland, Ohio, for two years, where he carried out further experimental work on the electronic properties of metals and alloys (in particular, de Haas–van Alphen effect and radio frequency size effects). On returning to the U.K. in 1969 he joined the Division of Electrical Science of the NPL as member of a group exploring the science and applications of the far infra-red and he is currently interested in solid state properties and their device applications in this spectral region.

Mr. A. Tonkin graduated in mathematics from Manchester University in 1961 and joined Elliott Automation Radar Systems as a microwave engineer. He is now Project Manager responsible for data and signal processing projects.

Mr. J. Savage graduated in physics from Queen Mary College, University of London, in 1969. He joined Elliott Automation Radar Systems as a Physicist and is now Section Leader responsible for digital signal processing.

Mr. D. V. Eddolls studied at Bristol College of Science and Technology, becoming a Graduate of the Institute of Physics in 1962. He joined the Allen Clark Research Centre of the Plessey Company in 1963, where he has been involved in the development of microwave devices based on gallium arsenide and of photoconductive and photovoltaic infra-red detectors.

Mr. H. E. G. Luxton graduated from Bath University of Technology in 1969 with a B.Sc. honours degree in Applied Physics. He has since been employed at the Allen Clark Research Centre as a Research Scientist. Prior to working on the development of a microwave-based I.R. detector he was concerned with the production of Gunn-effect solid-state microwave sources for operation at Q-band frequencies. Since completing the infra-red project he has carried out an investigation of the noise performance of gallium arsenide microwave field-effect transistors and at present is working on the development and application of these devices.

Mr. R. G. O'Rourke received the B.Sc. degree in physics in 1967 from the University of Nottingham. He has since been a Scientist at the Allen Clark Research Centre of the Plessey Company, where he has been engaged on development of Gunn diode oscillators in a microstrip environment, and microwave biased infra-red detectors.

Mr. H. C. Wright took a degree at the Thames Polytechnic and worked at the British Scientific Instrument Research Association and Mullard Research Laboratories before joining the Allen Clark Research Centre in 1967. His main work has been in semiconductor mechanisms.

U.D.C. 621.374.32

Computing Time Errors Introduced by Backlash Units

SUMADI SOSROPRAWIRO, M.Sc.*

SUMMARY

In a device using binary rate multipliers and reversible counters (up/down counters or bidirectional counters) to perform arithmetic operations, the result of computations could oscillate up and down around the exact answer. This oscillation can be minimized by means of backlash units (digital filters). However the introduction of the backlash units will cause an additional error on the computing time. This paper analyses the additional error in an experiment with a system performing multiplication.

* *National Institute for Instrumentation, Indonesian Institute of Sciences, Bandung, Indonesia.*

1. Binary Rate Multiplier (B.R.M.)

The b.r.m. has two inputs: a pulse train of input frequency f, and a number X in parallel binary form, where $0 \leqslant X < 1$.

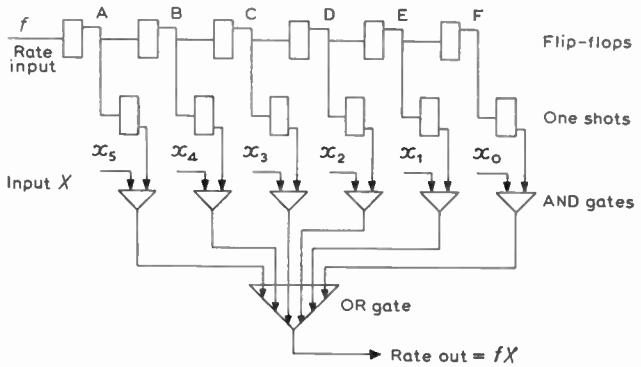

Fig. 1. Schematic diagram of a binary rate multiplier.

Figure 1 shows the diagram of a binary rate multiplier. It consists of a number of binary counters (flip-flops) whose outputs are fed to the pulse differentiators (one-shots) which trigger when the outputs of the flip-flops change from a logical '0' to a logical '1'. The output of each one-shot is ANDed with a control bit of the multiplier x. The output of these AND gates are, therefore, of pulse repetition frequency (p.r.f.) $f.2^{-1}$, $f.2^{-2}, f.2^{-3}, \ldots, f.2^{-n}$. The output rate

$$\begin{aligned} r_{out} &= f.x_0.2^{-n}+f.x_1.2^{-n+1}+f.x_2.2^{-n+2}+ \\ &\qquad +\ldots+f.x_{n-1}.2^{-1}. \\ &= f.2^{-n}(x_0.2^0+x_1.2^1+x_2.2^2+\ldots+ \\ &\qquad +x_{n-1}.2^{n-1}) \\ &= f.x.2^{-n} \end{aligned}$$

where

$$\begin{aligned} x &= x_0.2^0+x_1.2^1+x_2.2^2+\ldots+x_{n-1}.2^{n-1}. \\ &= \sum_{i=0}^{n-1} x_i.2^i \qquad \ldots\ldots(1) \end{aligned}$$

$x_0, x_1, x_2, \ldots, x_n$ are the binary coefficients of value 0 or 1. Assuming that

$$X = x.2^{-n}$$

then

$$r_{out} = f.X \qquad \ldots\ldots(2)$$

The number of pulses at the output of the b.r.m. during time T is TfX. Considering that $\Delta t = 1/f$, then

$$T = \sum_0^N X.\Delta t.$$

The number of pulses at the output of the b.r.m. is thus

$$f.\sum_0^N X.\Delta t = \int_0^T f.X.\mathrm{d}t. \qquad \ldots\ldots(3)$$

As the one-shots will trigger only when the flip-flops' outputs change from a logical '0' to a logical '1' then the outputs of the gates can not be coincident and the last pulse in one cycle (one cycle has 2^n pulses) will never be found at the output of the b.r.m. Stated otherwise, where the one-shots trigger only when the flip-flops outputs change from a logical '1' to a logical

'0', then the first pulse would disappear. The b.r.m. can be expressed as shown in Fig. 2.

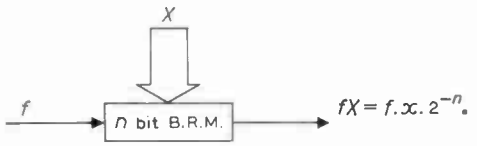

Fig. 2. Binary rate multiplier.

2. Division

The arrangement for division is shown in Fig. 3. The rate input f is constant. f and f' are equal in magnitude but out of phase. Assume that the number of bi-directional counter (b.d.c.), Z, is zero. The frequency coming to the minus input will then be: $fZY = 0$. However the plus input frequency to the bidirectional counter (b.d.c.) (count-up): $fX \neq 0$, and the counter will start to count up. Now Z will increase and the minus input frequency will increase until

$$fX = fZY \qquad \text{.....(4)}$$

When the two input frequencies to the b.d.c. become equal, the system will then be in equilibrium, the plus and minus pulses occur every second time and Z stays unaltered. From equation (4) it follows that

$$X = Z.Y$$
$$Z = X/Y \qquad \text{.....(5)}$$

Thus the system performs a division with independent variables X and Y. The time required by Z in the bidirectional counter to reach the equilibrium value can be determined by means of equation (3). Considering Fig. 3 the net number of pulses entering the b.d.c. during the time t is

$$\int_0^t f.X.\mathrm{d}t - \int_0^t f.Z.Y.\mathrm{d}t$$

2^n pulses correspond to $Z = 1$, therefore

$$2^n.Z = \left[\int_0^t f.X.\mathrm{d}t - \int_0^t f.Z.Y.\mathrm{d}t\right]$$
$$2^n.Z = f\left[\int_0^t (X - ZY).\mathrm{d}t\right] \qquad \text{.....(6)}$$

which has the solution

$$Z = X/Y + (Z_0 - X/Y)\exp(-fYt/2^n). \qquad \text{.....(7)}$$

It can be seen from equation (7) that Z varies from its initial value Z_0 towards the asymptote $Z = X/Y$ through an exponential transient. During the transient, X and

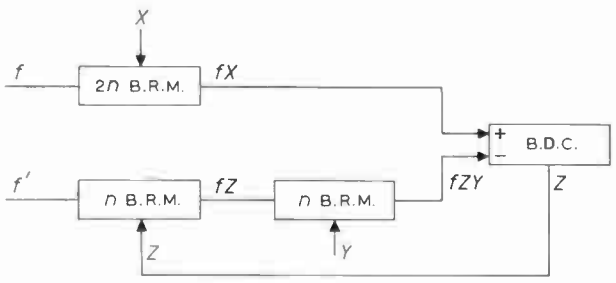

Fig. 3. The operation of division.

Y are assumed constant. X, Y and Z are quantities between 0 and 1.

In fact Z varies in steps of 2^{-n} and not continuously as it was assumed. Therefore equations (6) and (7) are approximate. The greatest accuracy that can be obtained is in general within $\pm 2^{-n}$ of the exact answer. The computing time may thus be defined as the time from when the new set of variables (X, Y) are put in until the error is $\pm 2^{-n}$.

Substituting $Z = X/Y - 2^{-n}$ in equation (7) we get

$$X/Y - 2^{-n} = X/Y + (Z_0 - X/Y)\exp(-fYt/2^n)$$
$$t = t_d = 2^n/fY.\ln 2^n(X/Y - Z_0) \qquad \text{.....(8)}$$

t_d is defined as 'division time'.

3. Square-Root Extraction

The system performing a square root extraction is shown in Fig. 4 The principle may be analysed in a similar manner as for a division. The net number of pulses entering the b.d.c. during the time t is given by

$$2^n \times Z = \int_0^t fX\,\mathrm{d}t - \int_0^t fZ^2\,\mathrm{d}t \qquad \text{.....(9)}$$

which gives the solution

$$Z = \sqrt{X}.\tanh[f.\sqrt{X}.t/2^n + \tanh^{-1} Z_0/\sqrt{X}] \qquad \text{.....(10)}$$

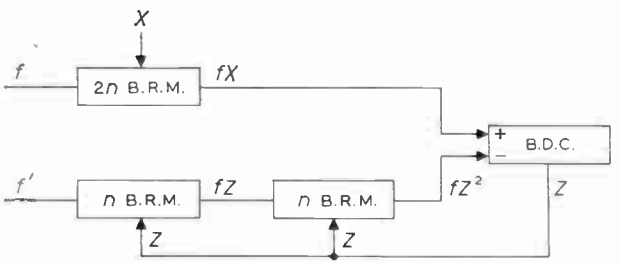

Fig. 4. Square-root extraction.

The time t_r required for the calculation until the error is 2^{-n} is found by substitution of $Z = \sqrt{X} - 2^{-n}$ in equation (10).

$$t_r = (2^{n-1}/f)\sqrt{X}\ln(2^{n+1}.\sqrt{X} - 1).(\sqrt{X} - Z_0)/(\sqrt{X} + Z_0). \qquad \text{.....(11)}$$

If $Z_0 = 0$, then

$$t_r = (2^{n-1}/f)\sqrt{X}.\ln(2^{n+1} \times \sqrt{X} - 1) \qquad \text{.....(12)}$$

4. Multiplication

The circuit diagram for generating multiplications is illustrated in Fig. 5. When the system reaches an equilibrium,

$$fXY = fZ$$
$$Z = XY \qquad \text{.....(13)}$$

The number of pulses to the b.d.c. during the time t is given by

$$2^n \times Z = \int_0^t fXY\,\mathrm{d}t - \int_0^t fZ\,\mathrm{d}t \qquad \text{.....(14)}$$

which when integrated gives

$$Z = XY + (Z_0 - XY)\exp(-f.t/2^n) \qquad \text{.....(15)}$$

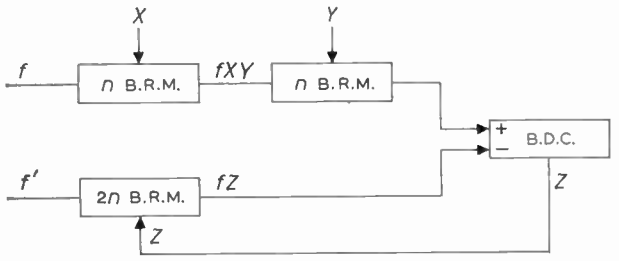

Fig. 5. Multiplication.

The time t required for multiplication until the error is 2^{-n} is found by substitution of $Z = X.Y - 2^{-n}$ in equation (15).

$$t_m = 2^n/f \times \ln 2^n(X.Y - Z_0) \qquad \text{.....(16)}$$

t_m is defined as the required time for multiplication.

Considering that the period of the input signal

$$\tau = 1/f$$

we obtain

$$t_m = 2^n.\tau.\ln 2^n(X.Y - Z_0) \qquad \text{.....(17)}$$

It has been found from experiments[4] that the values of time defined by equations (8), (12) and (16) may vary up and down by approximately a factor of 1·5. Furthermore, for small values of $x.y$, i.e. for $x.y = 1$, the introduction of two backlash units may cause t_m to much exceed its theoretical value defined by equation (16).

5. Frequency Fluctuation

In the analyses outlined above we assumed that the frequency coming out of the b.r.m. to be constant if the input quantities are constant. It is seen to be true only for average values. For times very much greater than $1/f$, the mean output frequency is exactly fX, but there occur fluctuation which will conflict with the assumption made earlier. When an equilibrium will be reached, we may say that the plus and minus frequencies are alike on the average. Because of the fluctuations, Z may vary some steps up and down around the equilibrium value. The oscillation of Z are often very irregular.

Another case when oscillations occur is when the answer to the calculation Z is such that it cannot be expressed by n digits (e.g., we cannot express the answer to 37/128 by 6 digits b.r.m.s).

6. Backlash Units

The fluctuation of Z can be decreased by means of devices called 'backlash units' or 'digital filters' as shown in Fig. 6. The principle of the filter is as follows. Pulses coming to the inputs of the backlash unit must be non-coincident. The first pulse of r_1 (plus pulse) clears bistable B so that B is at a logical '0', and sets bistable A so that A is at a logical '1', enabling NAND gate G_1. Further r_1 pulses are routed through G_1 and the b.d.c. counts up unless bistable A is reset by an r_2 pulse. The r_2 channel (the minus pulses channel) operates in a similar manner. If plus and minus pulses arrive alternately, nothing will be emitted.

7. Experiment

The block diagram of the experiment is illustrated in Fig. 7. The 'start' and the 'stop' of the b.r.m.s is synchronized with the input pulses by means of a J–K master-slave flip-flop. Using two backlash units and one 'divide by two' counter after the b.r.m.s, we could eliminate the fluctuation of Z. We did not succeed in eliminating the Z fluctuation either with one 'divide by two' counter plus one backlash unit, or with only two backlash units without 'divide by two' counter. From Fig. 5, the output of the b.d.c. is

$$Z = X.Y$$
$$Z = x.2^{-n} \times y.2^{-n}$$
$$Z = xy \times 2^{-2n}$$
$$Z = z \times 2^{-2n}, \quad \text{where } z = xy.$$

Hence the coefficient of Z is 2^{-2n} which means that the b.r.m. for Z number must be $2n$ bits b.r.m. as is shown in Fig. 7. According to Fig. 7, the output rate

$$f_0 = z \times 2^{-2n} f$$
$$f_1 = z \times 2^{-2n} f.2^{-1}$$
$$= z \times 2^{-2n-1} f$$

Considering that

$$\tau = 1/f$$
$$\tau_0 = 1/f_0$$
$$\tau_1 = 1/f_1$$

we obtain as a result

$$\tau_1 = 2^{2n+1}.\tau/xy. \qquad \text{.....(18)}$$

The maximum and the minimum values of the computing time t_c, the time required for multiplication in the experiment, can now be determined. The value t_c depends on the starting point and on the initial condition of the output(s) of the digital filter(s), whilst the starting point will depend on the initial condition of the b.r.m.s (initial condition of the outputs A, B, C, ... of the b.r.m.s). Assume that we use only one digital filter. If in the initial condition the A output of the back-lash unit is at a logical '1', the computing time t_c equals to the distance between the starting point and the first output pulse. Therefore the value t_c can vary from τ (minimum) up to τ_1 (maximum). Thus if at $t = 0$, A of the backlash unit is '1' then the computing time $\tau \leqslant t_c \leqslant \tau_1$. If in the initial condition, A of the backlash unit is at a logical '0' then the value of t_c will increase with one output period τ_1. The first pulse coming beyond the starting point will trigger the backlash

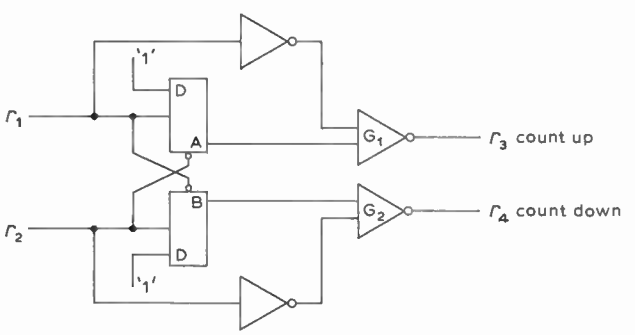

Fig. 6. Backlash unit or digital filter.

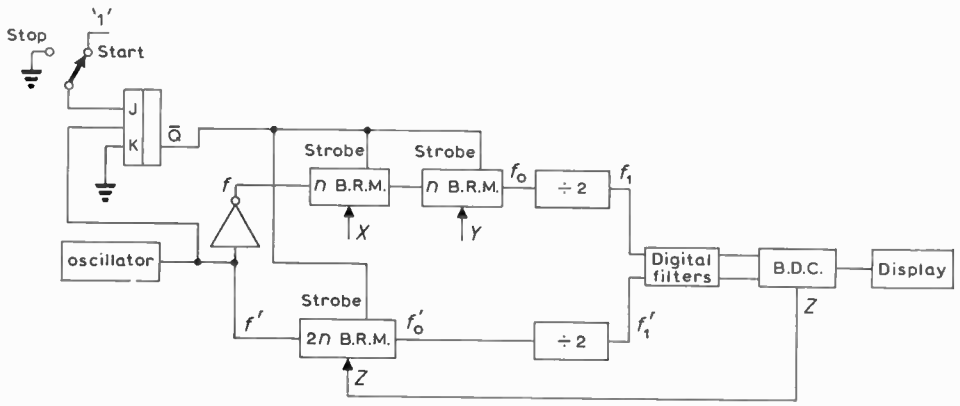

Fig. 7. The block diagram of the experiment.

unit so that A changes from a logical '0' to a logical '1'. Thus at $t = 0$ this pulse is blocked from the b.d.c. by the backlash unit. The second pulse passing the backlash unit is routed to the b.d.c. and makes one count-up. In this case the value of t_c may vary from $(\tau_1+\tau)$ up to $(\tau_1+\tau_1)$. In general, not knowing the initial conditions of the b.r.m.s and the backlash unit, we could say that the value of t_c may vary from τ up to τ_1, i.e.

$$\tau_{in} \leqslant t_c \leqslant 2\tau_{out} \quad \text{or}$$
$$\tau_{in} \leqslant t_c \leqslant (m+1).\tau_{out} \qquad \text{.....(19)}$$

where

τ_{in} is the period of the rate input (in our experiment τ),

τ_{out} is the period of the rate output (τ_1) and

m is the number of backlash units.

Consider that the number of the backlash units output, which in the initial condition are at a logical '0', is p, then the computing time

$$(\tau+p.\tau_1) \leqslant t_c \leqslant (p+1).\tau_1. \qquad \text{.....(20)}$$

In our experiment we used for multiplication 6-bit b.r.m.s, one 'divide-by-two' counter and two backlash units. The input frequency is 1000 Hz. For $xy = 1$, the period of the rate output

$$\tau_1 = 2^{13}/1 \text{ ms} = 8192 \text{ ms.}$$

and for $xy = 2$

$$\tau_1 = 2^{13}/2 \text{ ms} = 4096 \text{ ms.}$$

The results of measurements are recorded in Table 1 and Table 2. Here t_c theoretical means the time defined by equation (20). The average t_c measured is the average value of five measurements. It can be seen from Table 1 that the computing time t_c, for $z = xy = 1$, may vary from 1 ms up to 24·576 s. This phenomena may be considered as a computing time error. This error is introduced by the b.r.m.s and backlash units. The value of the error will depend on the input frequency, the number of the backlash units and the product xy ($xy \neq 0$) for a given number of bits of the b.r.m.s. The maximum error due to the initial condition of the b.r.m.s is equal to one output period τ_1 and the maximum error due to the initial conditions of the backlash units is equal to $m\tau_1$. Hence the total maximum error,

$$\Delta t_{max} = (m+1).\tau_1$$
$$\Delta t_{max} = (m+1).2^{2n+1}/xy.\tau \qquad \text{.....(21)}$$

where $xy \neq 0$. If xy increases, the error decreases.

Equation (21) is true only when the period of the output is constant. In fact the separation between the two following pulses are not always equal. When the output period is constant (the output pulses are coming regularly), then the maximum error will not depend on the starting point, in other words, on the initial conditions of the b.r.m.s. If the pulses coming at the output are irregular, then the maximum error will depend on the initial conditions of the b.r.m.s. This can be explained with the help of Fig. 8.

Table 1

$f = 1$ kHz $\quad xy = 1$

Initial conditions		Computing time			
A 1st backlash	A 2nd backlash	t_c (s) theoretical	t_c (s) measured lowest	average	highest
1	1	0·001– 8·192	5·62	6·34	7·41
1	0	8·192–16·384	10·18	10·45	11·74
0	1	8·192–16·384	12·86	14·58	14·72
0	0	16·384–24·576	17·84	18·70	19·41

Table 2

$f = 1$ kHz $\quad xy = 2$

Initial conditions		Computing time			
A 1st backlash	A 2nd backlash	t_c (s) theoretical	t_c (s) measured lowest	average	highest
1	1	4·096– 8·192	6·90	7·47	7·84
1	0	8·192–12·288	9·28	9·56	10·15
0	1	8·192–12·288	11·10	11·65	11·83
0	0	12·288–16·384	15·37	15·74	15·88

In this model the output rate is 9/16 of the input rate and $f = 1$ kHz. During one cycle there are 9 pulses (K, L, M, N, O, P, Q, R and S pulses) at the output.

If the initial conditions of the b.r.m.s are such that the starting point is at a point between K and L pulses and we use two backlash units whose outputs in the initial condition are at a logical '0', then the L and M pulses are blocked from the b.d.c. by the first and the second

Fig. 8. Output pulses of a 4-bit b.r.m. with $x = 9$ and $f = 1$ kHz.

Table 3

($f = 1$ kHz)

xy	t_o (s) eqn. (16)	t_o (s) measured	$\Delta t_{max.}$ (s)
2	5·66	15·48	12·28
4	11·32	17·07	6·44
6	14·68	17·55	4·09
8	16·98	21·38	3·07
10	18·90	24·90	2·45
12	20·40	25·27	2·04
14	21·60	25·28	1·73
16	22·70	24·80	1·51
18	23·60	25·30	1·34
20	24·50	29·14	1·22
24	26·00	29·03	1·01
32	28·40	33·21	0·73
40	30·20	33·09	0·61
50	32·00	33·61	0·48
60	33·50	37·74	0·40
63	34·00	39·13	0·38

backlash units respectively. The N pulse will be routed to the b.d.c. In this case.

$$\Delta t_{max} = 6 \text{ ms}.$$

But in the case where the starting point occurs at a point between M and N pulses, we get

$$\Delta t_{max} = 4 \text{ ms}.$$

We could see from equation (21) that for $xy = 1$ the maximum error is most significant. We can compare the computing time t_c defined by equation (16) with those measured in our experiment as it is shown in Table 3. Take for an example, $xy = 2$. The computing time defined by equation (16) will be 5·66 s, but the experiment gave a result of 15·48 s. This is due to the Δt_{max} of 12·28 s. Theoretically t_c for $xy = 4$ must be twice that for $xy = 2$, but in fact, as is shown in Table 3, the time required for $xy = 4$ is almost the same as the time required for $xy = 2$. The measurement of the t_c-measured in Table 3 have been done for only one time. However, many measurements has been observed and gave almost the same values. Only for $xy = 2, 4, 6$ and 8 the results may vary up and down with about 1·5, 1, 0·5, 0·4 seconds respectively. It might be that the small variation on the computing time originated from the small variation of the initial conditions of the b.r.m.s but not those of the backlash units.

8. Conclusions

The introduction of the backlash units will cause the computing time to be much larger (for small xy) than its theoretical value defined by equation (16), but for a large value of xy this additional error is not significant. Equations (8), (12) and (16) are approximate, in fact the computing time may be a little higher.

9. Acknowledgments

The author wishes to thank Professor Dr. A. J. Vendrik, Ir. G. J. H. Uyen and Mr. J. H. Bakker for their permission to do the experiment in the Laboratory of the Department of Medical Physics of the University of Nijmegen, and also Mr. K. B. Meisner for his assistance.

10. References

1. Parsons, B., 'Binary Rate Multiplier', Texas Instruments Application Reports.
2. Martin, J. D., 'Signal processing and computation using pulse rate techniques', *The Radio and Electronic Engineer*, **38**, pp. 329–34, December 1969.
3. Wood, P., 'A frequency meter with continuous digital presentation', *J. Brit. Instn Radio Engrs*, **26**, pp. 109–13, August 1963.
4. Lundh, Y., 'Digital techniques for small computations', *J. Brit. Instn Radio Engrs*, **9**, pp. 439–49, January 1959.
5. Yang, H. Z., 'Determination of maximum error of a binary multiplier', *Automation and Remote Control*, **21**, pp. 709–13, July 1961.
6. Meyer, M. A., Gordon, B. M. and Nicola, R. N., 'An operational digital feedback divider', *Trans. Inst. Radio Engrs on Electronic Computers*, EC-3, pp. 17–20, March 1954.

Manuscript first received by the Institution on 7th December 1971 and in final form on 19th April 1972. (Paper No. 1462/CC139.)

U.D.C. 621.396.962.25

An Application of Correlation to Radar Systems

A. TONKIN, B.Sc.*

and

J. SAVAGE, B.Sc.*

Based on a paper presented at a Colloquium on Correlation held in London on 25th November 1971.

SUMMARY

This paper considers an application of correlation techniques to radar systems. One particular form of the system, the frequency modulated continuous wave radar, is described and it is shown that with this form of radar, correlation can be obtained by a combination of mixing and spectral analysis.
A method of performing the spectral analysis using a digital fast Fourier transform spectral analyser is also described.

* *Marconi Elliott Avionic Systems Ltd., Elstree Way, Borehamwood, Herts.*

1. Introduction

A radar system relies for its performance on a comparison of the received signal with a record of the transmitted signal. Conventional radar techniques use a filter to act as this stored record. Although this is satisfactory for simple radar systems it is less so for radars using more advanced techniques or when the radar is to be used in a number of different environments, where the modulation waveform needs to be modified to match the environment. Digital filters have, in many of their forms, the capability of being varied at will, over a wide range of parameters, and are therefore particularly suitable for these radars. Digital logic is now being produced with sufficient speed to enable the development of a digital filter that can meet the requirements of some of these radar systems. In this paper detailed consideration is given to one form of system, namely, frequency-modulated continuous-wave (f.m.c.w.) radar. In this system, correlation between the received and transmitted signals is obtained by a combination of mixing followed by digital filtering. A brief explanation of the principles of this form of radar and of the processing required to obtain an optimum performance is first presented. The equipment which has been developed for this processing is a fast Fourier transform spectrum analyser. This analyser operates at high speed, has a high dynamic range and is compact and light. The basic principles of the fast Fourier transform are then outlined and the actual equipment implementation for the f.m.c.w. application is described.

2. The Frequency Modulated Continuous Wave Radar

Although the basic principles of a simple pulse radar are well known, those of more advanced systems such as the frequency modulated continuous wave radar, are less so. A brief outline of the general principles of this radar system will therefore be presented before embarking on a description of the associated signal processing equipment.

The f.m.c.w. radar relies on measuring the range of the target by coding the transmitted signal, by varying its frequency with time, and comparing this with the signal returned from the target. If the transmitted signal has a complex waveform $u(t)$ then it can be shown that the optimum signal processing is obtained by correlating the return signal with the complex conjugate of this waveform.†

The return signal is given by $u(t-\tau)\exp[-j\omega_D(t-\tau)]$, where τ is the propagation delay between transmission and reception and ω_D is the Doppler shift due to relative motion between target and radar. Thus the signal after processing is given by

$$h(T) = \int_{-\infty}^{\infty} u^*(t-T)u(t-\tau)\exp[-j\omega_D(t-\tau)]\,dt$$

The simplest coding for the transmitted signal, and the one most often used, is the linear frequency sweep.

† Rihaczek, A. W., 'Principles of High-Resolution Radar', (McGraw-Hill, New York, 1969).

Thus the complex signal waveform is given by:

$$u(t) = \exp\left[-j(\omega t + pt^2)\right]$$

Substituting this in the correlation integral for $h(T)$ gives:

$$h(T) = \exp\left[j\{\omega(T-\tau)+p(T^2-\tau^2)+\omega_D\tau\}\right]\times \times \int_{-\infty}^{\infty} \exp\left[jt\{2p(T-\tau)-\omega_D\}\right] dt$$

The integral at the end of this expression is the defining integral for the Dirac delta function. Thus $h(T)$ is zero except where

$$2p(T-\tau)-\omega_D = 0$$

or

$$T = \frac{\omega_D}{2p} + \tau$$

It can be seen that this value of T is a function of both the propagation delay and the Doppler shift. Separation can, however, be obtained by transmitting another waveform in addition, for example, with a different frequency sweep, and computing from the two correlation functions both the range and the Doppler shift.

This is not, however, the only way to process the signal. It will be noticed that if the integration kernel were multiplied by an arbitrary frequency shift then $h(T)$ would become:

$$h_1(T) = \exp\left[j\{\omega(T-\tau)+p(T^2-\tau^2)+\omega_D\tau\}\right]\times \times \int_{-\infty}^{\infty} \exp\left[jt\{2p(T-\tau)-\omega_D-\omega\}\right] dt$$

and as before $h_1(T)$ is zero except where

$$T = \frac{\omega_D-\omega}{2p} + \tau$$

However, if $\omega = (2p\tau-\omega_D)$ then $h_1(0)$ is zero. But $h_1(0)$ is given by:

$$h_1(0) = \int_{-\infty}^{\infty} u^*(t)u(t-\tau)\exp\left[-j\omega_D t\right]\exp_t\left[-j\omega t\right] dt$$

It can be seen that this is the spectrum of

$$u^*(t)u(t-\tau)\exp\left[-j\omega_D t\right]$$

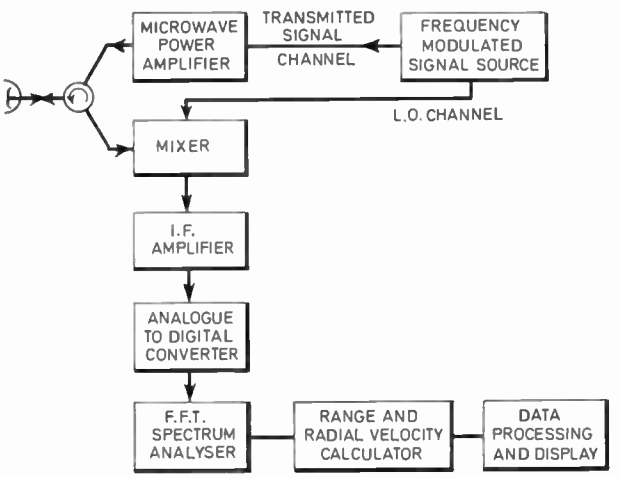

Fig. 1. Block diagram of a frequency-modulated continuous-wave radar system.

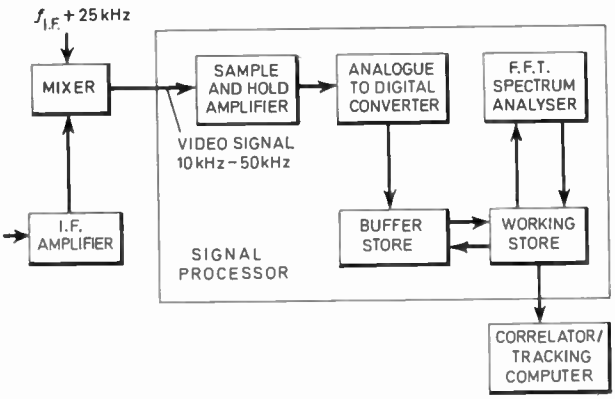

Fig. 2. A digital signal processor.

and so an alternative method of processing is to find the spectrum of this function. This function is, however, readily obtained as $u(t)$ is the current transmitted waveform, $u(t-\tau)\exp\left[-j\omega_D t\right]$ is the return signal, and the product of one with the complex conjugate of the other is the mathematical equivalent of mixing the signals. Thus this correlation can be achieved by mixing the return signal with the transmitted signal and then spectrum analysing the result.

A simplified diagram of an f.m.c.w. radar with this form of processing is shown in Fig. 1.

3. Principles of Fast Fourier Transform Filtering

The requirement for the signal processing has been reduced to that of mixing the return signal with the transmitted signal and then deriving the spectrum of the result. It is well known that the spectrum of a signal can be found by evaluating its Fourier transform. The principle of filtering by means of the fast Fourier transform is to convert the signal into a sequence of digital numbers each representing the instantaneous signal amplitude and to compute, digitally, the Fourier transform from these points, using an algorithm called the fast Fourier transform (F.F.T.). The signal processing equipment consists of a sampling circuit, an analogue-to-digital converter, a buffer store and an F.F.T. signal analyser (Fig. 2).

The fast Fourier transform algorithm is a method of efficiently computing the 'discrete Fourier transform' (D.F.T.) of a finite set of equally spaced samples. This algorithm can be readily understood by noting that the discrete Fourier transform can be separated into a linear sum of two half-size Fourier transforms, since the D.F.T. is defined by:

$$A_k = \sum_{r=0}^{N-1} X_r \exp\left[-j2\pi\frac{rk}{N}\right] \qquad k = 0 \to N-1$$

$$= \sum_{r=0}^{\frac{N-1}{2}} X_{2r} \exp\left[-j2\pi\frac{rk}{(N/2)}\right] + \exp\left[-j\frac{2\pi k}{N}\right] \sum_{r=0}^{\frac{N-1}{2}} X_{2r+1} \exp\left[-j2\pi\frac{rk}{(N/2)}\right]$$

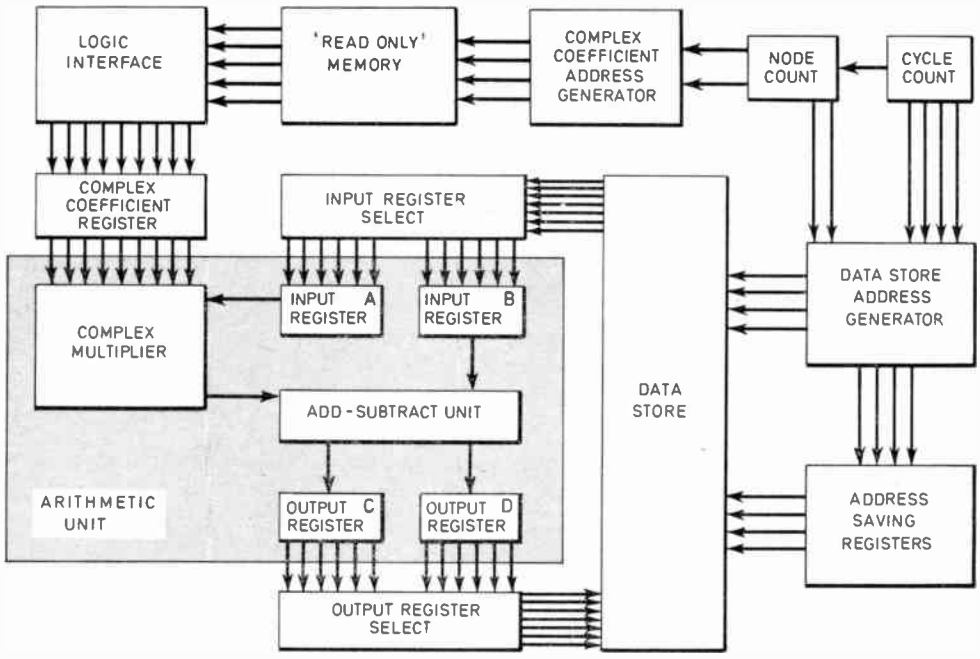

Fig. 3. Block diagram of a fast Fourier transform calculator.

Thus

$$A_k = B_k + \exp\left(-j2\pi \frac{k}{N}\right) C_k \qquad k = 0 \rightarrow \frac{N-1}{2}$$

or

$$A_k = B_k - \exp\left(-j2\pi \frac{k}{N}\right) C_k \qquad k = \frac{N+1}{2} \rightarrow N-1$$

where B_k and C_k are Fourier transforms of $N/2$ points each made up of the even and odd points respectively.

These transforms can in turn be reduced to two more Fourier transforms of half the points each, and so on until they become single points. Thus the whole transform becomes a series of iterations of the form

$$X_k = X_k + WX_j$$
$$X_j = X_k - WX_j$$

with appropriate values of k, j and W. It can be seen that there are $N/2$ such iterations per pairing of transforms and $\log_2 N$ pairings. As each iteration involves a single complex multiplication the whole transform requires $N/2 \log_2 N$ multiplications. The equivalent number of multiplications required for a simple-minded, coefficient by coefficient approach is N^2. Thus the fast Fourier transform technique reduces the number of multiplications considerably, for example, for a 1024 point transform the numbers of complex multiplications are 5120 and 1 048 576 for the F.F.T. and the direct method respectively.

4. Fast Fourier Transform Equipment Design

The equipment necessary for executing the fast Fourier transform (Fig. 3) consists of an arithmetic unit which performs the basic iteration $C = B + WA$ and $D = B - WA$, a random access memory for storing the complex numbers A, B, C and D and a read-only memory which contains the complex weighting coefficients W. The data store can be duplicated for a system where the input data are supplied continuously so that simultaneous collection of data and analysis can take place.

The analyser uses emitter-coupled logic (E.C.L.) in the arithmetic unit, where full use can be made of its high speed, yet employing relatively simple logic functions. In the control unit and store address generators, however, speed is not as important and transistor-transistor logic (T.T.L.) has been used so that full advantage can be gained from the availability of medium and large scale integration functions.

Both the 'read only' and the random access memories are of the bipolar semiconductor type which again contributes to the space efficiency of the system.

4.1. *The System Design Philosophy*

There are two basic ways of increasing the speed of a digital system. One is to reduce the time necessary for making a logic decision and the other is to make as many logic decisions at the same time as possible.

The former means using a faster type of logic, which in general means a faster transition between logic levels. In this case the working frequency of the interconnexion system must be increased and there comes a point where reflexions and cross-talk in wires or printed circuit tracks becomes excessive. This means that constant impedance transmission line interconnexion techniques must be used which increases costs as well as decreasing the packing density.

The latter, a highly parallel system, will have a speed which is directly proportional to the number of integrated circuits.

The aim of the system design was to take advantage of both techniques while avoiding the disadvantage of excessive use of either.

4.2. *The Arithmetic Unit*

Emitter-coupled logic was chosen for the arithmetic unit because, not only is it the most comprehensive range of fast logic currently available, but also it has a shorter propagation delay than T.T.L. although its transition time is not so fast as to necessitate elaborate transmission line techniques. Some care must be taken when interconnecting this type of logic over a distance greater than about three inches but this is seldom necessary. In order to achieve the best possible packing density, multilayer printed boards with plated-through holes have been chosen for use in the arithmetic unit in conjunction with flat packaged logic. In this way the necessarily close packing of conductors can be achieved by the inclusion of isolating conductor planes inside the boards.

The task of the complex multiplier is to perform four multiplications and add and subtract the result. Four unilateral iterative multipliers were chosen, as they are synchronous and enable a serial add/subtract unit to be used. This means a large saving in the number of logic elements especially with a long processor word where parallel arithmetic could increase the quantity of logic required by a factor of 20.

The unilateral multiplier (Fig. 4) in fact performs its function in a very similar manner to that in which conventional longhand multiplication is taught except that the addition is performed after each digit is multiplied instead of totalling at the end. The result of this cumulative addition at any stage in the multiplication is known as the partial product and is held in two registers in the multiplier, one for the sum bits and one for the carry bits.

In operation, the complex coefficient is supplied to the multiplier in parallel form from the complex coefficient register, while the data word is fed in serially from register A. The two numbers are assumed by the multipliers to be positive fractions and so a small amount of logic is included to take care of negative numbers and also to prevent the numbers in the processor exceeding unity. The output from the multipliers are converted to a 2's complement representation if negative before passing on to the add/subtract unit, so that from then on, the signs of numbers can be dealt with automatically.

The unilateral iterative multiplier, being of a synchronous type is not particularly fast in operation although when emitter-coupled logic is employed it is capable of multiplying 20-bit numbers in about 1·1 μs. It is, however, very efficient in its logic implementation and has an important advantage over other types of multiplier in that it performs multiplication in two distinct phases.

The first phase involves the input register A and the complex coefficient register supplying data to the multipliers until register A is empty. During this time the least significant part of the product is calculated and fed out of the multiplier. By the end of the phase the most significant part of the answer is held in the partial product registers. Because a constant word-length must be maintained in the processor, however, the least significant part of the product is not required and consequently the output shift registers C and D can remain static during this period.

The second phase involves the contents of the partial product registers being combined to form the real product. As each bit is calculated it is fed through the add/subtract unit together with the contents of input register B and the result is collected by output registers C and D.

This means that input register A and the complex coefficient register are free during the second multiplier phase and the output shift registers C and D are free during the first. It can be seen that provided the data store and the complex coefficient store have sufficiently short cycle times, all data transfers between the input/output registers and the stores can take place during multiplication. Normally duplications of all registers would be required in order to gain this type of speed advantage, but the two-phase property of the multiplier chosen for this processor means that in fact only input register B need be duplicated.

4.3. *Data Store*

In order to gain full advantage from the design of the arithmetic unit, the data store must be capable of two half cycles (two 'read' or two 'write' cycles) per multiplier phase or about 600 ns. There are two types of memory currently available which will satisfy this requirement.

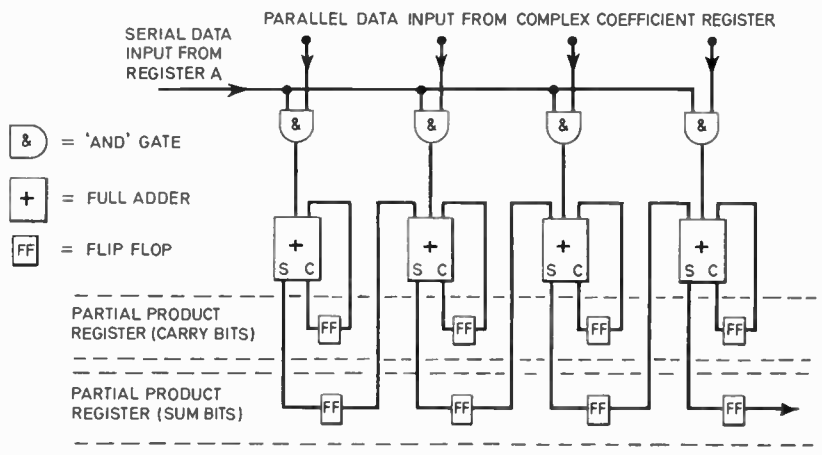

Fig. 4. Four-bit unilateral iterative multiplier.

One is a plated-wire magnetic memory system. This would be large, heavy and not easily 'ruggedized' for an airborne environment. The other type which is the one chosen for this system is an all-semiconductor integrated random access memory system using a 256-bit bipolar memory element which has a maximum cycle time of 400 ns. The random access memory system stores all data and coefficients in the form of double length complex words up to 40 bits long and has an overall half cycle time of 270 ns.

4.4. *Complex Coefficient Store*

The set of complex coefficients required by the processor is permanently stored in a read-only memory. The actual values required to perform a 1024 point F.F.T. are 512 incremental values each of sine and cosine covering the range 0 to π, which would require a memory capacity of 512 double length words. But by virtue of the symmetry of these functions only values of cosine from zero to $\pi/2$ are in fact required, for which a memory capacity of half this number of single length words is sufficient. The negative sign necessary for values of cosine greater than $\pi/2$ is supplied by the control logic. This further economy of space, however, means that the 'read only' memory must be accessed twice in each iteration, once for the real part and once for the imaginary part of the complex coefficient. But the type of memory chosen, a 256 bipolar device, is easily fast enough having a maximum access time of 100 ns.

4.5. *Control Logic*

Both the data store and the complex coefficient store have separate address generators. In each iteration of the arithmetic unit, the complex coefficient store is accessed twice and the data store performs two 'read' cycles and two 'write' cycles. This means that six different addresses must be generated in each iteration making a total of approximately 30 000 addresses for each thousand point F.F.T.

There are two possible methods of generating these addresses. The simplest of these is to use a conventional binary counter to address a suitably programmed 'read only' memory. This would be suitable for, say, a 64-point transform machine, where only 50 or so 'read only' memory elements would be necessary. A 1024-point transform machine, however, would require over 1000 such elements and consequently is not feasible for the present application.

Fortunately, the addressing sequences are not altogether random and can in fact be generated by reversing the order of the bits of a binary count, complementing and shifting.

These processes can be implemented using standard T.T.L. and m.s.i. components and as the final component count for both generators was less than 120, this method was chosen for the present system.

5. Conclusions

In this paper a method of implementing the correlation function required for optimum signal processing of an f.m.c.w. radar system has been presented.

A description of the actual equipment for this implementation is given which results in a compact high speed processor.

Manuscript first received by the Institution on 25th January 1972 and in final form on 29th March 1972. (Paper No. 1463/AMMS49.)